Ministry of Higher Education and Scientific Research
University of Babylon / College of Science
Department of Physics

Preparation and Characterization of (NiO:Cu/Si) Solar Cell by Aerosol Assisted Chemical Vapor Deposition (AACVD)

A Thesis

Submitted to the Council of College of Science, University of Babylon in Partial Fulfillment of the Requirements for the Degree of Master of Science in Physics

By

Zaid Mohammed Jassim Zwaid

(B. Sc. in Physics 2014)

Supervised By

Asst.Prof. Dr. Saba Abdulzahra O. ALShiaa

2021 A.D. 1443 A.H.

بِسْمِ اللَّهِ الرَّحْمَٰنِ الرَّحِيمِ

(وَيَسْأَلَونَكَ عَنِ الرُّوحِ قُلِ الرُّوحُ مِن أَمْرِ رَبِي وَمَا أُوتِيتُمْ مِنَ الْعِلْمِ إِلاَّ قَلِيلاً)

صدق الله العلي العظيم

سورة الاسرا ء

الآية(٨٥)

Supervisor Certification

I certify that this thesis entitled (**Preparation and Characterization of (NiO:Cu/Si) Solar Cell by Aerosol Assisted Chemical Vapor Deposition(AACVD)**) was prepared by (**Zaid Mohammed Jassim Zwaid**) under my supervision at partial fulfillment of the requirements for degree Master of science Physics.

Signature

Supervisor : **Dr. Saba Abdulzahra O. ALShiaa**

Title : Assistant Professor

Address : Department of physics – College of science – University of Babylon .

Data: / / 2021

Certification of the Head of the Department

In view of the available recommendation, I forward this thesis for debate by the examination committee.

Signature:

Name : **Dr. Abdulazeez O. Mousa Al-Ogaili**

Title: Professor

Address: Head of Department of physics – College of science – University of Babylon.

Data: / / 2021

Examining Committee Certificate

We certify that we have read this thesis entitled " **Preparation and Characterization of (NiO:Cu/Si) Solar Cell by Aerosol Assisted Chemical Vapor Deposition(AACVD)**" and, as an examining committee, examined the M.Sc. student " **Zaid Mohammed Jassim Zwaid**" in its content and that , in our opinion it meets the standards of a proposal for the degree of Master of Science in Physics with (Excellent) degree.

Signature :

Name : **Dr. Raheem G. Kadhim**
Title : Professor
Address : Department of Physics /
College of Science / University of Babylon
Date : / / 2021

(Chairman)

Signature :

Name : **Dr. Alaa Jewad Kadham ALgidsawi**
Title : Assistant Professor
Address : Al-Qasim Green University
Date : / / 2021

(Member)

Signature :

Name : **Dr. Nassar A. Al-Isawi**
Title : Lecturer
Address : Department of Physics /
College of Science/University of Babylon
Date : / / 2021

(Member)

Signature :

Name **Dr. Saba Abdulzahra O. ALShiaa**
Title : Assistant Professor
Address : Department of Physics /
College of Science / University of Babylon
Date : / / 2021

(Member and Supervisor)

Approved by the college committee on graduate studies

Signature:

Name : **Dr. Enas M. Al-Robayi**

Title: Professor

Address: Dean of the College of science /University of Babylon

Date: / / 2021

Dedication

To everyone who wants the best for this country...

For everyone who gave us hope and trust for someone...

To everyone who repeated to us calls for success…

For everyone who works for others...

Zaid

Acknowledgments

Firstly, I should thank my Almighty (Allah) for helping me in completing my thesis.

I would like to express my thanks, gratitude and appreciation to my supervisor Asst. Prof. Dr. Saba Abdulzahra O. ALShiaa for his extinguished efforts, sound advice and guidance that have helped in smoothing out every difficulty encountered during my work, Many thanks to the deanery of the college of science at Babylon University and the Department of Physics for offering me the opportunity to complete my dissertation. My great thanks are expressed to all my friends. Finally, many thanks and gratefulness to all my family members who always support me and alleviate difficulties I have faced during my work.

Zaid

Summary

The compound NiO:Cu thin films were prepared using a the Aerosol-Assisted Chemical Vapor Deposition (AACVD) deposition technique, it is a method that has proven its efficiency in preparing thin films within Nano scale ranges. Copper were with different doping percentage (Cu/Ni=0, 7.5, 10, 12.8 At. %) to deposition on substrates of glass and (n-type) and (p-type) silicon.

The crystal structure of the prepared films has been examined by X-ray diffraction method (XRD) and the results showed that all the prepared films are polycrystalline in the cubic phase with the highest peak at the plane (111) and at the angle (37.5^{o}), it showed an improvement in the crystal structure by increasing the height of the peaks. There is an increase in the crystallite size of the nanoparticles, decrease in the strain and the dislocation density and increase the lattice constants (a_o) when increasing the doping. This is an indication of improved properties of the prepared films. As for the results of the scanning electronic microscope (SEM) the images show the nanoparticles by increasing the doping and an increase in the grain size with the doping increases.

The optical properties of prepared films with thickness (45 - 62 ±6) nm were studied using optical transmittance measurements in the spectral region (330-1100) nm. It was noted that, the transition is direct allowed transition and the increase in doping copper percentage leads to a decrease in the optical energy gap of the NiO films from(3.5- 2.8eV), which decreases when the film thickness increases, so the thickness of the film increases with the increase in doping. The optical constants such as refractive index, extinction coefficient and dielectric constant have been calculated for all prepared films.

The electrical properties include Hall Effect were studied. The results show that the prepared films were p-type becomes n-type when the doping is increased (Cu/Ni=12.8%). The characteristics of the voltage-current in the dark and lighting state showed that the compound films are sensitive to light, where it‘s notice a decrease with a disparit in the current values in the dark state and an increase in the sensitivity of the samples after lighting in the forward and reverse bias, it was noted that the best efficiency of heterojunction is with a value of (2.8571429%) when depositing the type (p) film of the NiO:Cu sample on the Si (n) substrate at doping (Cu/Ni=10%) . It‘s noticed that there is a variation in the values (I_{sc}, V_{oc}, I_{max}, V_{max}, FF) when depositing isotype (p / p), (n / n) and un isotype (n / p), (p / n).

Contents

List of Symbols

Symbol	Physical meaning
A	Absorptance
a_o	Lattice Constants
A_c	Cross Sectional Area
A^*	Richardson Constant
α	Absorption Coefficient
B	Magnetic Field
b	Width of electrodes.
C_p	Specific Heat Capacity
d	The Inter Planar Distance
D	Average Crystallite Size
Δ	Dislocation Density
E_e	Electrical Field
E_g	Energy Gap
E_H	Hall Electric Field
E_p	Photon Energy
Δf	Band width
E_F	Fermi level energy
E_c	Conduction Band energy
E_V	Valence Band energy
h	Plank Constant
I-V	Current-Voltage
I_A	Absorbed Light Intensity

Symbol	Physical meaning
I_a	Sample current measured at ambient environment
I_o	Incident Intensity of Light
I_{sc}	Short Circuit Current
I_{ph}	Photocurrent
I_R	Reverse Voltage
I_s	Saturation Current
I_d	Dark Current
I_n	Noise Current
I_T	Intensity of the Transmitting Rays
$\vec{q}$	Wave Vector Photon Transferee
I_L	Light Current
k_o	Extinction Coefficient
$\overrightarrow{k}$	Wave Vector
k_B	Boltzmann's Constant
L	Distance between two electrodes
λ	Wavelength
M	Molar Concentration
n	Refractive Index
n^*	Complex Refractive Index
n_e	Carrier Concentration
N_D	Donors Concentration
N_A	Acceptors Concentration
P	Holes Concentration
P_{in}	Incident Power
q	Charge of Electron
R	Reflectance
R_H	Hall Coefficient
R_λ	Spectral Responsivity
R_e	Device Resistance

Symbol	Physical meaning
R_a	Resistance of the film sensor in Air
R_g	Resistance of the film sensor in Gas
S	Sensitivity
ε'	Micro Strain
ε_p, ε_n	Dielectric constants of p-type and n- type,
ε_i, ε_r	Imaginary and Real Part of Dielectric Constant
ε_p, ε_n	permittivity of two semiconductor materials
ε_s	permittivity of semiconductor
T	Transmittance
T_o	Absolute temperature
t	Film Thickness
T_s	Substrate Temperature
V	Applied voltage
V_{bi}	Built-in Potential
V_H	Hall Voltage
V_R	Reverse Voltage
υ	Frequency
V_{oc}	Open Circuit Voltage
ρ	Resistivity
ρ_o	Material Density
μ	Mobility
μ_p	Hole Mobility
μ_n	Electron Mobility
σ	Electrical Conductivity
σ_o	Minimum Electrical Conductivity
$\sigma_{D.C}$	D.C. Conductivity
σ_n	Excess Electron Conductivity
σ_p	Excess Hole Conductivity
τ	Carriers Lifetime
Θ	Bragg Diffraction Angle

Symbol	Physical meaning
T_{vap}	Evaporation temperature
F.F	Filling Factor
X	Width the Light Fringes
Y	Width the Dark Fringes
hkl	Miller Indices
H	Efficiency of Heterojuction

List of Abbreviations

Symbol	Physical meaning
AFM	Atomic Force Microscope
β (FWHM)	Full Width at Half Maximum
AACVD	Aerosol Assistant Chemical Vaper Deposition
C.B	Conduction Band
PCD	Photochemical Deposition
V.B	Valence Band
SGD	Deposition using Sol-Gel
CSP	Chemical Spray Pyrolysis
ECD	Electrochemical Deposition
CCP	Cubic Close Packed Structure
CBD	Chemical Bath Deposition
DSC	Differential Scanning Calorimetry
EDX	Energy-dispersive X-ray spectroscopy
SEM	Scanning Electron Microscope
FCC	Faced Centered Cubic
HCP	Hexagonal Close Packed Structure
ICDD	International Center of Diffraction Data

Symbol	Physical meaning
IR	Infrared
LED	Light Emitting Diode
PL	Photo Luminescence spectroscopy
R.M.S.	Root Mean Square
SPT	Spray Pyrolysis Technique
VIS	Visible Spectrum
UV	Ultra Violet Spectrum
XRD	X-Ray Diffraction
(NsM)	Nanostructured material

List of Figures

List of Tables

CHAPTER

ONE

INTRODUCTION AND LITERATUER SURVEY

1.1 Introduction

One of the significant branches of solid state physics that crystallizes into a branch of itself is Thin Films. The division is concerned with micro-devices, all of which have a very small thickness of less than 1μm[1]. Since the second half of the seventeenth century, the properties of the material in the form of thin films had attracted the attention of physicists, for that much theoretical research was carried out in this field, and then at the beginning of the nineteenth century, when the semiconductor entered into practice, the study of the practical side grew [2]. Because of the thickness of these films, depending on the type of the application and analysis, they are deposited on substrates made of various materials such as glass, quartz, silicon, aluminum, etc. [3]. It is worth mentioning that Chemical Vapor Deposition (CVD) as one of the main methods of synthesizing films, coatings, powders, composites, nanotubes, etc., CVD techniques have been developed for a wide range of applications [4,5]. CVD includes homogeneous and heterogeneous chemical reactions of gaseous reactants, and can provide structural control of extremely pure materials at atomic or nanometer scales. Challenges in the selection and delivery of chemical precursors, especially for multicomponent products, are often significant [6]. The absence of adequate volatile precursors and the difficulty in regulating the stoichiometry of the deposits are the key obstacles to further CVD technique applications [7]. The Aerosol-Assisted Chemical Vaper Deposition (AACVD) method uses aerosol droplets to transport the precursors as a variant of the conventional CVD technique. Chemical precursors need not necessarily be volatile, but merely soluble in any solvent from which the aerosol can be produced, with the help of inert or reactive carrier gases in AACVD based processes. If the precursors for traditional

CVD prove too in volatile or thermally unstable for the synthesis of the particular mate, it provides a useful way to manufacture films, coatings and other CVD products [8]. Under ambient pressure or low pressure, the AACVD process can be conducted. AACVD has also been conducted in open air for deposition of oxide or sulfide materials without a reaction chamber [9, 10].

1.2 Nanostructured Materials

Nano structured thin films is class of materials, which display improved mechanical, electrical, magnetic and optical properties obtained by the size effect. All exotic properties, such as hardness and durability, are most appropriate for manufacturing industry applications. Thin films with a super hardness of 40 to 105 GPa have recently been frequently published [11]. Toughness is the capacity of a material during deformation to fracture to absorb energy. The capacity of a material to resist the growth of a preexisting crack is fracture toughness Nanostructures have a volume between structures that are molecular and microscopic (dimensions in micrometers) [12].

1.3 Various Forms of Nanostructures

In nanotechnology, various classifications of nanostructures exist. Typically, nanostructures are characterized by their geometric properties. In general, nanostructures consist of Nano cages, Nano belts, Nano crystallites, Nano needles, Nano flowers, Nano fabrics, nanofibers, nanocomposites, Nano foams, Nano meshes, Nano pin films, Nano pillars, nanoparticles, Nano rods, nanoclusters, Nano powders, Nano shells, Nano wires, Nano tubes, quantum dots, and sculptured thin film [12].

The most common mode of their classification is the classification of nanostructures according to their dimensions. Form (dimensionality) of their microstructural constituents (boundary regions and crystallites) The three groups of NsM can be divided into four families, based on the chemical composition of the crystallites [13] as show in figure (1.1)

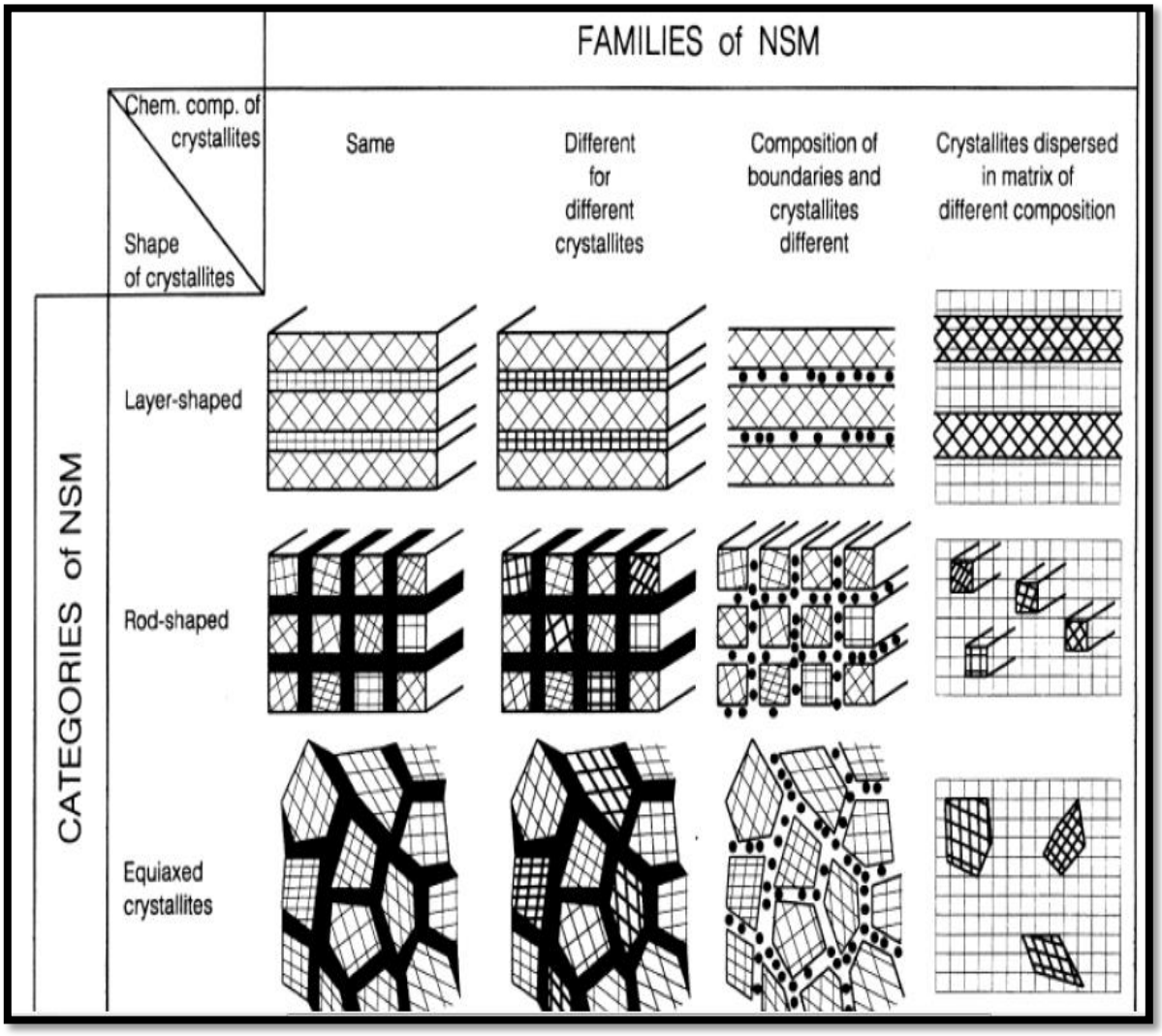

Figure (1.1): Nanostructured material (NsM) classification schemes according to their chemical composition and the dimensionality (shape) of the NsM-forming crystallites (structural elements [13].

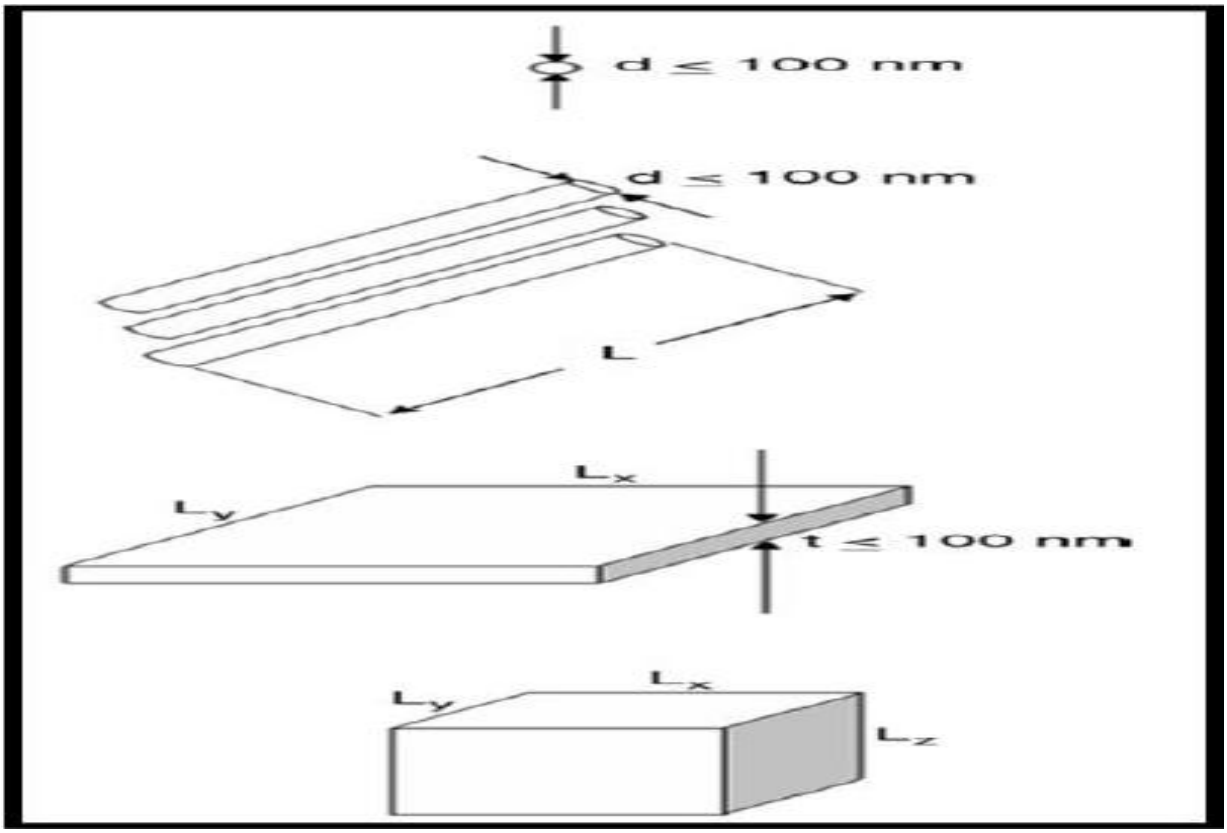

Figure (1.2): Nanostructure classification according to 0-D, 1-D, 2-D, and 3-D [13].

In the Nano metric size range, the dimensions of 0D nanostructures are (such as nanoparticles or well-separated Nano powders). Nanostructures of 1D have a dimension that is outside the range of Nano metric size as shown in figure (1.2). There is a rod shape and type of nanotubes, Nano rods, nanowires and Nano needles in these 1D nanostructures. Outside the Nano metric size spectrum, 2D nanostructures have two dimensions. These 2D nanostructures therefore imply plane-like structures and are made up of thin films, monolayers, and Nano coatings. There are three dimensions of the 3D nanostructures on the broad side of the Nano metric size spectrum. Many different types of these bulk 3D nanostructures shape themselves, which typically include nanocrystal line units that display the nanoscale's affected

properties due to the size effect [14]. Different distributions of nanoparticles or Nano crystallites, nanowire groups and nanowires may be used in a 3D nanostructure The nanostructures of 0D, 1D, 2D and 3D can be amorphous or nanocrystal line. You may also categorize the 2D and 3D nanostructures in more detail. A plane with a depth below 100 nm is the simplest form of a 2D nanostructure and other dimensions are bigger than Nano metric dimensions. This plan will reveal internal nanostructure dimensions, for example, nanocrystals (or Nano grains) with a nanoscale dimension, despite their external dimensions some new size-related properties different from those of a microcrystalline layer can be seen by this 2D Nano-crystalline layer[13]. The inside grains (crystallites) can be outside the nanoscale and yet still be treated as a nanostructured matter if the external thickness is left in the Nano metric size range in the Nano metric size range, the insider structural dimensions (for crystallites or grains) and outsider surface dimensions (exclusively their depth) can therefore be divided between the 2D nanostructures as inner nanostructured and non-internal nanostructured layers [15]. 3-D nanostructure measurements would not be found in any Nano metric size spectrum, but certain size-influenced properties are still seen. For example, with two or more phases with different properties, 3D nanocomposites can be acquired and their total synergistic properties cannot be acquired by each phase alone. The nanocomposite matrix has dimensions greater than the Nano metric scale and the amplifying material is normally within the range of Nano metric size. These 3D nanostructures, for example, nanoparticles, Nano flakes, nanotubes or Nano rods, can be classified by the form of amplifying phases. The 3D nanostructure in its inner structure can be microcrystalline or nanocrystal line.

1.4 Semiconductors

There are several semiconductor concepts. The term semiconductor has traditionally been used to describe a broad group of materials (different elements and chemical compounds) whose conductivity falls within a wide gap between conductive materials and insulating materials. In general solid materials can be defined as follows in terms of their electrical conductivity [16, 17, 18]: -

1. Conductivity (10^{3} -10^{8}) (Ω .cm) $^{-1}$ conductors such as copper and silver.
2. Conductivity (10^{-8} -10^{3}) (Ω .cm) $^{-1}$ semiconductors such as germanium (Ge) and silicon (Si).
3. Conductivity (10^{-18}-10^{-8}) (Ω .cm) $^{-1}$ insulated materials such as diamonds and quartz.

The basic characteristics of semiconductors can be determined by the following points [19. 20]: -

1. Self-conductivity (Intrinsic Conductivity) is demonstrated by a very high purity semiconductor and does not occur at low temperatures.
2. As well as having negative electrical conductivity, semiconductors have positive electrical conductivity.
3. Semiconductors have a negative thermal coefficient resistance, which is the adoption of their electrical temperature relation as opposed to what it is for metals.
4. When they contain impurities or certain defects, semiconductors are very sensitive.
5. During the photoelectric phenomenon or during a change in resistance, semiconductors are sensitive to light.
6. When a magnetic field is put on it, their relation is impaired.

In electronic applications, semiconductor sensitivity to these factors has rendered it a very significant material.

1.5 Classification of semiconductors

It is possible to classify semiconductors according to their crystalline structure to [20, 21]: -

1.5.1 Crystalline Semiconductors

a- Single Crystalline Semiconductors

These materials are distinguished by the fact that their atoms are geometrically arranged, replicated regularly, in equal dimensions and in three directions, in a systematic manner. It is called the long-range order, which achieves the atomic system's lowest free internal energy as in figure (1.3a).

b- Polycrystalline

It is a group of crystals, called grains, with a relatively large number of atoms. Grains are isolated from each other by boundaries. Each granule has a long-range structure, while crystalline granules have a (Short-range Order) as a whole and as shown in figure (1.3b). In determining their physical properties, most semiconductors are polycrystalline materials in which the grain boundary is very important, since these boundaries reflect crystalline defects that cause the electrostatic potential barrier to form on both sides of the granule, which impedes the flow of the majority of charge carriers [22].

1.5.2 Amorphous Semiconductors

These are atoms with a short-range arrangement. Their atoms are arranged randomly, so they cannot be counted as a repetition of the cell unit as shown in Figure (1.3c). The random state is thermodynamically unstable

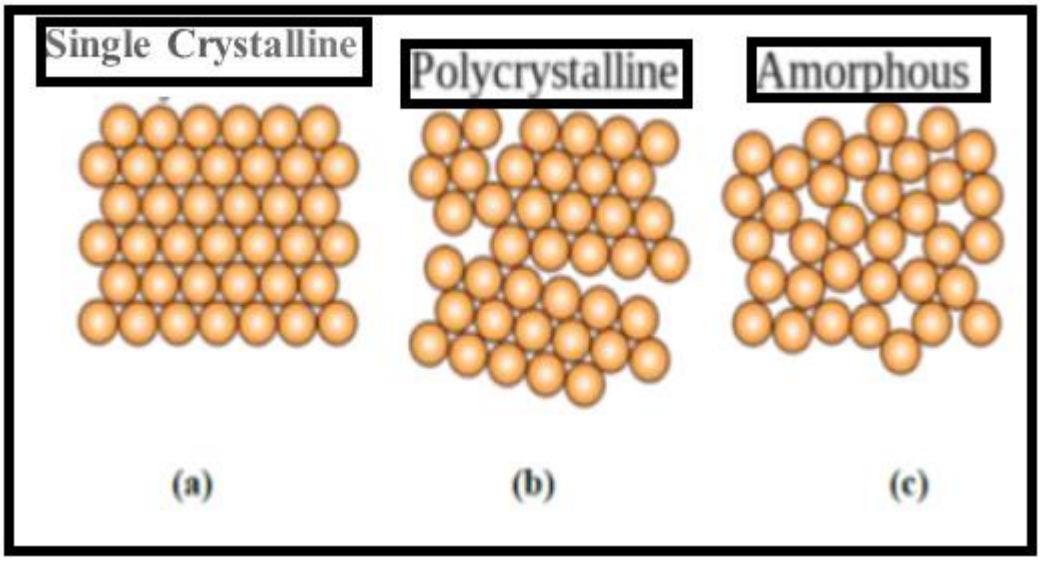

Figure (1.3): Order atoms in materials [22].

(a) Single Crystalline (b) Polycrystalline (c) Amorphous

From the study of X-ray diffraction patterns, crystalline semiconductors can be distinguished from amorphous, as the diffraction pattern is in the form of wide, low-light, concentric rings of random materials, in the form of sharp bright spots in monochromatic materials and in the form of high-Polycrystalline materials as in figure (1.4) [23].

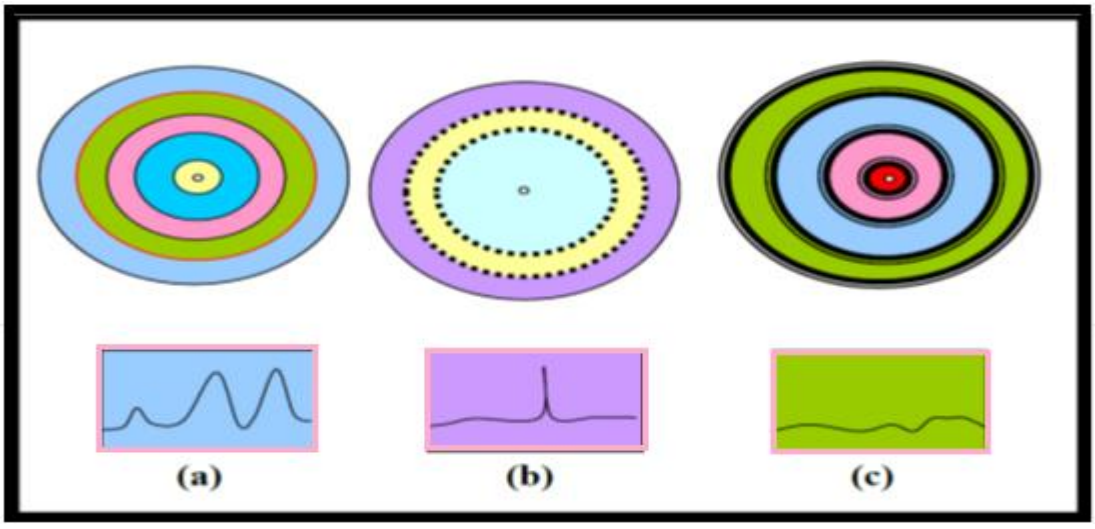

Figure (1.4): X-ray diffraction of crystalline, polycrystalline and amorphous materials [23]. (a) Polycrystalline (b) Single crystalline (c) Amorphous

Semiconductors can be classified into the following [16]: -

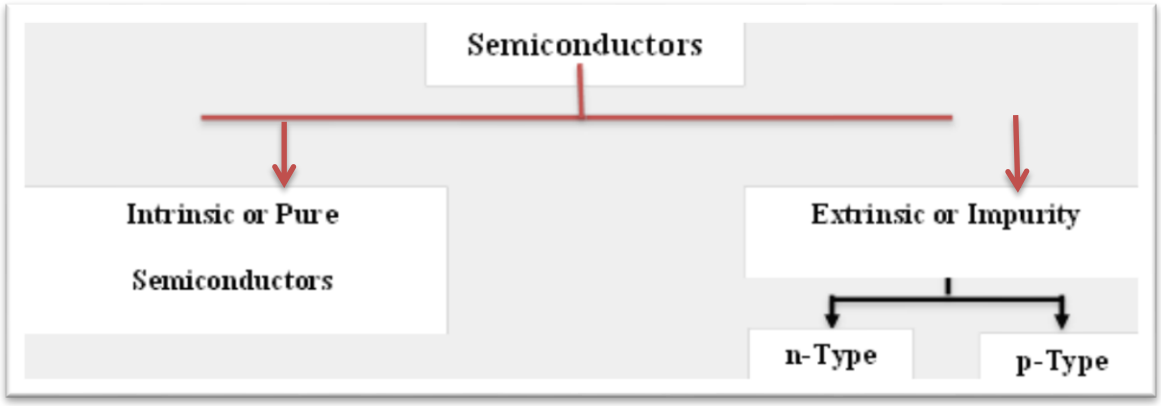

1.6 Intrinsic Semiconductors

Intrinsic semiconductors are referred to as pure and impurity-free semiconductors such as pure Si, Ge, and their valence band is entirely packed with electrons at absolute zero, while the conduction band is totally empty. A certain amount of electrons in the valence band will be thermally excited and moved to the conduction band when the temperature of the pure semiconductor is increased, leaving behind a number of holes, the electrons arriving at the conduction band can fill this band in a molecule and when an electrical field is shed on them will be ready for electrical conductivity The holes created in the valence band are filled directly by neighboring electrons moving in a direction opposite the direction of the field and the hole is transferred to the field. The concentration of electrons is known to be equal to the number of holes in a semiconductor. (i.e) [16, 24]:

$n = p = ni$ …….. (1-1)

As:

ni: intrinsic currier concentration.

n : concentration of electrons.

p: concentration of holes.

The Fermi level is in the middle of the forbidden energy gap in pure semiconductors, as in the following equation [25]:

$$E_F=(E_C+E_V)/2 \quad \text{…….. (1-2)}$$

Whereas:-

E_F: Fermi energy level.

E_C: conduction band energy.

E_V: valence band energy.

1.7 Extrinsic Semiconductors

The deliberate addition of impurities by grafting or doping to the pure semiconductor is called a procedure that is suitable for most applications. This is why the semiconductor impurity is categorized into two groups according to the type of impurities applied to it, the first is the type of semiconductor (n-type) which is called the negative type because electrons are the majority of its charge carriers (Majority Carries) and the gaps are the minority carriers and the second is the positive type semiconductor (p-type) because the majority of the positive type (p-type) are electrons. As for the Fermi stage in the grafted semiconductor, in the positive-conducting semiconductor, the negative-conductor semiconductor is found creeping near to the conduction band and the valence band [24, 26]. Doping controls the characteristics of the semiconductor as well as the heat treatment, but the doping effect is more suitable because the change in temperature is undesirable, so doping is preferable in the regulation of semiconductor conductivity [27] .

1.8 Literature Survey

As described by many researchers, nanostructured nickel oxide thin films have been prepared using several deposition methods.

SA. Mahmoud et al. (2011) [28],Showed The effect of varying substrate temperatures on the structural and optical dispersion properties of NiO films was investigated , Using SPT, nickel acetate of a 0.05 M solution in ethanol was deposited. This was achieved on an ultrasonically cleaned glass substratum at a substrate temperature of (225 - 350 °C). The diameter of the nozzle was 0.7 mm, the deposition time was 15 s and the spraying time was 3 min. The spraying nozzle height was held at 35 cm. Furthermore to achieve a homogeneous film, the rate of spraying was kept at15 cm^3/min. For temperature measurements, a thermocouple was used. At a low substratum temperature of 225 °C, the XRD model provided amorphous films. A single-phase cubic structure was formed with preferential growth along the (1 1 1) plane at above 275 °C. The refractive index relies on the temperature of the substrate and thin film thickness.

S. C. Chen et al.(2011) [29], Deposited NiO:Cu composite films with varying copper content ranging from 0 to 18.17 % . The p-type conductivity is shown by the hall measurement for all copper-saturated NiO films. Furthermore, the NiO film transmission decreases continuously from 96% to 43% with the copper content increasing from 0% to 18.17%. XRD patterns of copper-doped NiO films indicate that the NiO films with copper content greater than 6.97% only occur and crystallize NiO peaks. Copper + ions that contribute to p-type conduction and weaken the crystallinity of NiO-Cu compound films with a

higher proportion of copper are replaced by a large number of capillary sites of Ni2 + ions in NiO crystals.

A.M. Reddy et al. (2011) [30], Deposited NiO films by using the DC reactive magnetron sputtering process. They showed in scanning electron microscopy micrographs of the NiO films as a function of thickness. The films produced at a thickness of 150 nm have irregular grain shapes. Uniform grain size distribution and large grain size can however, be seen in the thickness of 250 nm films. In addition, 550 nm of smaller grain and smooth structure could be obtained in the film thickness.

S. Sriram, and A. Thayumanavan (2013)[31], Showed NiO films were prepared using precursor solutions using spray pyrolysis process. (XRD studies show that films prepared from ancient solution (21 nm) have samll grain size as indicated in SEM studies compared to film prepared from fresh solution (60.3 nm). In optical studies, higher band gap could be obtained in films prepared without aging precursor (3.6 eV).

R.A. Ismail et al. (2013)[32], Have reported NiO thin films in the presence of nickel chloride salt solution using a spray pyrolysis process. The films were deposited at different temperatures on substrates such as glass and silicon. As shown by XRD research, the deposited films at 280^{o}C have an amorphous composition. And at higher temperatures, the films display the cubic structure. There is no marked difference between the results obtained from the XRD in crystallite size.

K. H. Kim et al. (2014) [33], Showed Copper doped nickel oxide (NiO:Cu) thin films using the technique of electrodeposition, nanocrystal line grains with spherical shaped particles shown the surface morphology of both the un doped and doped thin films. The optical tests showed a decrease in band gap energy for the un doped , 2 % and 3 % respectively, from 3.34 eV to 3.32 eV and finally to 3.20 eV. The refractive index peaked between 2.60 and 2.65, with major differences in the visible and NIR range in the measured extinction coefficient values of doped thin films.

V. Gowthami et al. (2014)[34], Deposited a(0.3M) aqueous nickel chloride solution on a glass slide using SPT. The goal was to test the parameters of the oscillator (optical dispersions) of the thin film NiO. The temperatures of the substrates ranged from 350 °C, 400 °C and 450 °C. The focus was on optoelectronic devices that make use of thin films and interference devices for semiconductors. Optical dispersion has been taken into account because it reveals knowledge that is useful in determining microscopic properties. Substratum nozzle distance of 7 cm, volume of 0.5 ml per min and optimized airflow of 1.2 kg/cm2 have been retained. For the NiO films, optical transmittance spectra were recorded from 300 nm to 1100 nm wavelengths. The thickness of the film increased as the transmission decreased. Transmittance variation was from 30 % to 90 % as the thickness of the film decreased. There was a direct band difference of 3.54 eV, 3.43 eV and 3.37 eV.

Y. Zhao et al. (2014)[35], Showed the effect of partial oxygen pressure on the properties of NiO films was investigated, the XRD patterns show that when

the partial oxygen pressure drops from 80% to 0%, the strength of the (200) peak decreases.

M. Jlassi et al. (2014)[36], NiO film was prepared at different annealing temperatures using the sol gel method. The XRD study shows that there were polycrystalline structures in all annealed films. Meanwhile a single large unstructured XRD line is shown in as-deposited films. It was possible to find a prevailing peak corresponding to (200). As the annealing temperature decreased from 600 to 300 ^{o}C, the intensity of this peak decreased. On the other hand, as the annealing temperature rises, it is clear that all the films display high clarity in the visible and near infrared sections. This results in films with strong transmission for that purpose.

M.M. Gomaa et al. **(2016)**[37], Found that the films were gray in colour and strongly adherent to the substrate. They observe that the thickness and grain size were varied from 0.028-0.23 μm, and 14-17 nm, respectively as the volume of sprayed solution was increased from 30 to 75 ml. In another case, the band gap changes from 3.58 to 3.4 eV with increase in the film thickness. They explain that may be attributed to the changes in homogeneity and crystallinity of the films.

M. Vigneshkumar et al. (2016)[38], Focus on the antireflection coating for NiO thin films in solar cells. NiO films were deposited on glass substrate using a 0.5 M aqueous solution from nickel chloride of a temperature at 350 °C, A reflectance of 7% was obtained of 550 nm. This low value gives an indication that it can be used as an antireflection coating material in solar cells. The refractive index was recorded at 550 nm to be 1.871. Calculated

optical direct band gap energy from the prepared NiO thin film was found to be 3.25 eV.

AA. Yadav, and U. Chavan. (2016)[39], Studied effect of substrate temperature on various physical and electrochemical properties of NiO thin films. This was done by using nickel chloride precursor spray deposition of NiO thin films. The thin films were deposited at 425 °C, 450 °C, 475 °C and 500 °C temperatures. Cubic polycrystalline nickel oxide confirmed the structural analysis. The surface morphology showed a porous surface with randomly formed heaps that were inhomogeneous. It was found that optical band gap energy was in the range of 3.04-3.28 eV. The electrical resistivity confirms NiO semiconducting behavior with energies of activation at room temperature of 0.30 to 0.38 eV.

-W. Chen et al. (2018)[40], Prepared high quality hole transport layers are at room temperature without further processing by spin-coating copper doped nickel oxide (Cu:NiO) nanoparticle. An increase in conductivity in Cu:NiO films relative to NiO is observed in line with theoretical calculations predicting that Cu doping results in acceptor energy levels similar to the valence band limit compared to gap states of nickel vacancies in undoped NiO. In both Cu+ and Cu2+ states, Cu in Cu: NiO can be identified, and the replacement of Ni2+ with Cu+ leads to both increased carrier concentration and mobility of the carrier. In addition, the films exhibit increased work function which allows enhanced charge transfer and extraction in accordance with increased conductivity. These factors contribute to an improvement in all

parameters of photovoltaic output and, subsequently, to an improvement in the efficiency of the inverted solar cells.

R. O. Ijeh et al. (2019)[41], prepared nickel oxide (NiO) thin films with p-type Cu doped (5 a%) using a sol–gel solution process and investigated their structural, optical, and electrical characteristics by X-ray diffraction (XRD), optical transmittance and current–voltage (I–V) characteristics. The crystallinity of the NiO films improved with the addition of Cu dopants, and the grain size increased from 38 nm (non-doped) to 50 nm (Cu-doped). The transmission of the Cu-doped NiO film decreased slightly in the visible wavelength region, and the absorption edge of the film red-shifted with the addition of the Cu dopant. Therefore, the width of the optical band gap of the Cu-doped NiO film decreased as compared to that of the nondoped NiO film.

S. Benramache et al.(2020)[42], The nickel chloride hexahydrate (0.8M) and copper (II) chloride dehydrate (Cu/Ni = 0, 2.15, 4.3, 8.6 and 12.9 %) were used to prepare the Cu doped NiO thin films as the thin films were formed by a spin coating process in 2020. At a crystallization temperature of 600 C, the Cu doped NiO thin films were heated at 2 h. The thin films obtained by the spin-coater process have a film thickness of 400 nm. A polycrystalline with a cubic structure (200) peak was observed in the prepared Cu doped NiO thin films. The optical property demonstrates that the thin films prepared have a transmittance of about 70%. The minimum bandgap energy of Cu doped NiO thin films is 3.85 eV at 12.9 %, the thin film deposited at 8.6 %. The maximum value of urbach energy is 425 meV. The thin films of Cu doped NiO have a high electrical conductivity of 8.6 %, Because of the existing

phase and higher electrical conductivity, the prepared Cu doped NiO thin film was sufficient for gas sensing applications.

1.9 Aim of the Work

I. Analysis of structural, optical and electrical properties of prepared (NiO:Cu) thin films by Aerosol-Assisted Chemical Vapor Deposition (AACVD) on glass and silicon substrates

II. Analysis of the effect of Cu doping on the structural, optical and electrical properties of films and on Si(p)/(NiO: Cu and Si(n)/(NiO: Cu) hetro-junctions by Aerosol-Assisted Chemical Vapor Deposition (AACVD) form, film thickness, grain size, surface roughness, optical energy gap.

III. Fabrication a device heterojunction Isotype (p-p) type,(n-n)type and heterojunction un isotype (p-n)type,(n-p)type.

IV. Investigating the optimization conditions for prepared (NiO:Cu) solar cell manufacturing.

CHAPTER

Two

Theoretical Part

2.1 Introduction

This chapter includes a general description of the theoretical part containing the general information about (NiO: Cu) and heterojunctions, as well included characteristics structural, optical, and electrical properties of (NiO: Cu) thin films deposited on glass and Si wafer substrate.

2.2 NiO properties

Thin films with a NaCl-type structure of nickel oxide (NiO) have been of attractive interest because they have excellent chemical stability, preferring optical, electrical and magnetic properties [43]. There is several on deposition of NiO thin films were by various techniques such as Sol-Gel methods [44], chemical vapor deposition [45], and spray pyrolysis techniques [46]. Numerous reference results and previous studies have shown that reactive sputtering with a sputtering pressure in the range of (0.1-1 Pa) and in a pure oxygen atmosphere using a heated substrate can achieve superior electrical and optical properties of NiO films. NiO is with a wide band gap of 3.6 eV [47]. NiO is a promising material for variety applications, such as solar thermal absorber[48]. However it is only difficult to find a sufficient stable semiconductor device with an adequate band gap for visible absorption, the need for reactions. Thus in order to minimize the energy gap, the substrate temperature must be increased and the Cu must be increased in order to obtain an adequate energy gap.

Due to their uses in semiconductors, mirrors, sand coating lenses and many other applications, thin films has become increasingly appealing in physics and engineering. There are applications in industry in areas such as optical electronics, communications, coatings, electricity generation, and energy conservation.

In microelectronics and semiconductor applications, thin films are still very commonly used. The thin film industry is rising as rapidly as proper applications can be implemented by scientists and engineers [49].

Table (2.1): Properties of Nickel Oxide

Formula	NiO
Crystal structure	Rock salt (Octahedral)
Electron configuration	$3d^8$
Cation	Ni++
Optical basicity	0.915
Oxide ion polarizability	High
Molar mass	74.6928 g/mol
Density	6.67 g/cm3
Melting point	1957^oC
ΔHf for metal oxide formation per oxygen atom @ 298 K	245.2 kJ/mol
Bandgap	2.0-4.3 eV
Type of conductivity	P-type
Dielectric constant	10
Coefficient of refraction	2.23
Refraction index (n_D)	2.18

2.3 Heterojunctions

It is known as a basic contact (intimate contact) between two semiconductor materials or a junction resulting from different energy gap semiconductors, constant electrical insulation, electronic winding and working

function [50], but the composition should be similar. There is however a difference in the lattice constants of the two compounds. This is called heterojunction lattice incompatibility and can be categorized into abrupt and graded based on the distances during the transition from the first semiconductor material to the other ending near the interfering surface (the separation surface) in the abrupt heterojunction, the transition takes place within a few atomic distances (≤ 1μm) figure (2.1a), where as in the gradient it takes a few longer diffusions as in figure (2.1b):

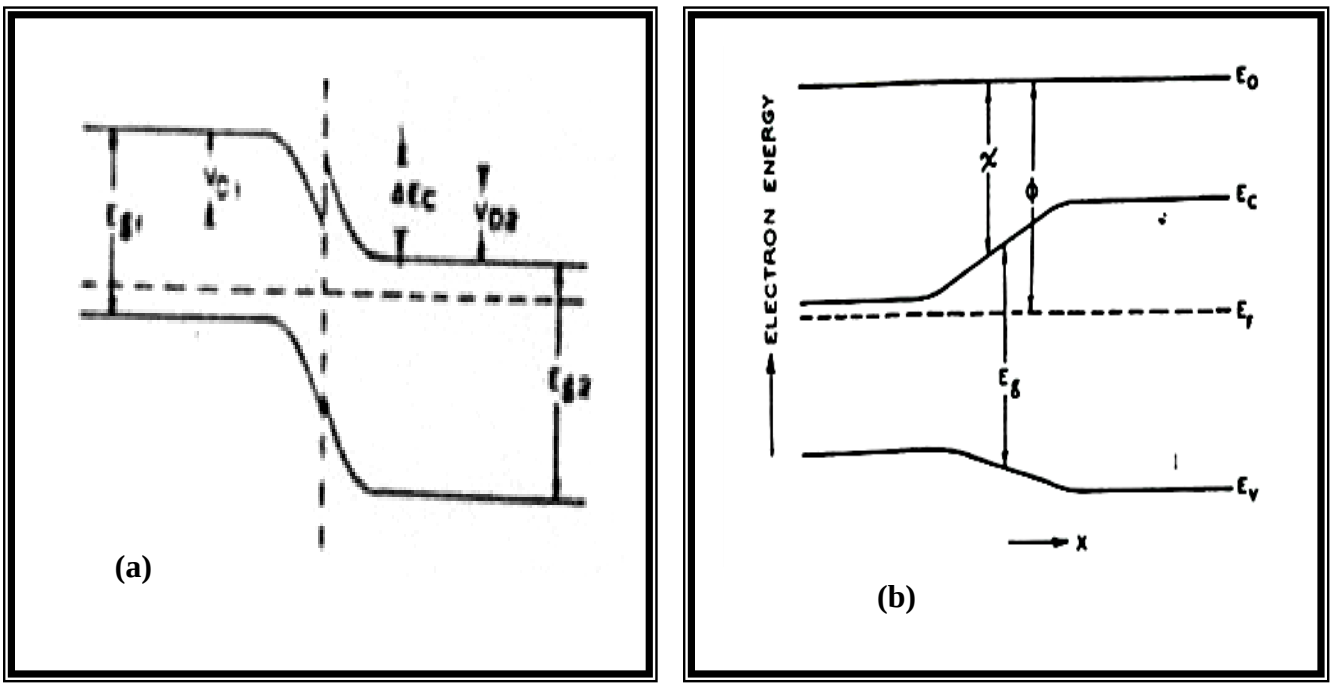

Figure (2.1):a. band energy diagram of heterojunction abrupt (n-p)
b **.**Graded (p-n)[50].

In contrast to the gradual heterojunction [51], which has little clear theoretical formula to explain the transition zone of this heterojunction, there are many theories which illustrate the abrupt heterojunction. If a

semiconductor has the same type of conductivity, the heterojunction can be categorized on the basis of the type of electrical conductivity on either side of the heterojunction, then it is called an isotype such as n-n and p-p, if the conductivity of the two semiconductors is different from the asymmetric heterojunction, it is called an isotype such as n-p and p-n over time, heterogeneous competition with homogeneous [52].

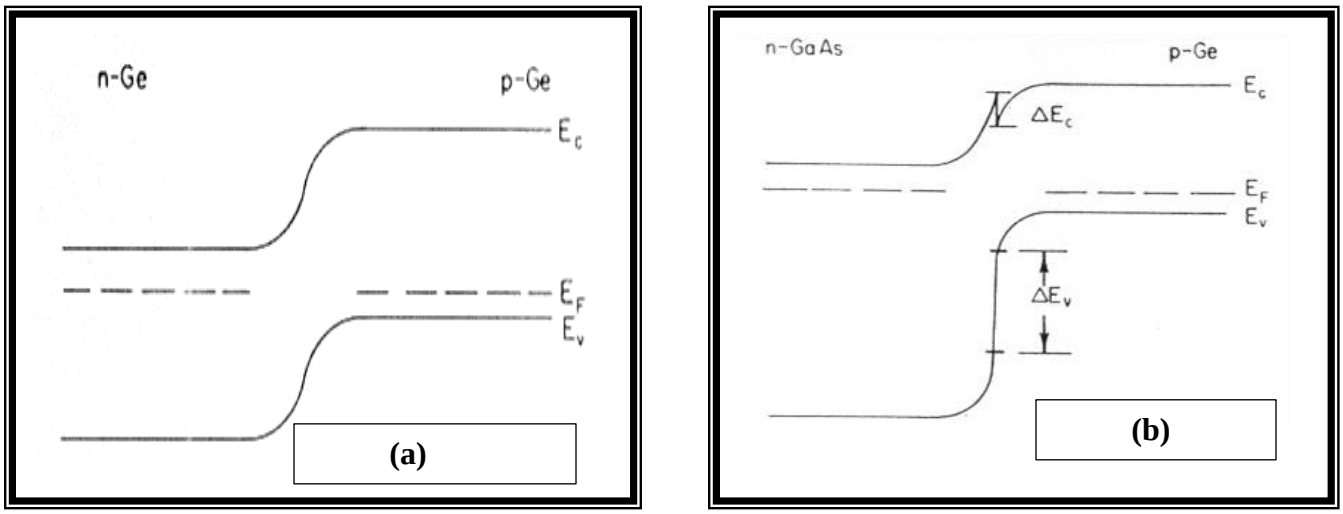

Figure (2.2): a. Scheme band energy of homo junction (n-p)
b. Diagram band energy of heterojunction (n-p)[52].

2.4 The Aerosol-Assisted Chemical vapor deposition (AACVD)

Aerosol-assisted chemical vapor deposition (AACVD) is a technique that includes the atomization into fine droplets of a precursor solution that are dragged through a mobile nozzle by a hot air flow to a heated reaction zone where chemical reactions occur. This work provides a description of the electrical and electronic components for AACVD implementation [53]. Due to the low instrumentation costs needed for its implementation and the numerous applications in the field of sold state research, the aerosol-assisted chemical

vapor deposition (AACVD) technique is becoming increasingly popular [54]. Via installing their own equipment to make depositions with different types of coatings, these two features allow companies and universities to advance in research and application processes. For example, Monárrez et al., using this technique, synthesized magnetite nano-particles in a carrier gas reactor[55,56], But if the idea is to obtain thin films, the precursor solution, as described by a carrier gas and a nozzle, must be nebulized and transported to the substrate. P Lim et al. to deposit TiO_2 on tin oxide glass-coated surfaces [57]; or, as in the study by Jagdeep et al., which deposited nanostructured $CoFe_2O_4$ thin films [58]. The method used in this work follows experimental information close to those used by Pizá-Ruiz et al, where $CuFeO_2$ thin films were deposited on borosilicate glass coated with a thin film of TiO_2 and ZnO [59]. The AACVD method consists essentially of a nebulizer that atomizes the precursor solution which, with the assist of hot air, rises to a given flow through a nozzle and is deposited on a film-generating substrate. The physical characteristics of this film (thickness, uniformity, structure, etc.) depend on the substrate temperature, the carrier gas and the nozzle movement speed [55, 59].

AA CVD method involves atomizing a precursor solution into fine aerosol droplets of sub-micrometer size that are delivered to a heated reaction zone and are undergo to evaporation, decomposition, and to form the desired products by homogeneous and/or heterogeneous chemical reactions. AACVD tackles the availability and distribution concerns of chemical precursors as a variation of traditional CVD processes [60]. A schematic diagram of AACVD is shown in figure (2.3).

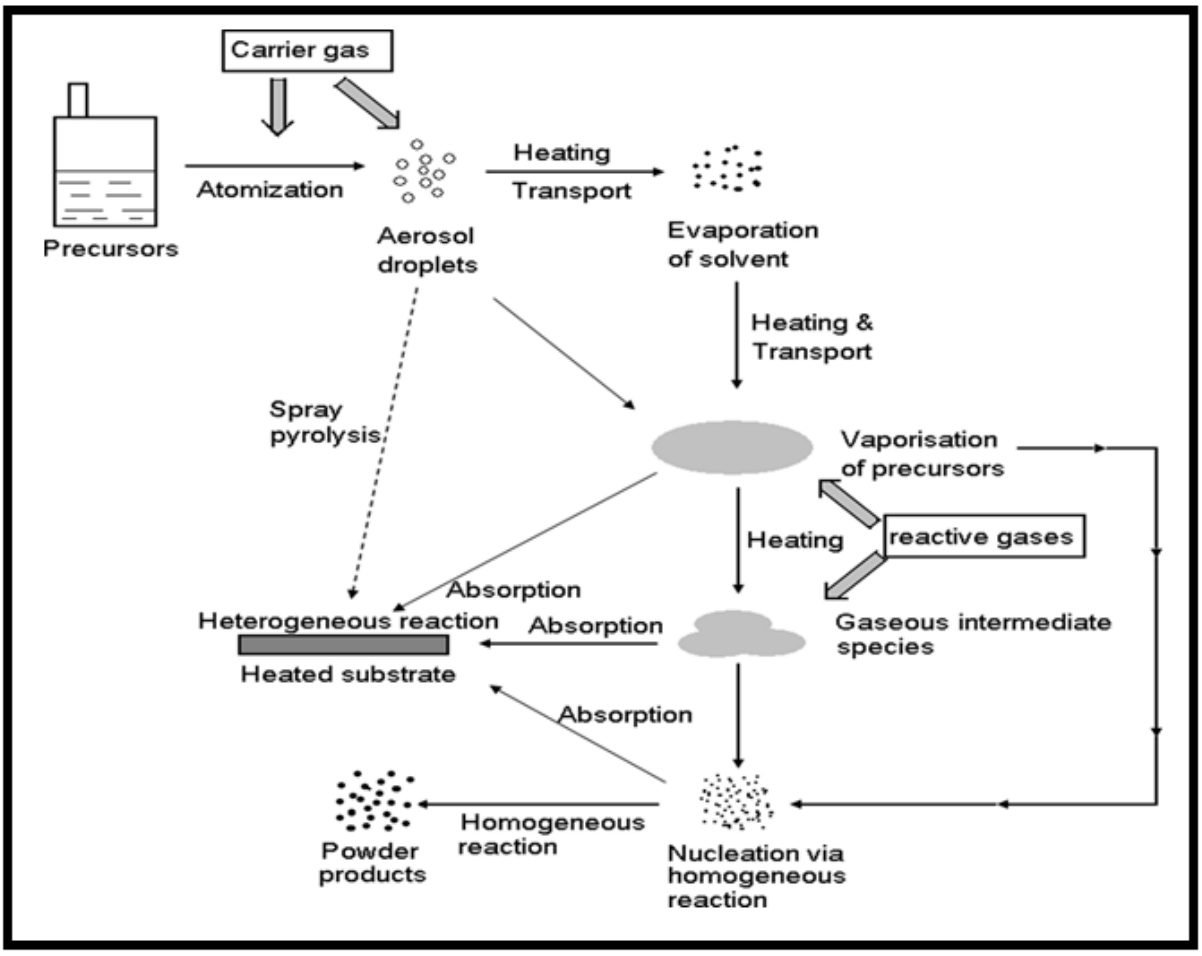

Figure (2.3): Shows the (AACVD)[60].

As the requirement for precursor volatility and thermal stability becomes less stringent, high-quality AACVD system products can be manufactured at a lower cost. Compared to the conventional CVD method, the AACVD method presents some key advantages:[61]

I. Wider range and availability of precursors for low-cost high-quality CVD products, which is a critical problem for mass production.

II. Simplification of the supply and vaporization of precursors by means of a precursor aerosol generation.

III. High deposition rate obtainable from a high mass-transport rate of the precursor and a potential increase in the selection of precursors.

IV. Since AACVD can work under low pressure, ambient pressure or even in an open atmosphere, the reaction environment is more flexible;

V. Simplification of the synthesis, with precise stoichiometric power, of multicomponent materials. AACVD can combine the advantages of both traditional CVD and spray pyrolysis processes as a result of the aerosol transport of precursors and the related CVD deposition mechanism. In most CVD-related fields, it has attracted growing interest and has been widely used to synthesize various CVD products, such as films, coating powders, as well as nanotubes, etc.

2.5 Structural Properties

2.5.1 X-Ray Diffraction

One of the commonly used experimental techniques for determining lattice parameters is X-ray diffraction, the desired orientation of the crystal. The XRD mechanism is simple. The constructive diffractions (or interference) from parallel planes of atoms with inter-planar spacing (d) occur when a monochromatic X-ray beam occurs on a crystal sample if Bragg's law is satisfied. As show figure (2.4)[62].

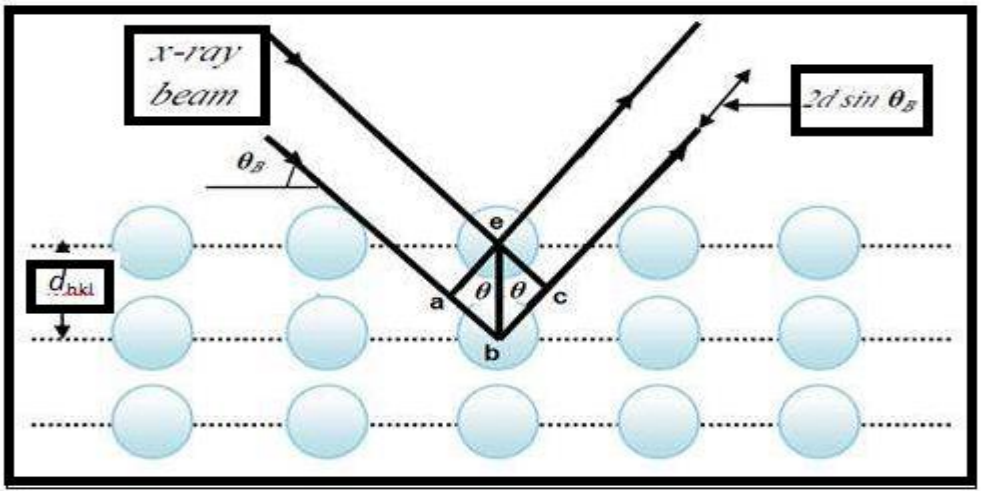

Figure (2.4): Explains crystalline levels and Bragg's law[62].

$$2d \sin\theta = n\,\lambda \quad \cdots\cdots\cdots\cdots\cdots\cdots (2-1)$$

Where:

n: is an integer that indicates the order of the reflection.

θ: is Bragg diffraction angle of the XRD peak (degree).

λ: is the wavelength of the X-ray beam.

By measuring the Bragg angle θ, the inter planar distance (d) can be obtained if the wavelength of the X-ray beam is known.

2.5.1.1 Parameters Calculation

XRD is typically used to measure various parameters that could be used to describe the studies of the films that have been deposited.

A. Full Width at Half Maximum (FWHM)

It was possible to calculate the FWHM (β) of the preferred orientation (peak) as it is equal to the width of the line profile (in degrees) at half of the maximum intensity [63].

B. Average Crystallite Size (D)

In order to evaluate the size-strain parameters (micro strains and crystallite sizes), the average grain size (D), the single line method is one of many line profile analysis methods based on a Voigt function that can be calculated using the Scherer formula [63]:

$$D = \frac{0.94\,\lambda}{\beta \cos\theta} \quad \cdots\cdots\cdots\cdots\cdots\cdots (2-2)$$

β: FWHM (radian)..

C. Micro Strains (ε')

The crystal defects lead to a change in the distance of the interlayer (d) or in other words, the change in the distance between the atomic surfaces means that the crystal has a deformation, which means that (d) is not the same in every point of the crystal points that leads to all parts of the crystal, reflecting the X-rays at an angle different from the other component. Micro strain (ε ') occurs at the growth of the film created by expansion or compression lattice, calculated from the following relationship. [64]:

$$\varepsilon' = \frac{\beta \cos\theta}{4} \quad \cdots\cdots\cdots\cdots\cdots\cdots (2-3)$$

D. Dislocation Density (δ)

It describes the number of dislocation lines density that cut the unit area in the crystal and the crystallite size (D) information that can account for dislocation density (δ) resulting from the following equation called Williamson and Smallmans equation crystallite size. [65]:

$$\delta = \frac{1}{D^2} \quad \cdots\cdots\cdots\cdots\cdots\cdots \qquad (2-4)$$

2.5.2 Scanning Electron Microscope (SEM)

Scanning electron microscope (SEM) with energy dispersive X-ray spectroscopy is the best known and most widely-used of the surface analytical techniques. High resolution images of surface topography, with excellent depth of field, are produced using a highly-focused, scanning (primary) electron beam. The primary electrons enter a surface with energy of (0.5–30kV) and generate many low energy secondary electrons. The intensity of these secondary electrons is largely governed by the surface topography of

the sample [66]. An image of the sample surface can thus be constructed by measuring secondary electron intensity as a function of the position of the scanning primary electron beam. High spatial resolution is possible because the primary electron beam can be focused to a very small spot (<10 nm). High sensitivity to topographic features on the outermost surface (< 5 nm) is achieved when using a primary electron beam with energy of < 1 kV. In addition to low energy secondary electrons, backscattered electrons and X-rays are generated by primary electron bombardment. The intensity of backscattered electrons can be correlated to the atomic number of the element within the sampling volume [67, 68].

2.6 Optical Properties of Semiconductors

An intrinsic effect is related to the optical properties of a semiconductor. The electron-hole pair generation occurs directly or indirectly, depending on the intrinsic position of the top of the valence band (V.B) and the bottom of the conduction band (C.B) in the band structure [69, 70]. The semiconductor absorbs the photon from the incident beam, depending on the energy of the photon. Absorption is associated with the electronic transition in the material starting at the absorption edge between the V.B and the C.B, which corresponds to the minimum energy difference (E_g) between the lowest (C.B) and the limit maximum (V.B). If the energy of the photon (hv) is equal to or greater than the energy gap (E_g), then it will interact with a valence electron, lift the electron into the C.B and create a pair of electrons and holes. The maximum wavelength (λ_c) of the incident photon generating an electron-hole pair is known as [71].

$$\lambda_c(\mu m) = \frac{hc}{E_g} = \frac{1.24}{E_g(eV)} \dots\dots\dots\dots\dots\dots (2-5)$$

Where:

h: is Plank's constant (6.625×10^{-34} J.s).

c :is velocity of light .

E_g :is the optical energy band gap.

The photon flux intensity decreases exponentially according to the Lamberts equation with distance through the semiconductor [72].

$$I_T = I_o \exp(-\alpha t) \dots\dots\dots\dots\dots\dots\dots (2-6)$$

Where:

I_o,I_T : are the incident and the transmitted photon intensity in (W/cm^2) respectively.

t : is the thickness of the film in (cm) .

α: is the absorption coefficient, which is defined as the relative number of photons absorbed per unit distance of semiconductor.

2.6.1 The Fundamental Absorption Edge

The fundamental absorption refers to the transitions of band-to-band or excitation (i.e. the excitation of an electron from the band of valence to the band of conduction), manifested by a sudden increase in absorption that can be used to evaluate the semiconductor's energy gap. You may divide the absorption regions into three regions. [73]:

a) High absorption region

This region is shown in figure (2.5). In part (A), the magnitude of absorption coefficient (α) is larger or equal to (10^4 cm^{-1}). From this region the magnitude of forbidden optical energy gap ($E_g^{opt.}$) can be introduced.

b) Exponential region

This region is shown in Figure (2.5). In part (B) the value of absorption coefficient (α) is equal to (1 cm^{-1}<α< 10^4 cm^{-1}). It refers to the transition between the extended levels from the (V.B.) to the local levels in the (C.B) and from local levels in (V.B) to extend the levels in (C.B).

c) Low absorption region

The absorption coefficient (α) in this region is very small. It is (α< 1 cm^{-1}). The transition happens in this region because of density of state in mobility gap resulted from structural faults, as in figure (2.5), the part (C).

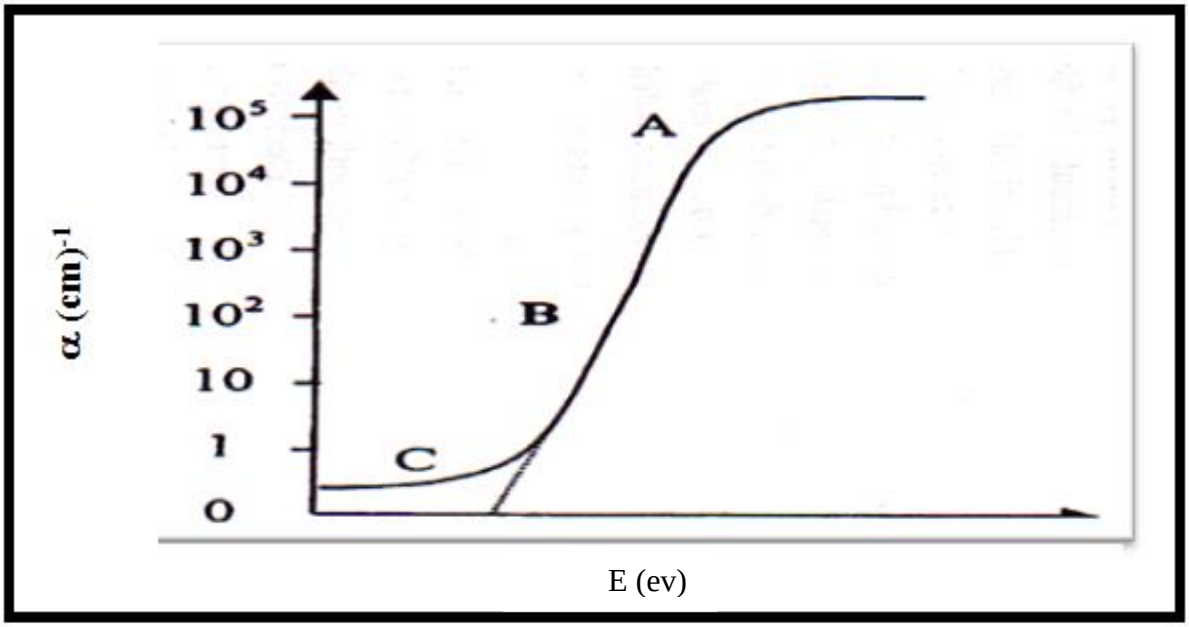

Figure (2.5): The variation of absorption edge with absorption regions [74].

2.6.2 Electronics transition

The radiation absorption, which contributes to the electronic transition between the bands of valence and conduction, is divided into a direct and indirect transition, as shown in the figure (2.6) [75].

In semiconductors, the direct transformation occurs when the bottom of (C.B) is precisely over the top of (V.B).This means that they have the same value of wave vector, i.e.(ΔK=0) in this state the absorption appears when ($h\upsilon=E_g^{opt.}$). For the conservation of energy and momentum rules, this form of transformation is necessary. There are two types of such direct transitions [76].

a) Allowed direct transitions

The transformation takes place at the same wave vector Δ K = 0 from the top points in the (V.B) and the bottom point in the (C.B) for momentum conservation, as shown in Figure (2.6.a).

This transition is described by the following relation [77]:

$$\alpha h\nu = B'\,(h\nu - E_g)^{1/2} \ldots\ldots\ldots\ldots\ldots\ldots (2-7)$$

Where:

υ: is the frequency in (Hz)

B′: Constant depended on type of material (is inversely proportional to amorphousity).

r =1/2 for Allowed direct transitions.

b) Forbidden direct transitions

If a transition occurs between states of the same wave vector, which is not equal to zero, the transition occurs from near the top of the wave vector

(V.B) and from the bottom of the wave vector (C.B), as shown in Figure (2.6.b). The transition is referred to as the forbidden direct transition, where the absorption coefficient for this form of transition is [77]:

$$\alpha h\nu = B' (h\nu - E_g)^{3/2} \dots\dots\dots\dots\dots\dots (2-8)$$

Also indirect transitions have two type of transition**:**

c) Allowed indirect transitions

The bottom of (C.B) is not above the top of (V.B) in the curve for the indirect transition in this case (E-K). Electron transits from (V.B) to (C.B) are not perpendicular if, before and after the transfer, the value of the electron wave vector is not equal to zero ($\Delta K \neq 0$). This form of transformation occurs with the help of a particle called "Phonon" to maintain the law of energy and momentum [78], so a phonon is required to preserve momentum [79]:

$$h\nu = E_g \pm E_p \qquad \dots\dots\dots\dots\dots\dots\dots (2-9)$$

Where:

E_p is the energy of an absorbed or emitted phonon , is (-) when phonon absorption, and (+) when phonon emission.

For the permissible indirect transition, as shown in Figure (2.6.c), the transition takes place from the top of the valence band to the bottom of the conduction band, so that[78]:

$$\alpha h\nu = B' \left(h\nu - E_g\right)^2 \qquad \dots\dots\dots\dots\dots\dots (2-10)$$

(d) Forbidden indirect transitions

Prohibited indirect transitions take place from any point near the top of (V.B) to any point other than the bottom of (C.B), as seen in the figure (2.6.d). The transition absorption coefficient with phonon absorption is given by [80]:

$$\alpha h\nu = B'\left(h\nu - E_g\right)^3 \ldots\ldots\ldots\ldots\ldots\ldots\ldots (2-11)$$

Experimentally, it is possible to distinguish the degree of the absorption coefficient between direct and indirect processes; α takes values from (10^4 to 10^5) cm^{-1} for direct transitions and (10 to 10^3) cm^{-1} for indirect transitions at the edge of absorption.

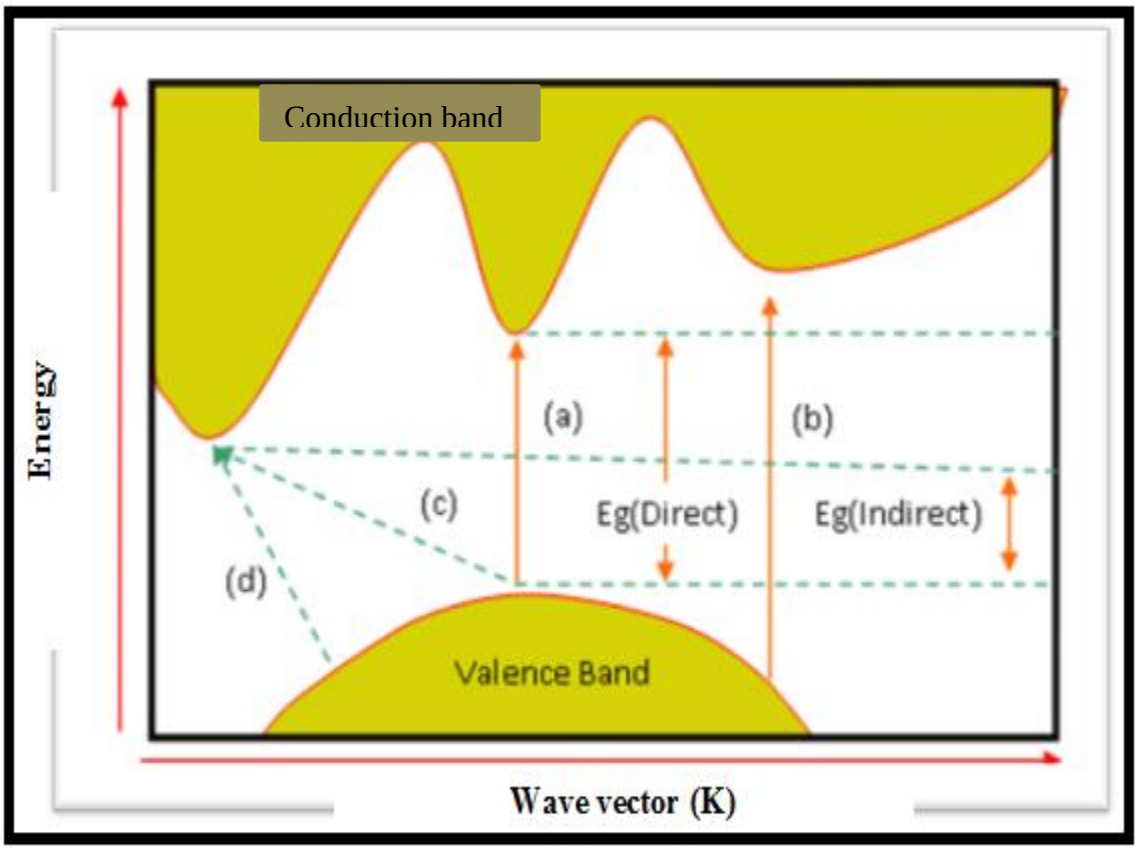

Figure (2.6): The transition types [75].

(a) Allowed direct transition. (c) Allowed indirect transition.

(b) Forbidden direct transition. (d) Forbidden indirect transition.

2.6.3 Absorptance (A)

Absorption can be defined as the ratio of the material's absorbed light intensity (I_A) to the incident light intensity (I_o) [79]:

$$A = \frac{I_A}{I_o} \quad \cdots\cdots\cdots\cdots\cdots\cdots (2-12)$$

2.6.4 Transmittance (T)

The ratio of the intensity of transmitting rays (I_T) through the film to the intensity of the incident rays (I_o) on it is given by transmittance as follows. [80]:

$$T = \frac{I_T}{I_o} \quad \cdots\cdots\cdots\cdots\cdots\cdots (2-13)$$

As a function of wavelength, we can also find a transmittance through the exponential relationship of both absorption and transmittance that [77]:

$$A = \log\left(\frac{1}{T}\right) \quad \cdots\cdots\cdots\cdots\cdots\cdots (2-14)$$

2.6.5 Reflectance (R)

Reflectance can be obtained from absorption and transmission spectrum in accordance to the law of conservation of energy by the relation [81]:

$$R + T + A = 1 \quad \cdots\cdots\cdots\cdots\cdots\cdots (2-15)$$

2.7 Optical Constants

Optical constants are very significant parameters since they define the material's optical behavior, including optical constants.

2.7.1 Absorption Coefficient (α)

The absorption coefficient is defined as a decrease in the ratio of incident ray energy flux relative to the distance unit in the direction of diffusion of the incident wave. The absorption coefficient (α) depends on the photon energy incident (hυ) and the form of semiconductor characteristics (n or p), where electronic transitions of type (n) or (p) and the energy gap are prohibited. According to Beer Lambert low [82]:

$$\alpha = \frac{1}{I}\frac{d[I]}{dt} \quad \cdots\cdots\cdots\cdots\cdots\cdots\cdots\cdots (2-16)$$

Also α can be given by:

$$\alpha = \frac{2.303 \times A}{t} \quad \cdots\cdots\cdots\cdots\cdots\cdots\cdots\cdots (2-17)$$

In semiconductors, a powerful function of the wavelength or photon energy is the absorption coefficient. The energy of photons is given by [82]:

$$E = h\upsilon \quad \cdots\cdots\cdots\cdots\cdots\cdots\cdots\cdots (2-18)$$

2.7.2 Extinction Coefficient (k_o)

The imaginary part of the complex refractive index is represented (n*) [80]:

$$n^* = n - ik_o \quad \cdots\cdots\cdots\cdots\cdots\cdots\cdots\cdots (2-19)$$

Where:

n : the real part from refractive index , equal (c/v).

v : velocity of light in material.

n*: The complex refractive index is defined by the following equation, which depends on the material form, crystal structure (grain size), crystal defects, crystal stress and extinction coefficient (k_o). [83]:

$$k_o = \frac{\alpha\lambda}{4\pi} \quad \cdots\cdots\cdots\cdots\cdots\cdots\cdots\cdots (2-20)$$

2.7.3 Refractive Index (n)

It is the ratio of light velocity in a vacuum to velocity in a medium. This index shows the degree to which electromagnetic waves influence a subject. The refractive index (n) value was determined using an equation based on the coefficient of reflectance and extinction (k_o), as shown in the following equation. [83] :

$$R = \frac{(n-1)^2 + k_o^2}{(n+1)^2 + k_o^2} \quad \cdots\cdots\cdots\cdots\cdots\cdots (2-21)$$

The refractive index can be expressed through the following equation.[83]:

$$n = \left[\left(\frac{1+R}{1-R}\right)^2 - (k_o^2 + 1)\right]^{\frac{1}{2}} + \frac{1+R}{1-R} \quad \cdots\cdots\cdots\cdots\cdots (2-22)$$

2.7.4 Dielectric Constant

A reaction between incident radiation and the material's charges will occur when a light incident occurs on the atoms in the material. This would contribute to the polarization of material charges. [79]:

$$\varepsilon = \varepsilon_r - i\varepsilon_i \quad \cdots\cdots\cdots\cdots\cdots\cdots (2-23)$$

Where:

ε_r : is the real part of the complex dielectric constant,

ε_i : is the imaginary part of it.

The following expressions can be used to measure the dielectric constant in its two parts. [84]:

$$\varepsilon_r = n^2 - k_o^2 \quad \cdots\cdots\cdots\cdots\cdots\cdots (2-24)$$

$$\varepsilon_i = 2\, n\, k_o \quad \cdots\cdots\cdots\cdots\cdots\cdots (2-25)$$

2.8 The Electrical Properties of Semiconductors (Hall Effect)

The electrical properties of semiconductors depend on the existence of pure or doped, crystalline or amorphous semiconductors. The electrical properties of the materials are detected not only by the chemical composition, but also by the arrangement of the atoms in the solid, and the presence of defects can be minimized by several methods, such as the annealing process, when the electron states in the energy gap resulting from the electrical properties of the material. Significant electrical characteristics are transport features such as the Hall effect [85,86].

Hall Effect is one of the rich sources of knowledge about the conduction properties of semiconductors. The main benefit of calculating the Hall effect is to find out the volume unit concentration charge for carriers, the measurement will directly give the type of carrier, even quantify the concentration of carriers mobility. In order to observe this effect, electric and magnetic fields are necessary [87]. The ratio of the generated voltage is divided by the current and the product of the magnetic field (I× B) by the thickness factor, called the Hall coefficient (R_H), which is known as the characteristic of the material from which the conductor is produced, since its value depends on the form, number and characteristics of the current-constituting charge carriers. When in the presence of a z-directional magnetic field (B), a steady current (I) follows along the x-axis from left to right, electrons are initially exposed to the Lorentz force and drift towards the negative y-axis, resulting in an excess surface electrical charge on the side of the sample and creating a transverse voltage. The Hall voltage (V_H) is known as this transverse voltage [88]. As seen in the figure (2.7) [87].

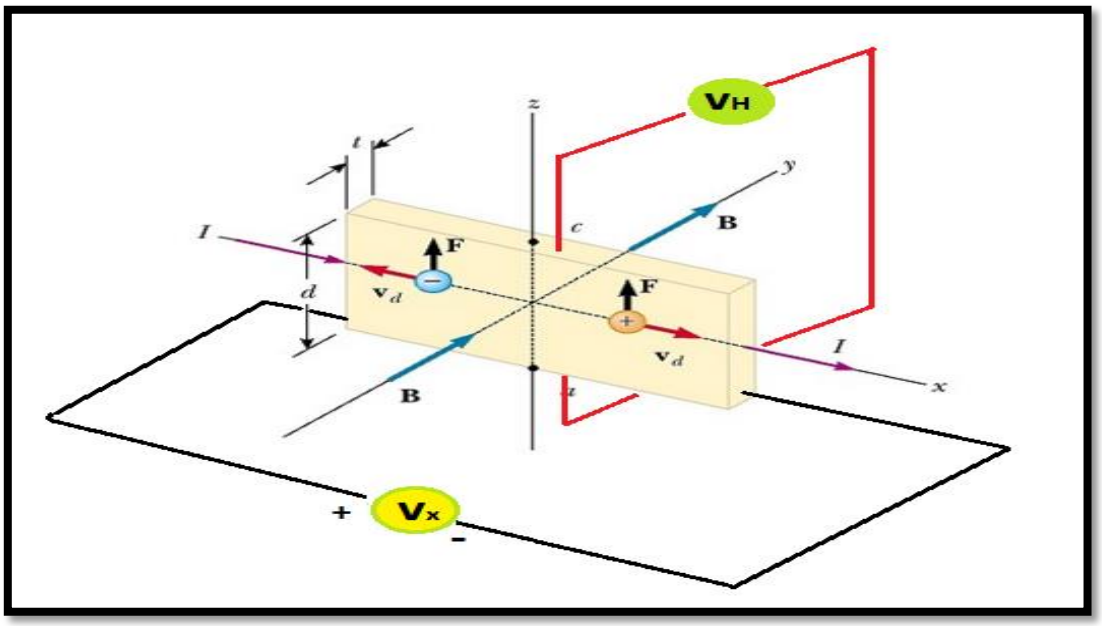

Figure (2.7): Schematic diagram of Hall Effect [87].

The Hall coefficient (R_H) is calculated by measuring the voltage of the Hall that generates the field of the Hall across the thickness (t) sample. It can be defined by [89]:

$$R_H = \frac{V_H}{I} \cdot \frac{t}{B} \qquad \cdots\cdots\cdots\cdots\cdots\cdots\cdots (2-26)$$

Carrier concentration can be determined by using the fallowing [89]:

$$n_H = \frac{-1}{qR_H} \quad \text{for electrons} \qquad \cdots\cdots\cdots\cdots\cdots\cdots (2-27)$$

or

$$n_H = \frac{+1}{qR_H} \quad \text{for holes} \qquad \cdots\cdots\cdots\cdots\cdots\cdots\cdots (2-28)$$

The charge carriers generating the current are deflected to the front edge of the sample with the control current and magnetic field directions shown in figure (2.7), so the current is mostly due to electrons (as in the case of an n-type sample), the front edge becomes negatively charged. It is positively

charged in the case of conduction of holes (p-type sample). So we can determine the type of semiconductor we've been using from the sign of the Hall coefficient (R_H) in the equation (2.28 and 29). We may assess the mobility of Hall from (σ) and (R_H) [89].

$$\mu_H = \sigma\,|R_H| \cdots\cdots\cdots\cdots\cdots\cdots (2-29)$$

or

$$\mu_H = \frac{\sigma}{n_e q} \cdots\cdots\cdots\cdots\cdots\cdots (2-30)$$

2.9 I-V Characteristics

The current supplied to the load by the cell is the current resulting from the difference between the light current (I_L) and the dark current (I_D), and the latter arises from the bias due to the induced voltages (V). Assume that the current passing at the junction can be represented by one exponential equation:

$$I = I_L - I_o\left[\exp\frac{eV}{mkT} - 1\right] \quad \ldots\ldots (2-31)$$

$$I = I_L - I_D(V) \quad \ldots\ldots (2-32)$$

Where (m) a quantity of numbers that takes up one or two numbers. The relationship between this equation's current and voltages can be plotted in the usual manner as in figure (2.8) [90].

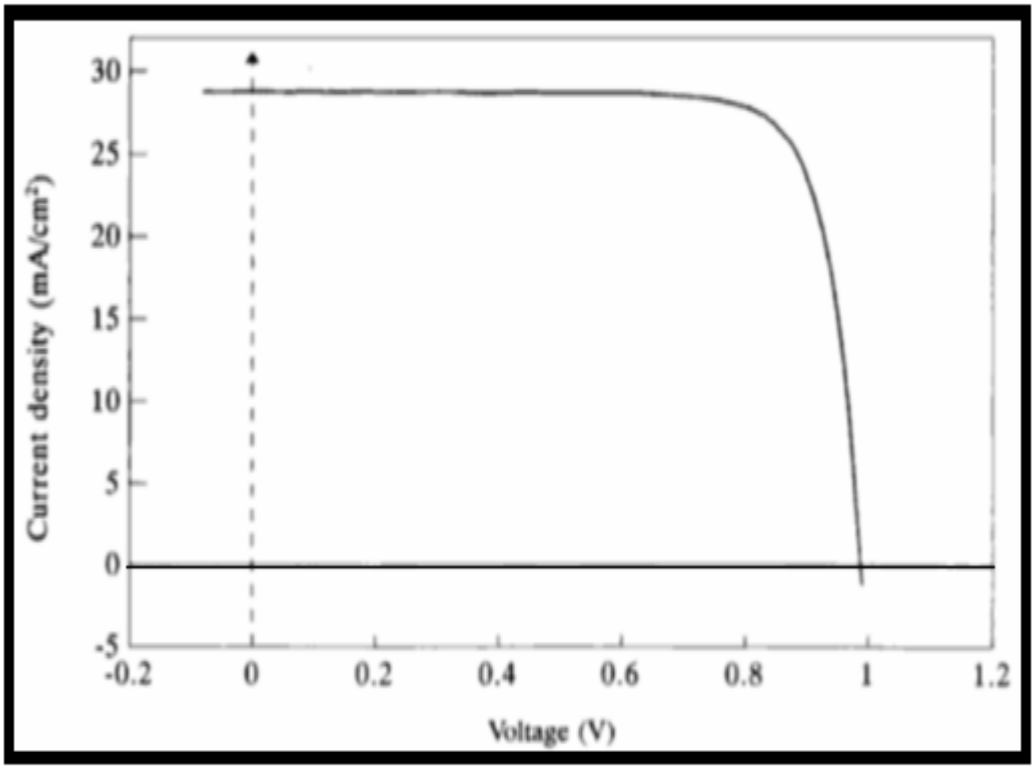

Figure (2.8). The relation between current and voltages [90]

Returning to figure (2-8), the highest current value can be obtained when a cell acts as a generator, when the value (V= 0) and equation (2-31) give the short circuit current under the closed-circuit condition:-

$I_{SC} \approx I(V=0) = I_L$ .....(2 – 33)

If the junction is held in the state of the closed-circuit such that (I = 0) voltages with the highest value reached in the first quarter are biased. These voltages are called voltages of the open circuit (V_{OC}). Its value is such that the bias current absolutely cancels the photon current, i.e.

$I_L = I_O (V_{OC})$

In case of open circuit, from equation (2-31) we find that

$V_{OC} = m\frac{kT}{q} \ln[\frac{I_L}{I_O} + 1]$ .....(2 – 34)

Through the above parameters, the alternative form is written [91].

$I=I_{SC}[1- \exp(\frac{e(V_{OC}-V)}{mkT})]$ .....(2 – 35)

The maximum power point represents the curve area between (I_{OC}) and (V_{OC}) the p-n cell operating area as a generator, as shown in Fig (2-9). The maximum value of the power dispersed in the load is an operating point(I_m, V_m). This point is called the maximum power point where the maximum voltage is expressed by V_m and the maximum current passing through the solar cell by I_m. Values of V_m and (I_m) can be obtained from the extreme case's normal state:

$\frac{dp}{dV}=0$ or $0 = d(IV)_m \approx I_M dV + V_M dI$ .....(2 – 36)

Which: can be written as:

$$\left[\frac{dI}{dV}\right]_M = -\frac{I_M}{V_M} \qquad \text{.....(2 – 37)}$$

Which is the general condition of the extreme case and the result is when applied to a cell defined by equation (2-33). [92]

$$I_M = \frac{I_L + I_Q}{1+\frac{m\ k\ T}{e\ V_M}} \qquad \text{.....(2 – 38)}$$

The cell-specific equation must also be met:

$I_M = I_L - I_O[\exp\frac{eV_M}{mkT} - 1]$ .....(2 – 39)

An approximate analytical solution can be used:

$\frac{I_M}{I_L} = I - a^{-b}$ .....(2 – 40)

Where:-

$$a = 1 + \mathrm{In}\frac{I_L}{I_0} \qquad b = \frac{a}{a+1} \qquad \ldots\ (2-41)$$

$$\frac{V_M}{V_{oc}} = 1 - \frac{ln\ a}{a} \qquad \ldots\ldots\ldots (2-42)$$

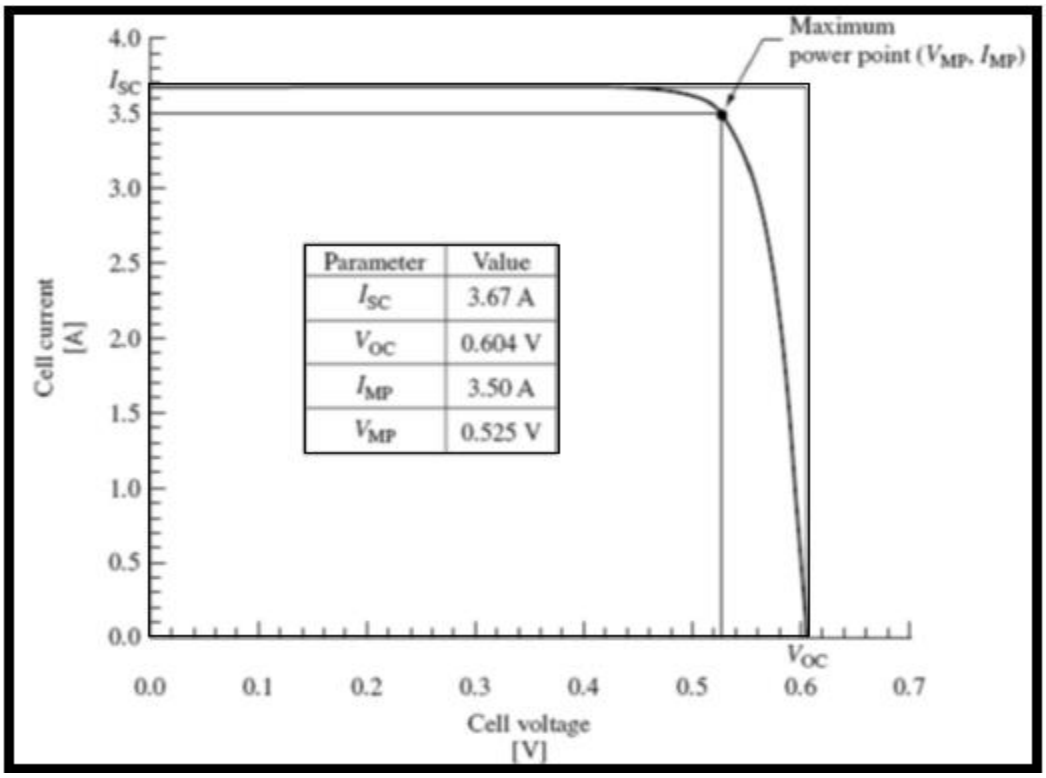

Figure (2.9): The p-n cell working area [92]

It is possible to reflect the product of V_m, I_m, which gives the best ability to deliver to the load, as in figure (2.10) according to the shaded rectangle area. It is an area smaller than the region that corresponds to the multiplication of V_{OC}, I_{SC} (the maximum current can be extracted from the cell divided by the maximum voltage). The division's product is defined as the filling factor and given by:

$$FF = \frac{I_M \cdot V_M}{I_{SC} \cdot V_{OC}} \qquad \text{..... .....(2 - 43)}$$

Its value, however, is always less than one and provides a quantitative measure of the curve's form and its properties.

The filling factor is an important functional parameter for many semiconductor crystalline cells and does not change much with different devices (Si, GaAs, InP and others). The maximum power obtained from the cell can be written using the definition of the fill factor with the following relationship: [93].

$$P_M = FF\ I_{SC} V_{OC} \qquad \text{.....(2 – 44)}$$

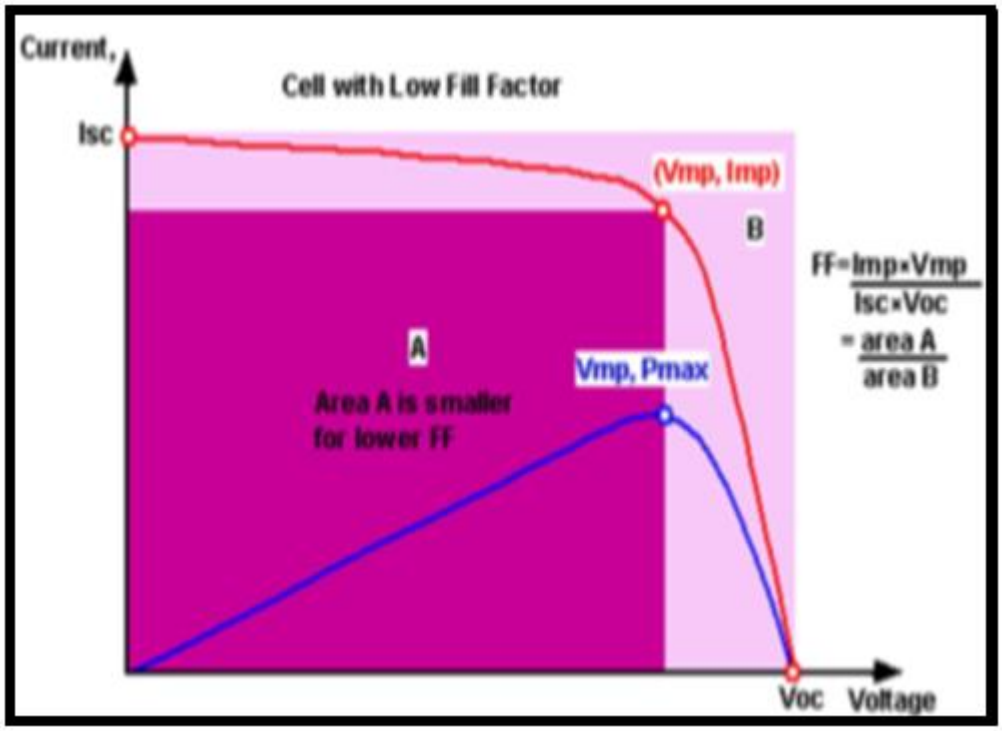

Figure (2.10): Current-voltage characteristics of a p-n cell [94].

The following approximation can be deduced using the terms in the equations (2-31) and (2-32) and a simple equation can be written to determine the filling factor:

$$FF = 1 - \frac{\ln a - 1}{a} \qquad \text{.....(2 – 45)}$$

It can be expected from this equation that the value of (FF) does not alter much and depends on the cell and the operating conditions. As a consequence, the equation (2-44) illustrates the maximum power dependency on the closed-circuit current and the open-circuit voltage (under simple operating conditions or parameters). A solar cell's energy conversion efficiency is defined as the ratio between the maximum electrical power provided to the load and the radiation power (P_L) that falls on the cell. [93]: -

$$\eta = \frac{I_M V_M}{P_L} = \frac{FF \, . I_{SC} \, . \, V_{OC}}{P_L} \qquad \text{.....(2 - 46)}$$

CHAPTER THREE

Experimental Work

3.1 Introduction

This chapter includes a description of all tools and devices used in this work which are shown in Diagram (3.1).

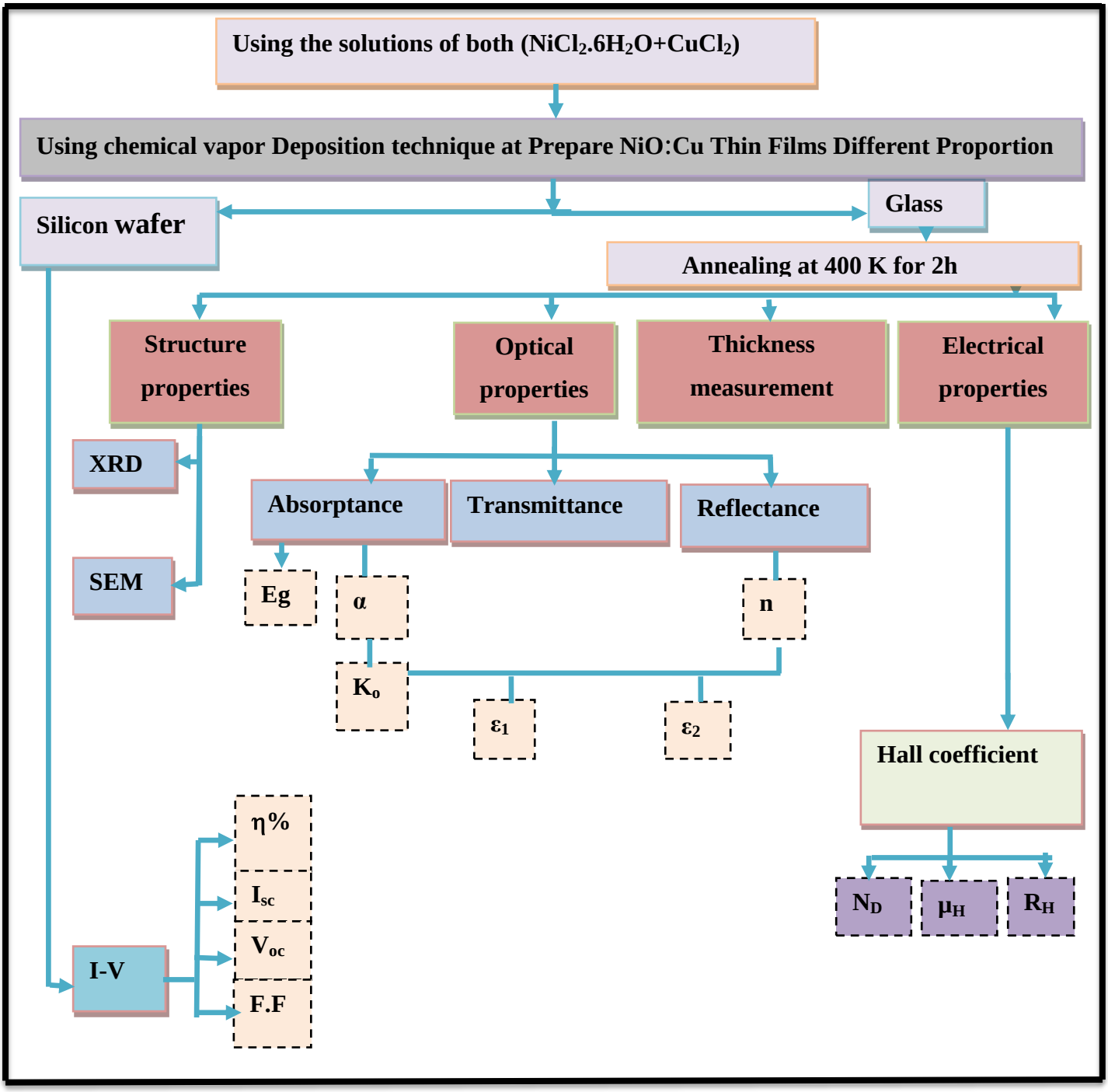

Figure (3.1): A schematic diagram explains the main steps for procedure.

3.2 Preparing the Solution

Prepared be a solution of nickel chloride hex water ($NiCl_26H_2O$). Molecular weight is 237.69g/mol. Prepare the solution with 0.35M molarity by dissolving 33.27g of nickel chloride salt in 400 ml of water. Step by step stir the solution for an hour in the magnetic stir device to ensure that it is completely dissolved. Shown in figure (3.2a)

Prepare the solution with 0.1M molarity by dissolving 1.34g of copper chloride salt ($CuCl_2$) in 100 ml of water. Step by step stir the solution for an hour in the magnetic stir device to ensure that it is completely dissolved. Shown in figure (3.2b)

Figure (3.2): a) Solution of nickel chloride hex water ($NiCl_26H_2O$)
b) Solution of copper chloride ($CuCl_2$)

3.3 Substrates Cleaning

Glass and silicon substrate (p-type and n-type) were used to precipitate samples, as well as used to make structural, optical and electrical measurements of thin films , The glass bases have been cleaned before being used in the deposition process by the following steps:

1. Washing slides or glass substrate with water and washing detergent powder and wipe it with a clean soft cloth in order to get rid of dust and oil stains suspended and to get rid of dirt suspended.
2. Then washing the glass substrate with distilled water well, and then put in place in the ultrasonic bath for a (15) minute
3. Glass slides are extracted from distilled water and washed with laboratory ethanol with high purity (99.9%) and then placed in the glass container again and flooded with alcohol the container is placed in the ultrasonic apparatus for (15) min be ready for use the film can then be deposited on them.
4. Immerse the silicon substrates in a container containing a mixture of 10% HF and 90% ethanol alcohol with 97% purity for ten minutes.
5. Silicon substrates are extracted from the container and the deposition process is done directly.

3.4 Deposition Process by AACVD

The devices shown in figure (3.3) were used in the deposition process. An ultrasonic nebulizer was used to form an aerosol from the material to be deposited and to form thin films, and the aerosols were transferred from a device by a hose to the chamber.

This chamber contains a heater, as well as two holes, one for entering the material to be deposited and the other for exit of unwanted products and easy passage of the fumigant.

The substrate is placed on the heater. At a temperature (200 °C ±10), and at a distance (12 cm± 2), the sample was deposited with the doping ratio shown in the Table (3.1).

After that, the banned films were annealed for two hours at 400 ° C, to obtain crystalline films and get rid of the defects that may have occurred in the deposition process.

Figure (3.3): The Aerosol-Assisted Chemical Vapor Deposition devices used by the researcher

The Table (3.1): Show the volumes taken from $CuCl_2$ added to $NiCl_2.6H_2O$ to obtain the proportions necessary to prepare

Sample	0.35M $NiCl_2.6H_2O$ (ml)	0.1M $CuCl_2$ (ml)	Deposition time (hour)	Cu/Ni At. %
NiO	100	0	1	0
NiO:Cu	80	20	1	7.5
NiO:Cu	75	25	1	10
NiO:Cu	70	30	1	12.8

3.5 Thin Films Thickness Measurement

The thickness of the prepared films were measured using the optical interference method using a He-Ne laser with a wavelength (632.8) nm and angle incident of 45° as shown in figure (3.4). The principle of operation of this method is based on the principle of interference of light waves reflected from the surface of the prepared films and those that are reflected on the substrate on which the films were deposited are prepared and the thickness of the films can be calculated using the following relation[95]:

$$t = \frac{y}{x} \times \frac{\lambda}{2} \quad \text{.....(3.1)}$$

Where:

λ: Represents the wavelength of the laser light

t: The thickness of the film

y: width the dark Fringes

x: width the light fringes

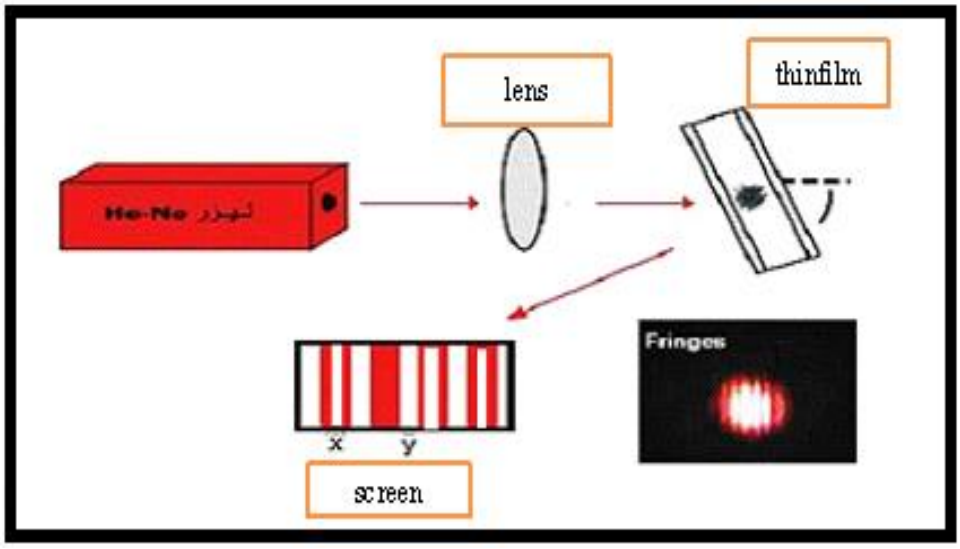

Figure (3.4): Thin film thickness measurement scheme by optical interference [95].

3.6 Structural Measurements

3.6.1 X-ray diffraction (XRD)

An X-ray diffraction technique was used to determine the crystal structure of the compound NiO: Cu films and the samples were examined with a Shimadzu (XR - DIFRACTOMETER / 6000) device at the University of Babylon, which is shown in figure (3.5) and has the following specifications:

Target: Cu

Wavelength: 1.5406A°

Voltage: 40 Kv

Current: 30 mA

Range (2Θ): (30 – 80) deg

A computer program was used to calculate the parameters of the lattice dimensions. The strain (Ɛ) and the dislocation density (δ) theoretically and compare them with the practical values of the graphs.

Figure (3.5): X - ray diffraction device

3.6.2 Scanning Electron Microscopy (SEM)

The morphological properties of NiO:Cu thin films have been measured by sending the samples abroad (Islamic Republic of Iran).

3.7 Optical Measurements

Optical measurements involve the absorbance and transmittance spectrum of NiO:Cu films were performed by (UV-Visible Spectrophotometer / 2700) two-beam supplied by the English company (CECIL), The sample on which the film is deposited is well placed in the substrate window so that the light rays perpendicularly to the thin film .A non-precipitated glass sample with a thin film placed in the source window is also used as a reference to eliminate the glass effect for the purpose of measuring the absorbance of thin film only,, The optical energy gap (Eg) was measured as well as measuring the rest of the optical constants finite include the refractive index (n), absorption coefficient (α) ,extinction coefficient (k_o) , dielectric constant in part real (ε_r) and imaginary (ε_i) and figure (3.6) illustrate the image of the device used.

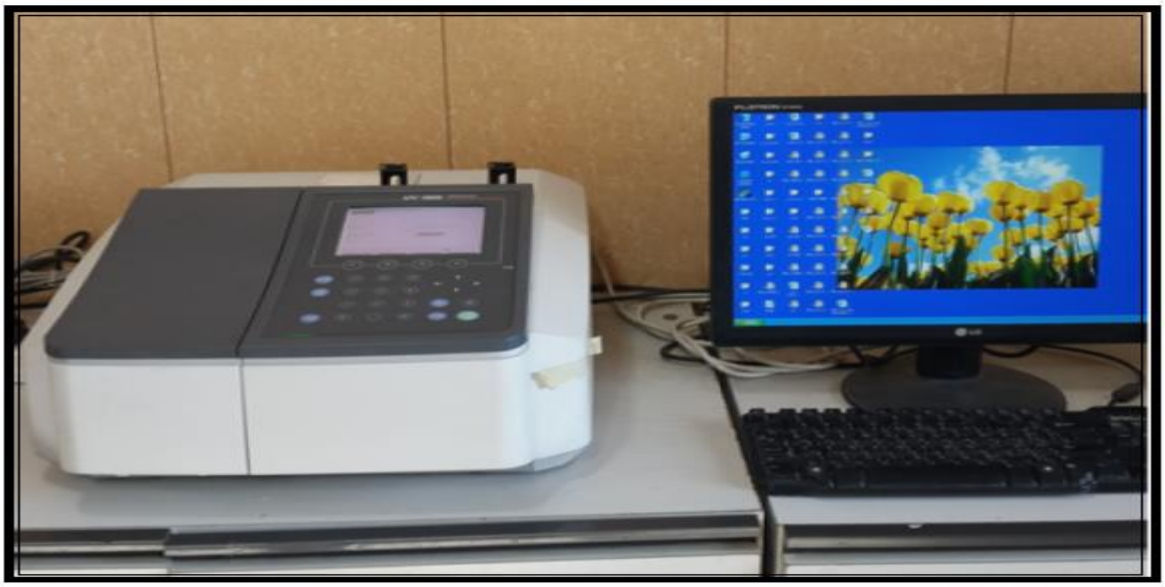

Figure (3.6): UV-Visible Spectrophotometer device**.**

3.8 Electrical Properties (Hall Effect Measurement)

Measurements of Hall effect on prepared films were carried out to determine the type of charge carriers and to find the Hall coefficient (R_H) ,carrier concentration ,mobility and resistivity, Using device(Measurement Hall Effect System) from type (HMS 3000) manufactured by (EcopiA) Taiwanese origin as shown in figure (3.7), Using a magnetic field of intensity (B = 0.55 Tesla) and through the relationship between (V_H) and (Is) ,it is possible to identify the type and density of charge carriers If the relationship is direct, the film is a positive type (p-type) If the relationship is inverse. The film is negative (n-type), this measurement is done in Polymer Laboratory– University of Babylon, College of Science – Department of Physics.

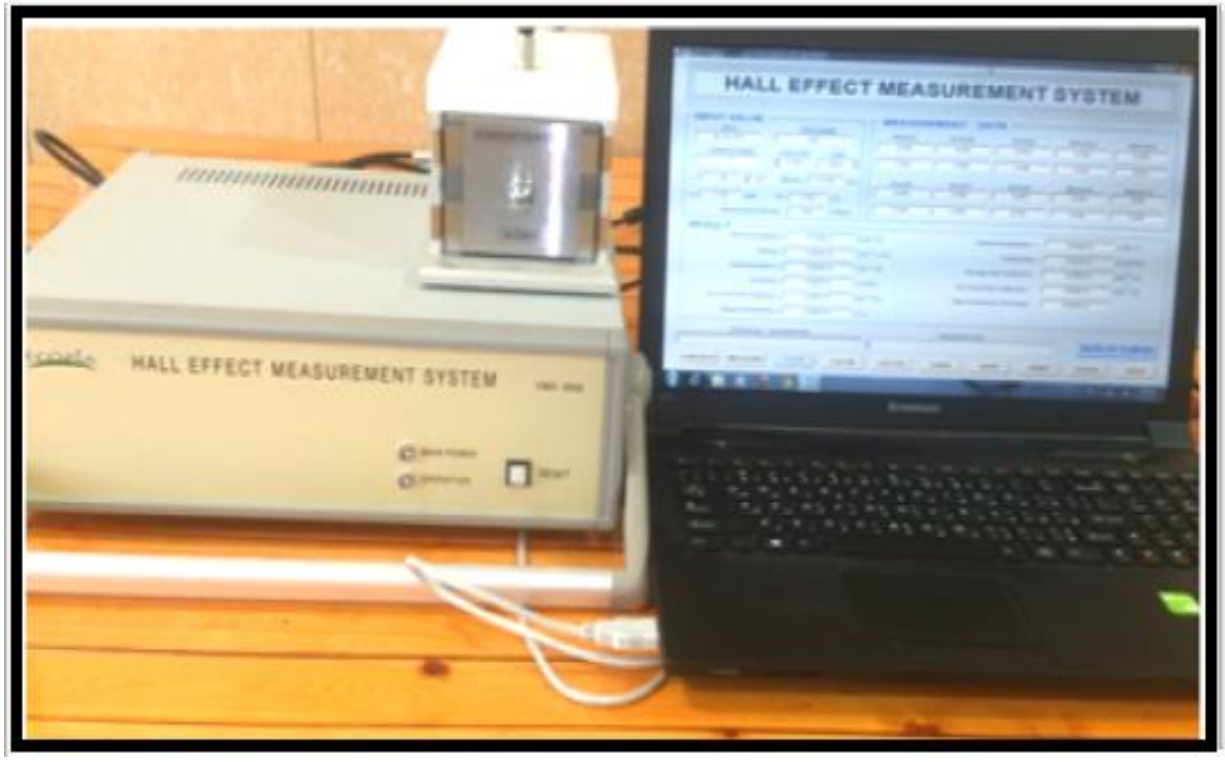

Figure (3.7): Hall Effect measurement system (HMS-3000).

3.9 Current-Voltage Characteristic Measurements for Si(n,p)/ NiO:Cu Heterojunction

The system shown in Figure (3.8) was used to precipitate gold electrodes on both sides of the substrate (Si/NiO:Cu) heterojunction of various types Si (n), and Si (p) with carrier density ($5\times10^{15}cm^{-3}$) and with orientation (100) For type (p) and (111) for type (n) by using sputtering technique of type (CRESSINGTON-108), for the purpose of studying the properties of current - voltage in the cases of darkness and lighting and to determine the sensitivity of light using the electrical circuit diagram was shown in figure (3.9) consisting of a device(DEGETAL MULTIMTER) of type (AUTO – RANGE DMM) for the purpose of measuring current and from power supply (DC) of type(DAZHENG) Its voltage ranges from (0 – 2) V and from a light source (halogen lamp) with a radiative power (100) mW. The dark current was first recorded as a function of multiple voltages by placing samples in a dark chamber and then re-measurements in the presence of the light source. These measurements were made at room temperature 300 K. and the surface area of the samples was (4 × 4) mm^2.

Figure (3.8): Electrode deposition system by sputtering technique

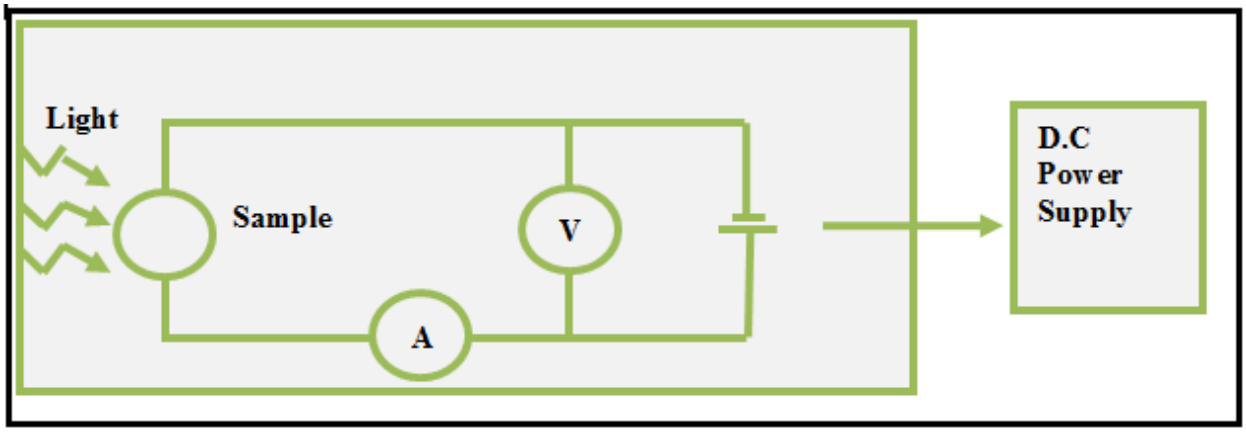

Figure (3.9): Circuit diagram for measuring current-voltage characteristics

CHAPTER FOUR

Results, Discussion, Conclusions and Suggestions

4.1 Introduction

The results of the experimental measurements and tests of structural, optical, electrical, solar cell properties for the deposited thin films will display in this chapter. The structural properties for NiO:Cu are covers by the study of XRD, SEM .The optical properties are studied, the optical energy gap and some other parameter such as absorption coefficient, extinction coefficient both real and imaginary part of the dielectric constant, refractive index, as a function of wavelength are determined, also the electrical properties Hall effect and electrical measurements of heterojunctions including current-voltage in two case of darkness and lighting properties.

4.2 Structural Properties

In this section the surface structural and morphological properties of NiO:Cu thin film of deposited on a glass substrate were examined.

4.2.1 X– Ray Diffraction Analysis (XRD)

The synthesis of the prepared films (NiO:Cu) was identified by AACVD and different doping of copper. It was found that the film have a polycrystalline and cubic polycrystalline structure at crystalline planes (111) and (200) which are corresponding at angles ($2\Theta = 37.2^{o}$)and ($2\Theta = 43.2^{o}$) respectively. When the doping is increased, noticed a rise in the peaks and became sharp for the crystal planes and the appearance of the peak at the angle ($2\Theta = 37.2^{o}$) which returns to the crystal plane (111) the results obtained from X-ray diffraction were confirmed with ICDD (International Center for Diffraction Data) card number (00-152-2025) observed that the preferred directions (111) when doping change from (0-12.8 %) and other preparation conditions are constant. When increasing the doping, it notic

observed an increase in the peaks relative to the crystalline planes with a decrease in the value of FWHM this indicates an increase in crystallite size, this result agrees with [42]. The effect of doping on the average crystallite size calculated using the FWHM from Scherrer equation (2-2) was also studied. The increase in doping results in a small increase in the value of the lattice constants this is due to an increase in the value of the distance between crystalline levels (d_{hkl}) with the increase of doping noted that the stress decreases when the doping increase, causing an increase in grain size. Also noted, the dislocations density decreases with increasing doping as in Table (4-1) and decreases with increasing crystallite size. Because the relationship between them is inverse and that means an improvement in the crystal structure, i.e. in the grain size as shown in Figures (4.1), (4.2), (4.3), and (4.4).

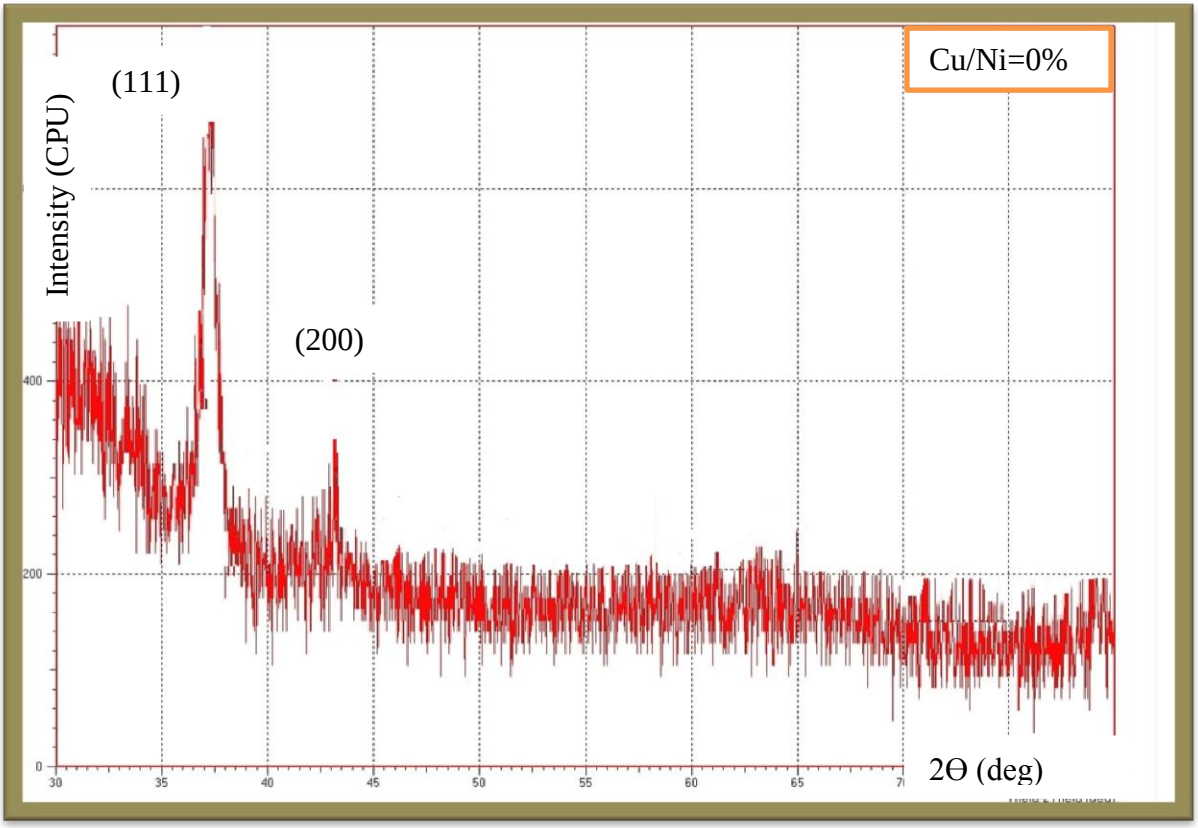

Figure (4.1):X-ray diffraction of NiO film.

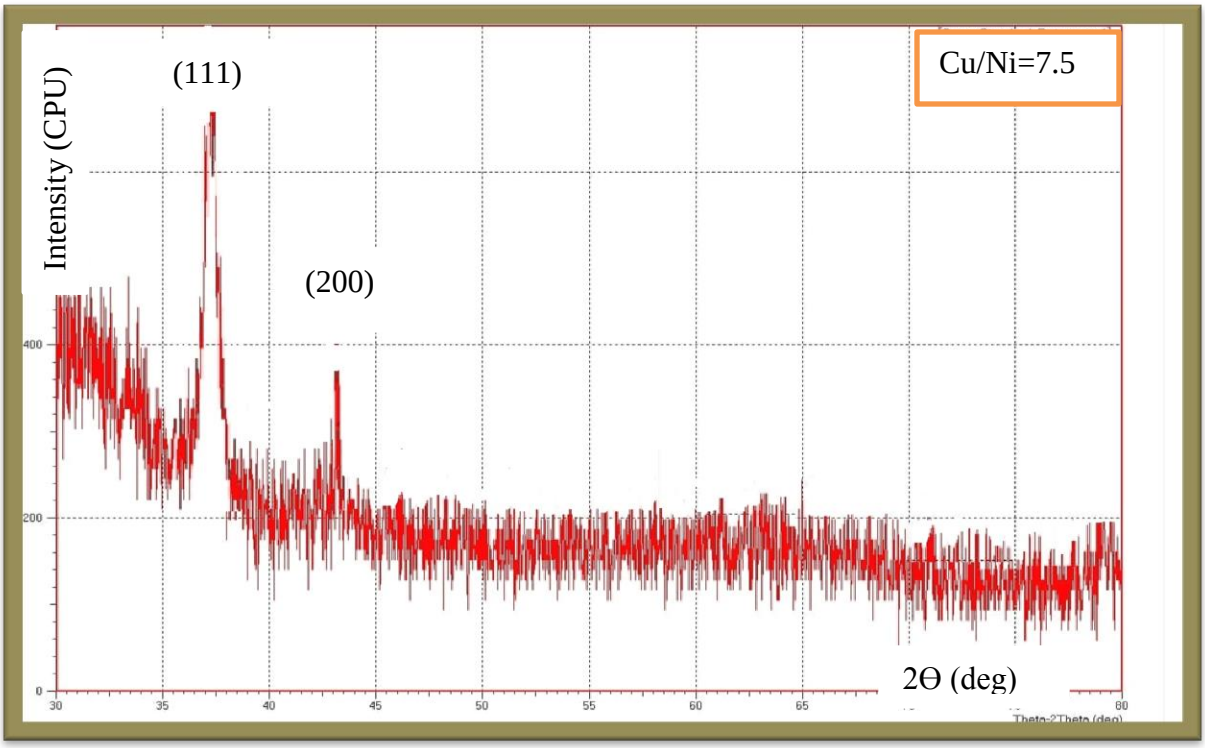

Figure (4.2):X-ray diffraction of NiO:Cu film prepared with doping Cu/Ni=7.5%.

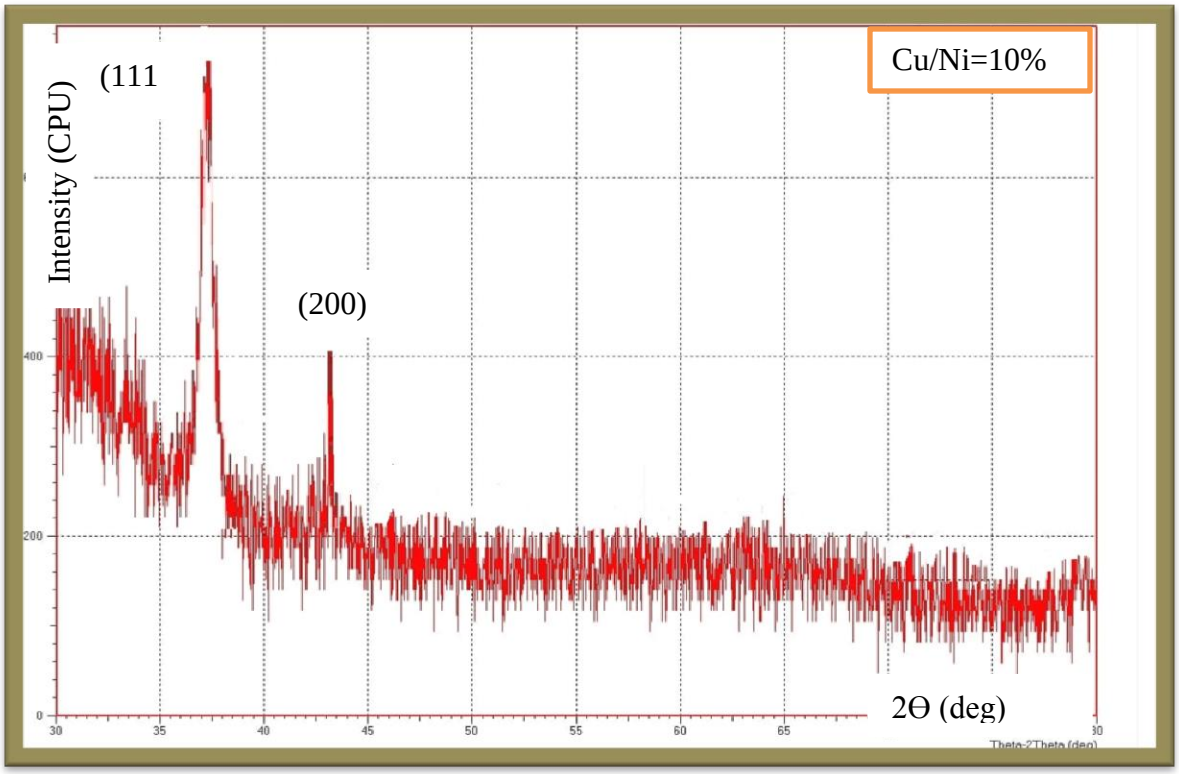

Figure (4.3):X-ray diffraction of NiO:Cu film prepared with doping Cu/Ni=10%.

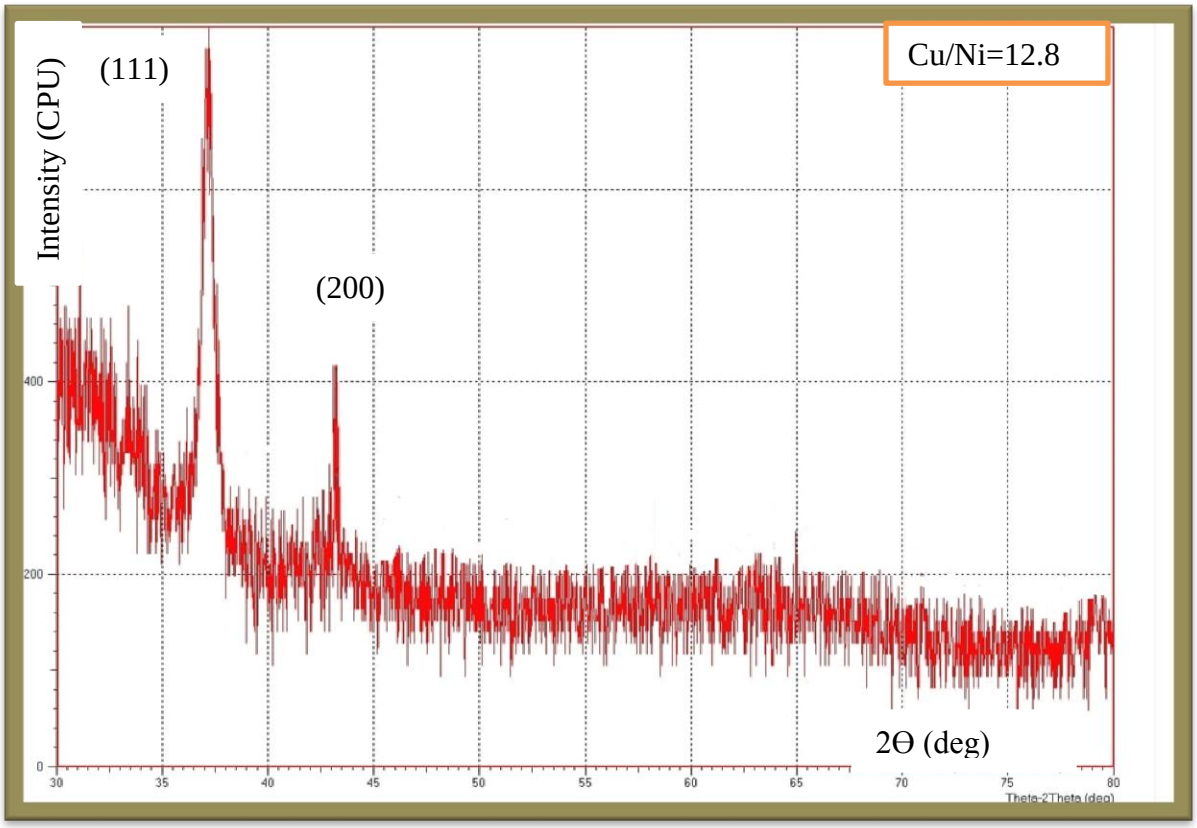

Figure (4.4):X-ray diffraction of NiO:Cu film prepared with doping Cu/Ni=12.8%.

Table (4.1): X-ray Diffraction Screening Parameters for NiO:Cu films samples at Different doping

Dop. Cu/Ni (At%)	2θ (Deg.)	FWHM (Deg.)	Int. (a.u)	d (nm)	G.S (nm)	hkl	a (nm)	strain (ε') nm	dislocation density (δ) nm^{-2}
0	37.2	1.6	650	0.241	5.236	(111)	4.82	0.006616551	0.036463371
	43.2	0.51	315	0.209	16.746	(200)	4.18	0.002069031	0.003565558
7.5	37.3	1.53	665	0.241	5.478	(111)	4.86	0.006325218	0.033323033
	43.4	0.48	340	0.208	17.805	(200)	4.14	0.001945976	0.003154049
10	37.45	1.38	715	0.240	6.076	(111)	4.8	0.005702576	0.027085426
	43.44	0.42	405	0.208	20.352	(200)	4.14	0.001702493	0.002414149
12.8	37.5	1.35	740	0.239	6.212	(111)	4.78	0.005577782	0.025912935
	43.5	0.4	420	0.208	21.374	(200)	4.06	0.001621084	0.002188791

4.2.2 Scanning Electron Microscope (SEM)

The scanning electron microscopy images for the undoped and Cu doped NiO thin films are in all Figures (4.5), (4.6), (4.7), and (4.8). The micrograph reveals that both un doped and doped NiO thin films are made of Nano crystalline grains. The surface micrograph of the un doped NiO thin film has uniform distribution of structured grains. There is evidence of homogeneous, spherical, dense, devoid of cracks indicating adhesiveness of grains. Figure (4.5) shows the electron microscopy images show of the (NiO) grain size, it is noted that the grains are distributed regularly on the surface of the film with found some defects and accumulation of molecules (NiO) in certain sites without other sites however, there are aggregations of grains and they take a spherical shape resulting from the mixing of some grains with each other due to the evaporation and deposition conditions on substrates. the low Cu doping concentration has almost no change in the surface morphology with NiO films.As shown in figure (4.6) films show a continuous, uniform, and crack-free surface, with the substrates completely covered by the (NiO:Cu) , shows that Cu, Ni, and O elements are uniformly distributed in the (NiO:Cu) films, indicating the successful incorporation of Cu+ ions.It is revealed from that the Cu doping results in a smoother surface with a lowersurface roughness ,this resulte agrees with other paper resulte [96]. When increases doping Cu ,it is noted increases the size of the nanoparticles others are irregular in shape, although grouped together but not contiguous, or may resulted from the assembly of spherical particles which may confirmed by the dotted lines that, as show figure (4.7)and figure (4.8) shows images of NiO:Cu films(at ratio Cu/Ni=12.8),it is noted increases the grains size with increases doping Cu.

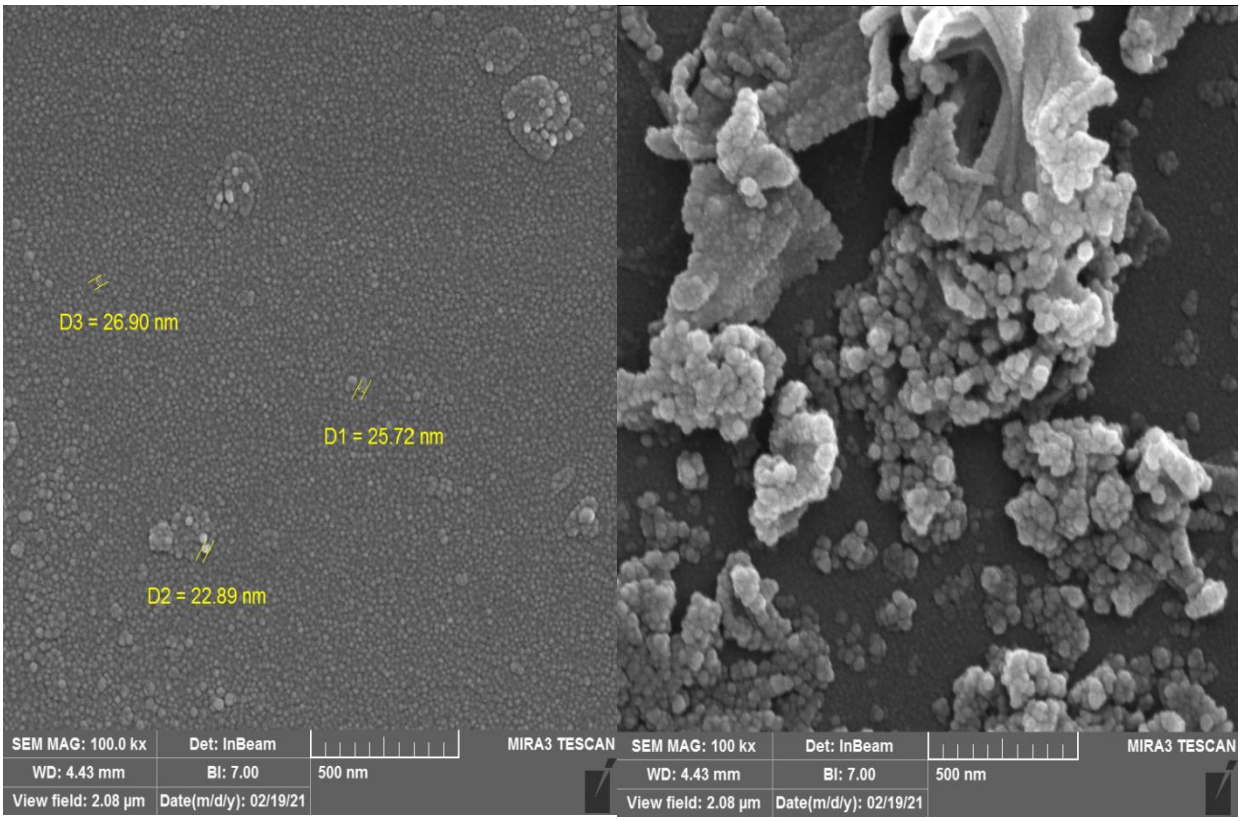

Figure (4.5): SEM images of NiO film

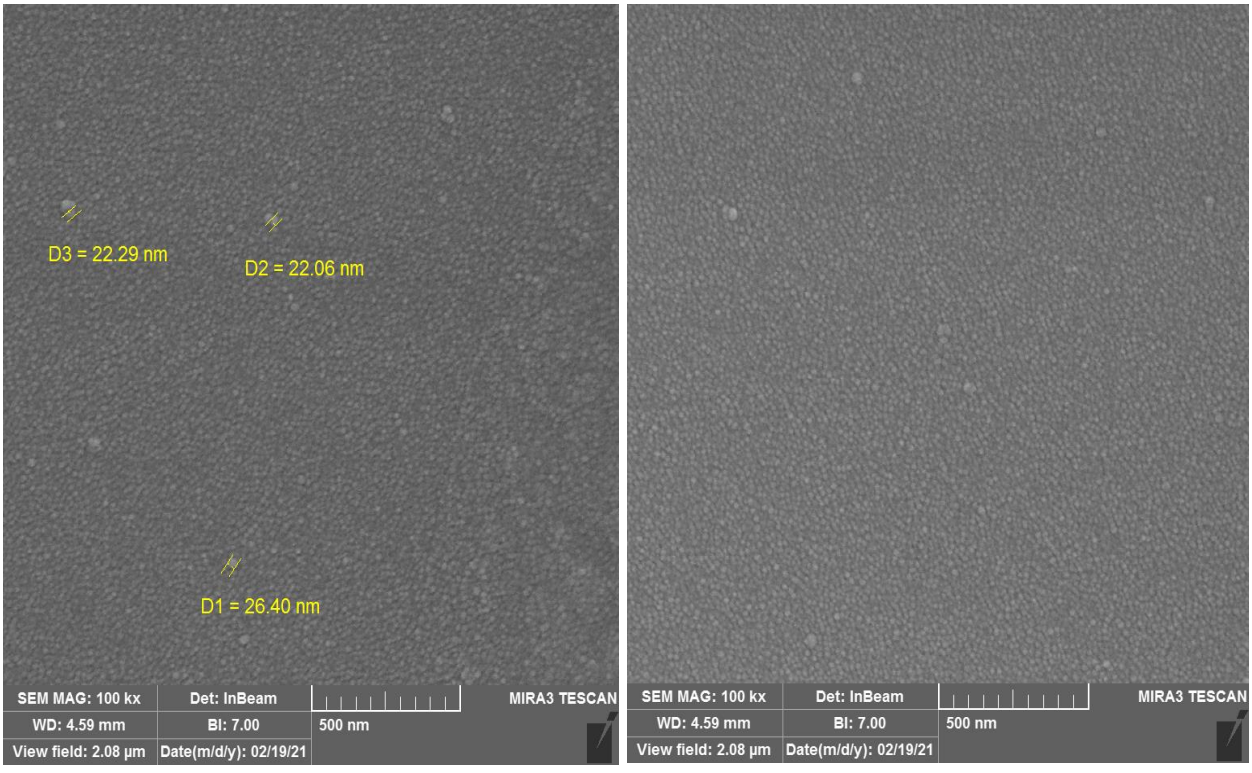

Figure (4.6): SEM images of NiO:Cu films prepared with doping Cu/Ni=7.5 %

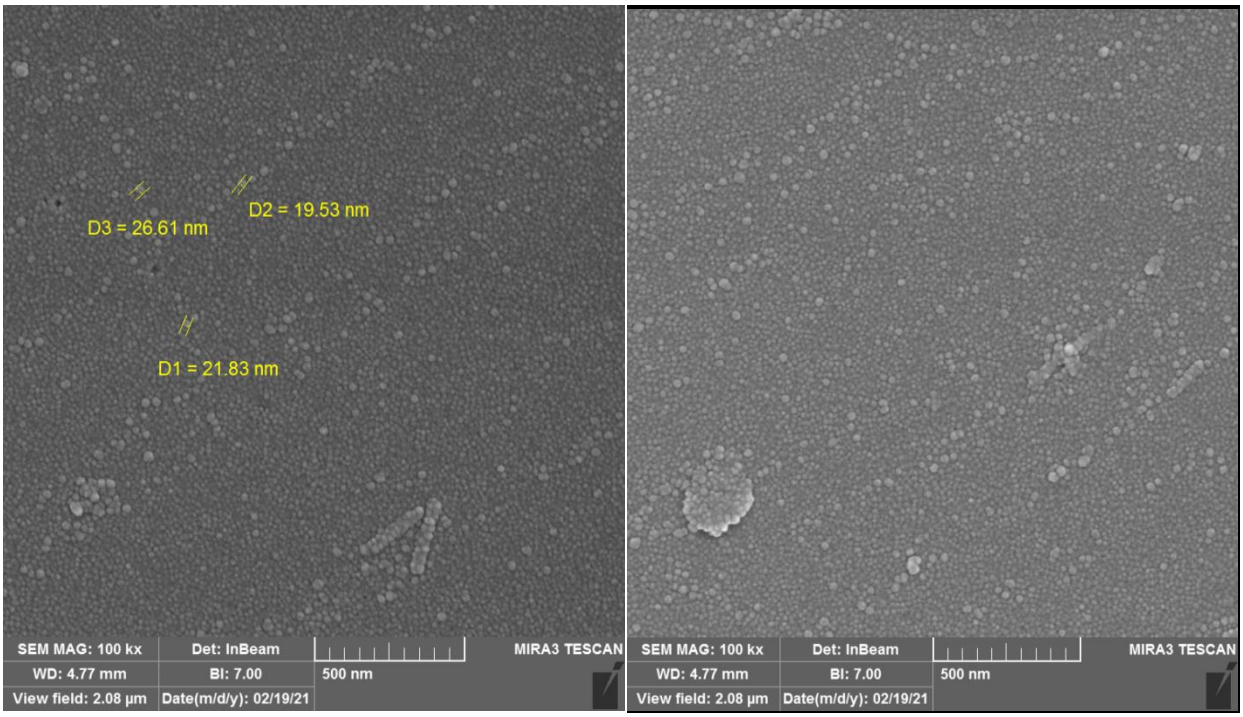

Figure (4.7): SEM images of NiO:Cu films prepared with doping Cu/Ni=10 %

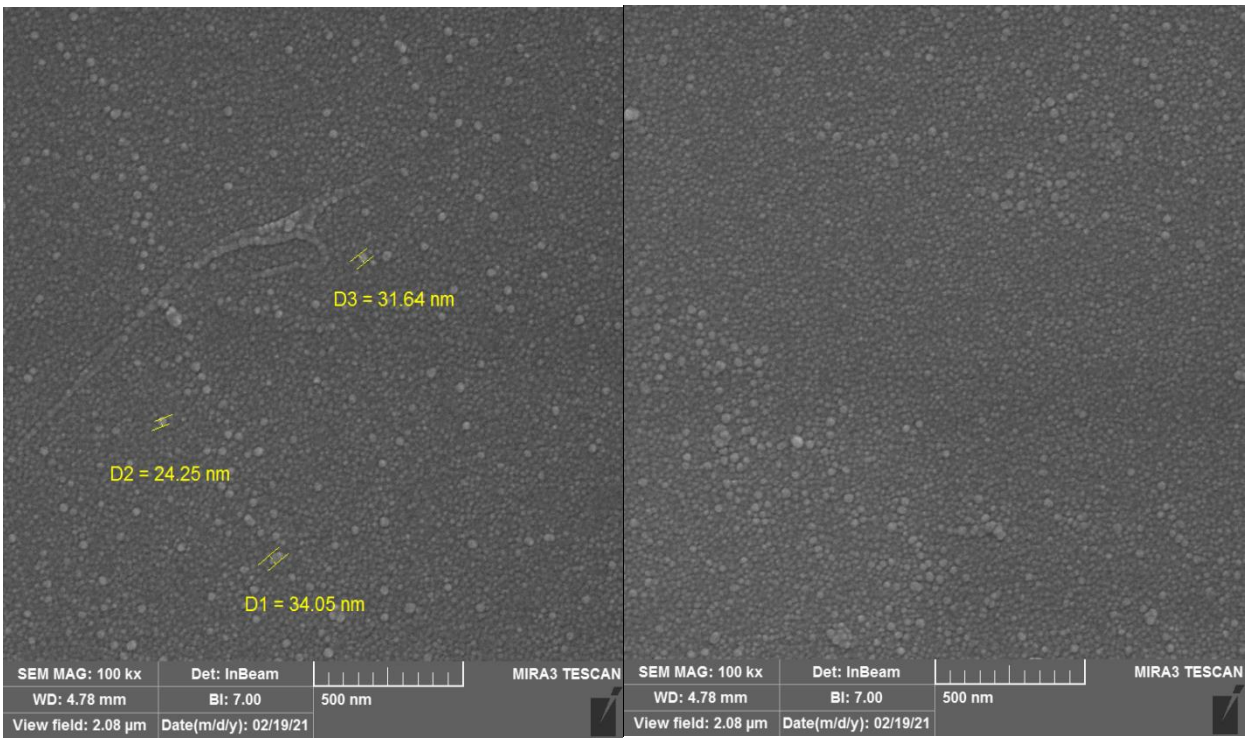

Figure (4.8): SEM images of NiO:Cu films prepared with doping Cu/Ni=12.8 %

4.3 Optical Properties

The optical properties for deposited NiO:Cu films on glass substrate by the Aerosol-Assistant Chemical vapor deposition technique (AACVD) at Different doping have been determined by using UV-VIS-IR transmittance spectrum in the range of (330–1100) nm. The study of the optical properties is useful in the task of the nature of the practical application that can be used to record film material.

4.3.1 Absorbance Spectrum

It was found that the absorption of all samples appeared in the UV range at wavelength (330) nm. The absorption of NiO:Cu films prepared with different doping decreased with the increasing of wavelength. Figure (4.9) shows the relationship between the absorbance and wavelength of NiO:Cu films prepared with different doping.

It notice that the absorbance decreases with increasing wavelength for all the prepared thin films.

This result means that incident photon is not able to excite the electron and transfer it from valence band to the conduction band because the energy of incident photon is less than the value of the energy gap value of the semiconductor. This leads to the absorbance decrease with increasing of wavelength. While increasing absorbance when increasing the doping copper, this result agrees with refer [41].

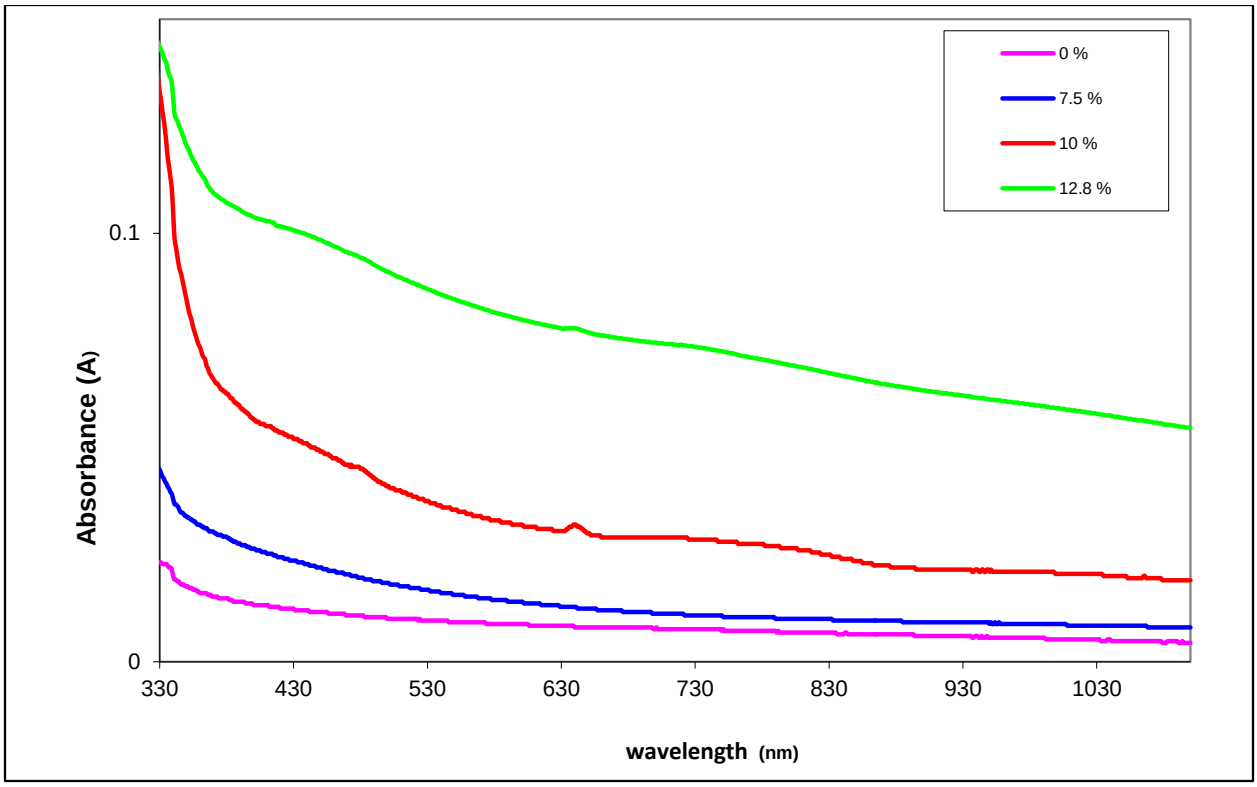

Figure (4.9): Absorbance spectrum as a function of wavelength for at different of Cu doped NiO thin films**.**

4.3.2 Transmittance Spectrum

Figure(4.10) explain the relationship between transmittance and wavelength for NiO:Cu films prepared by different doping of Cu. Transmittance demonstrated behavior opposite of absorbance as shown transmittance of prepared films decreases with increasing of doping and increased thickness of films. The variation of optical transmittance of NiO:Cu films prepared with different doping from Cu. As seen from these spectra's the transmittance of Cu doped NiO thin films were decreased with increasing Cu concentration in the visible region, the maximum transmittance of Cu doped NiO thin films were obtained for NiO pure. The

transmission of Cu doped NiO thin films at higher concentrations in the visible region was decreased due to the increase in absorption.

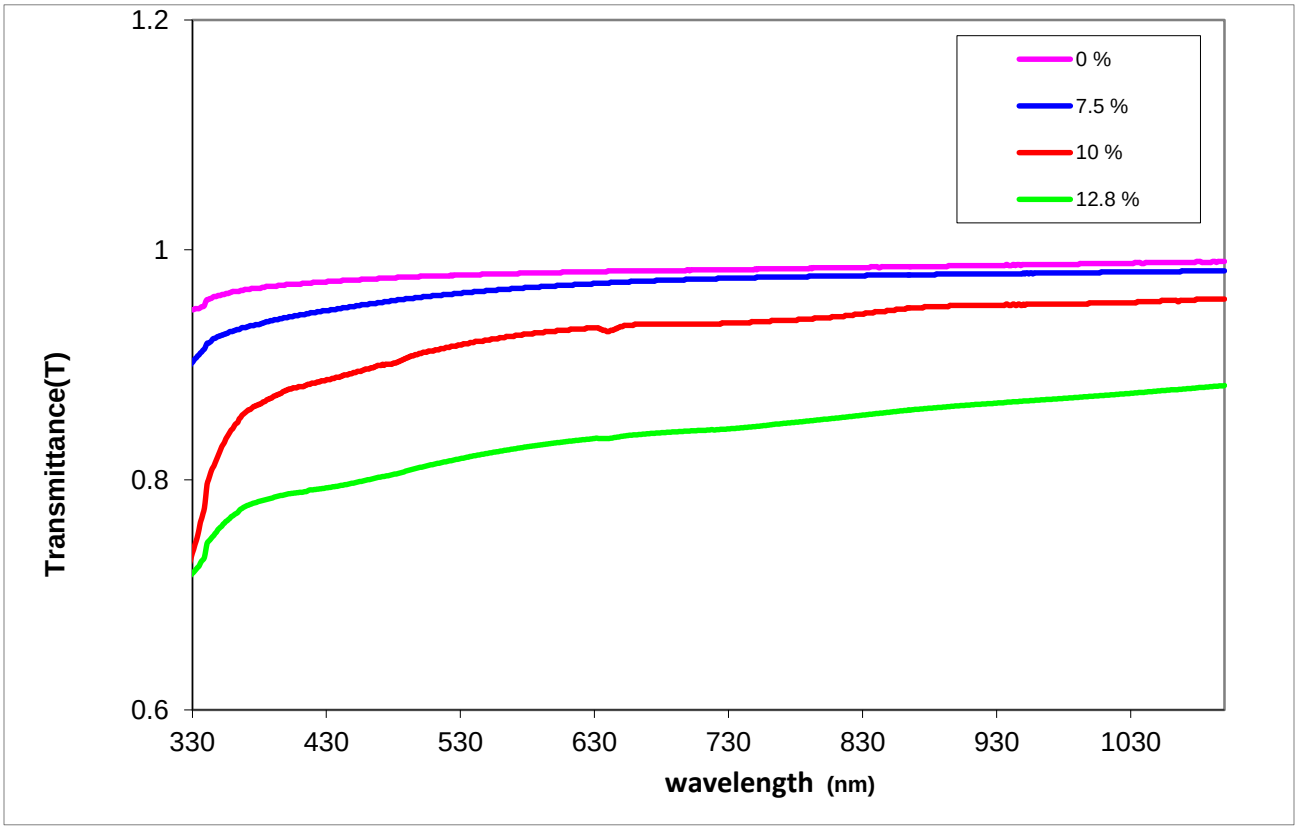

Figure (4.10): Transmittance spectrum as a function of wavelength for at different of Cu doped NiO thin films**.**

4.3.3 Absorption Coefficient

Figure (4.11) shows the optical absorption coefficient as a function of the incident wavelength of NiO:Cu films prepared with different doping agents and it has been observed that all the thin films prepared have an absorption coefficient that increases with increasing doping and decreases with increasing wavelength, this result agrees with refer[41]. The figure (4.11) shows that the absorption coefficient of the film gradually increases with doping. This is because the absorption value parameter indicates the ability of the film material to absorb the

energy of the incident radiation and the increase in doping increases the thickness of the prepared films.

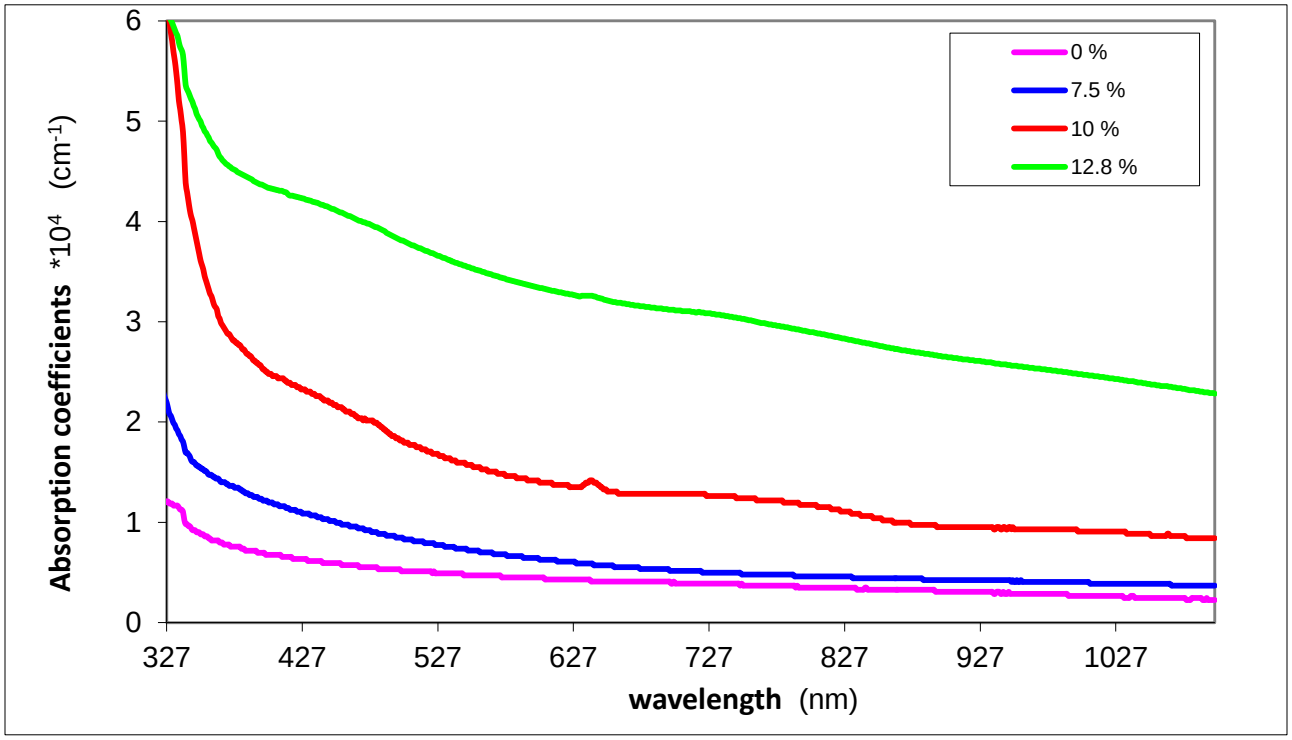

Fig: (4.11): Absorption coefficients as a function of wavelength for at different of Cu doped NiO thin films.

4.3.4 Optical Energy Gap

From Figure (4.12), the optical energy gap of NiO films deposited on glass substrates and different doping from Cu, this figure shows the relation between $(\alpha h\upsilon)^2$ on the y-axis and photon energy ($h\upsilon$) on the x-axis, Where the optical energy gap of the allowable direct transition from the tangent extension of the curve was calculated to convergence the photon energy axis at point $(\alpha h\upsilon)^2 = 0$, since intersection point represent the optical energy gap of the allowed direct electronic transitions and was found to decrease as doping copper increased , This means that the optical energy gap values can be controlled by changing the doping when prepared NiO films. observed that when calculating the energy gap, found that its

value ranges between (3.5 –2.8eV) this result is agreement with[42].Table (4.2) shows the optical energy gap values for NiO films at different doping from Cu, the energy gap decreases from increasing the doping copper when preparing the films.

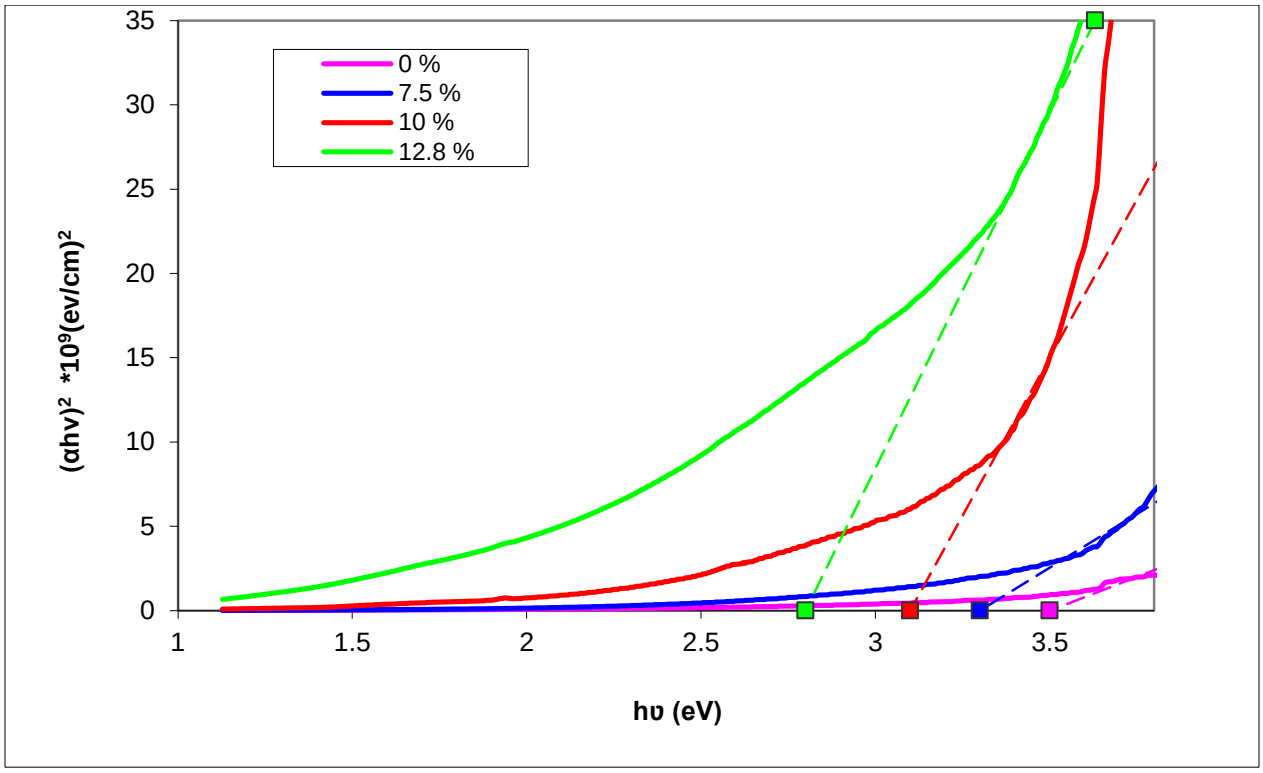

Figure (4.12): The optical energy gap for the allowable direct transition for at different of Cu doped NiO thin films.

Table (4.2): The values of optical energy gap for NiO thin films at different doping of Cu.

sample	Cu/Ni At. %	E_g (eV)
NiO	0	3.5
NiO:Cu	7.5	3.3
NiO:Cu	10	3.1
NiO:Cu	12.8	2.8

4.3.5 Extinction Coefficient

The relation between extinction coefficient and wavelength of deposited NiO films is shown in figure (4.13). In general, it is clear that the extinction coefficient (k_o) increases with increasing of doping of copper for all prepared samples. It is clear that (k_o) value for NiO films, In general since the increasing doping for copper of NiO samples leads to decrease the optical energy gap as a result of absorbance increases.

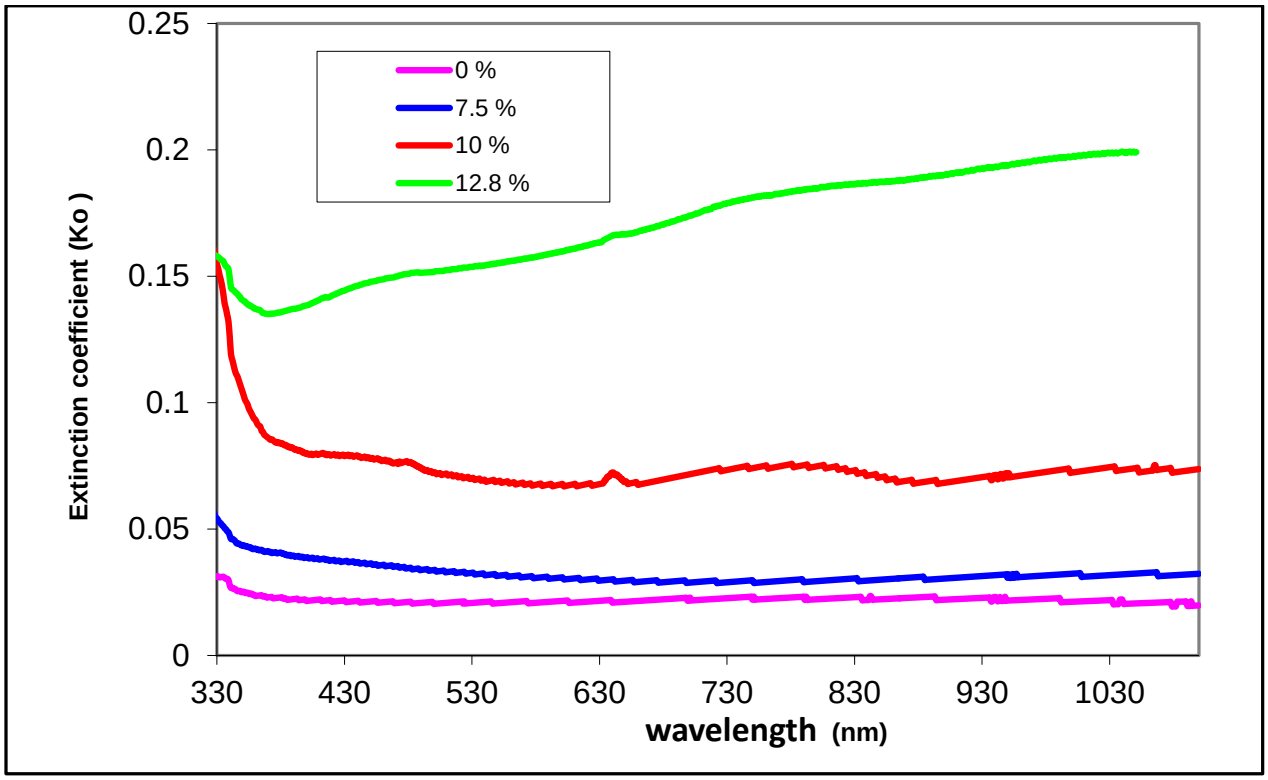

Figure (4.13): Extinction coefficient as a function of wavelength for at different of Cu doped NiO thin films.

4.3.6 Refractive Index

The variation of the refractive index versus wavelength in the range of (330–1000) nm for NiO films at different doping of copper is shown in figure (4.14). It can be noticed from this figure that the refractive index (n) increases

when the doping increase with wavelengths and then decrease with the decrease of doping . This behavior can be explained on the basic of that increases doping leads to make prepared samples less dense , which in turn decreases propagation velocity of light through the sample which results increasing of the refractive index (n) when decreases doping

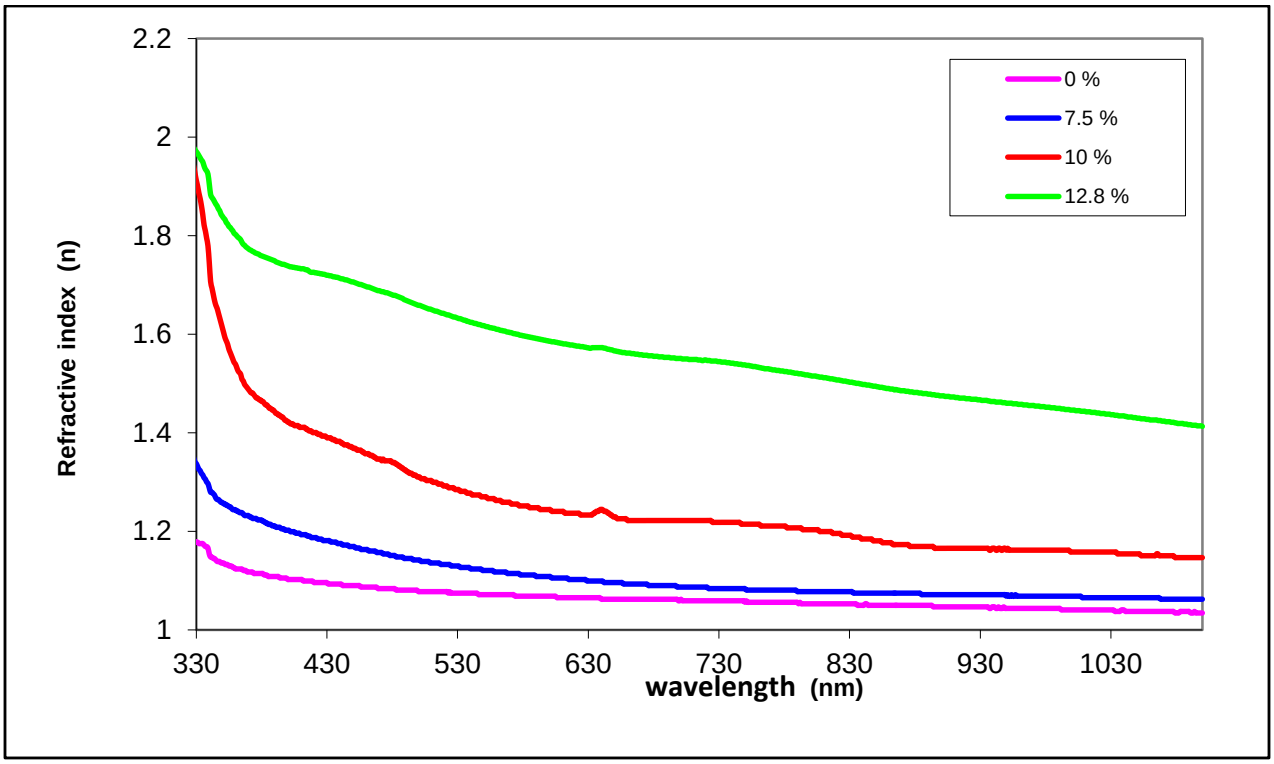

Figure (4.14): Variation of refractive index as a function of wavelength for at different of Cu doped NiO thin films**.**

4.3.7 Dielectric Constant

Figure (4.15) shows the real dielectric constant of NiO films prepared at different doping of copper. Noting from the figure that the real dielectric constant increases when the doping. Figure (4.16) illustrates the change of the imaginary dielectric constant of NiO films in different doping. It is noted from the figure that the value of the imaginary dielectric constant decreases when increase wavelength.

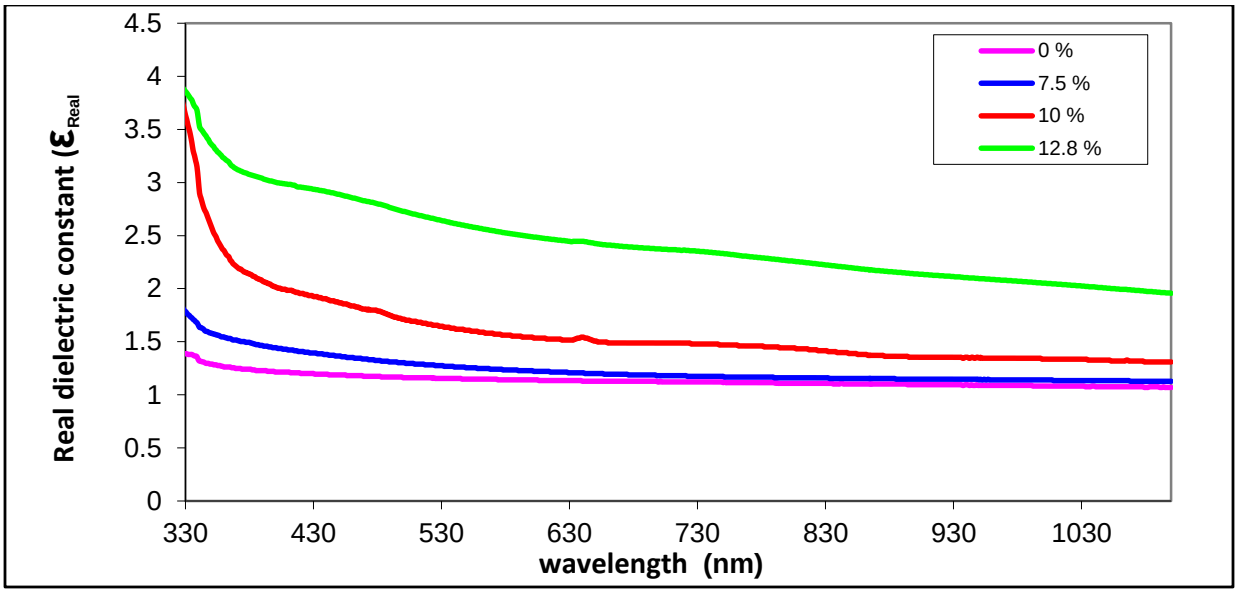

Figure (4.15): Real dielectric constant as a function of wavelength for at different of Cu doped NiO thin films.

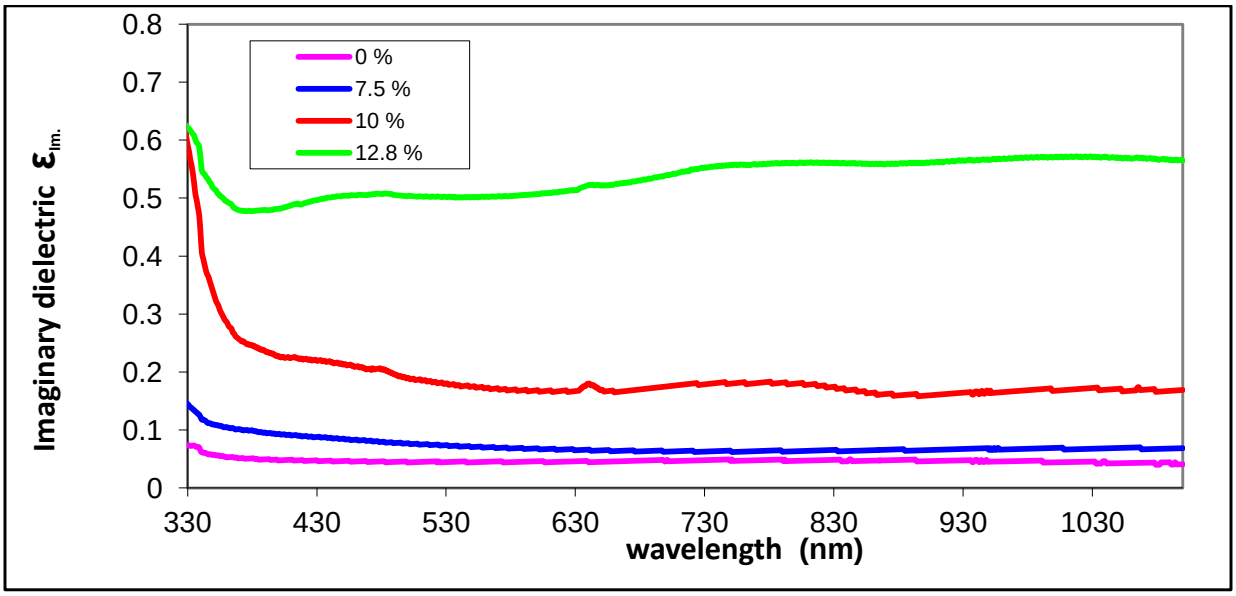

Figure (4.16): Imaginary dielectric constant as a function of wavelength for at different of Cu doped NiO thin films**.**

4.4 Effect of Dopping on (NiO:Cu) Films Thickness and Optical Energy gap

The figure (4.17) indicates that the band gap energy decreased with the increase in Cu concentration to the maximum value of 2.8 eV with 12.8 at. % Cu, this decrease can be explained by the interfaces site Share between Ni and Cu,

which was seen for the vacancy in oxygen.[42]. The Figure (4.18) indicates that the thickness increased with the increase in Cu concentration to the maximum value with 12.8 at. % Cu, this increase can be because decrease density.

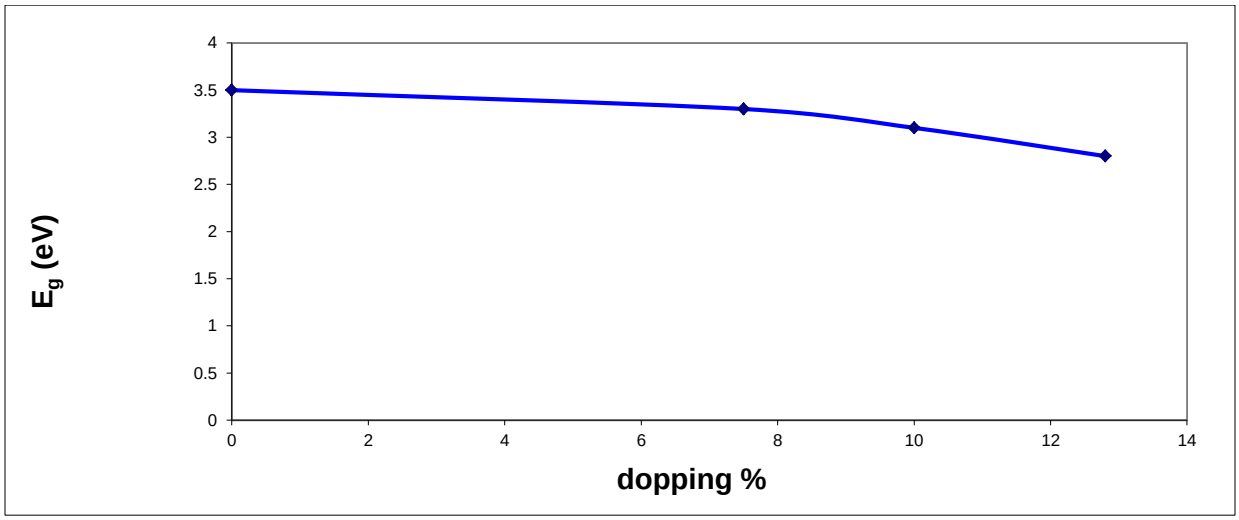

Figure (4.17) . The variation of bandgap energy of NiO doped thin films at several Cu concentrations

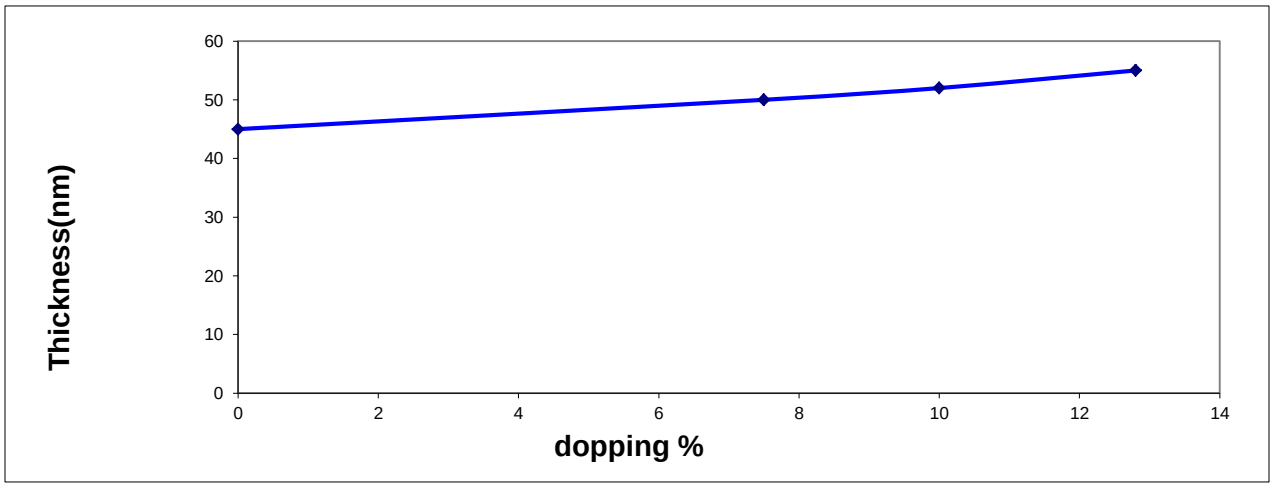

Figure (4.18) . The variation of thickness of NiO doped thin films at several Cu concentrations

4.5 The Electrical Properties of(NiO:Cu)Thin Films (Hall Effect Measurements)

The electrical properties of thin NiO films deposited on glass substrate, which involve Hall Effect, were investigated with increasing doping copper.

It is necessary to know the electrical properties of the Hall coefficient (R_H). Depending on the value of the incident magnetic field (B), the film is vertically placed in front of that field. Hall effect measurements of NiO films were analyzed for different doping copper in order to determine the form of charge carriers, their concentration, Where it was found that the carrier form of the NiO films is a positive type (p-type), Hall coefficient (R_H) value, the NiO:Cu (when doping rate Ni/Cu = 12.8 %) films were converted from p-type to n-type from hall coefficient (RH) value as the doping copper increases, the NiO:Cu (when doping rate Ni/Cu = 12.8 5) value was converted from hall coefficient (R_H) value, The explanation for this change is the increase in doping, which has resulted in an increase in the film's grain size. It is noted from Table (4.3) by using a computer program that the values of conductivity, resistivity, concentration (n_H) and hall coefficient (R_H) for the type of carrier (n) are different, but the values of mobility increase as the doping increases.

Table (4.3): Hall Effect parameters for NiO films at different doping for Copper.

sample	Concentration of Carriers n_H cm^{-3}	Conductivity $\sigma(\Omega.cm)^{-1}$	Resistivity $\rho(\Omega.cm)$	Mobility $\mu_H(cm^2/V.s)$	Hall Effect $R_H(cm^{-3})$	Type of Carriers
NiO	3.749×10^{13}	1.642×10^{-13}	6.09×10^{12}	1.9×10^{-5}	4.933×10^{4}	**p-type**
NiO:Cu Cu/Ni =7.5%	5.287×10^{12}	2.315×10^{-11}	4.319×10^{10}	1.26×10^{-3}	1.523×10^{5}	**p-type**
NiO:Cu Cu/Ni =10%	1.952×10^{12}	3.138×10^{-8}	3.187×10^{7}	0.1	3.198×10^{6}	**p-type**
NiO:Cu Cu/Ni =12.8%	-3.81×10^{11}	3.863×10^{-5}	2.589×10^{4}	6.325×10^{2}	-1.637×10^{7}	**n-type**

4.6 I-V Characteristics for Si(p,n) /(NiO:Cu) Heterojunction in Light and Dark.

It is important to study current-voltage properties in the dark and lighting state because it is a clear indication of the possibility of using the compound NiO:Cu as a light-sensitive material (solar cell).It notice observe the effect of light is evident in the change of current and voltage values for the samples prepared for the NiO compound at different doping for copper. All figures show that values the current in the dark state are less than the lighting state in the forward and reverse biases of all films. As it is note that the current values are disparit for the forward and reverse bias when changing the doping. It is noted from figure (4.19) that the electrical current of the Si (n) sample flow at NiO pure in the light and dark state because of the low potential barrier formed at the junction (p-n) of the sample, less current pass through the heterojunction in the dark state.

Figure (4.20) show that the electrical current of the Si (n) sample decrease flow at NiO:Cu in the light and dark state because of increase the potential barrier formed at the junction (p-n) of the sample.

The figure (4.21) that the electrical current of the Si (n) sample increase flow at NiO:Cu in the light and dark state because of increase the grain size and decrease the potential barrier formed at the junction (p-n) of the sample.

The increase doping turns NiO:Cu semiconductor from p-type to n-type is evident. when the (n) film is deposited on the Si (n) substrate, as in figure (4.22) for type (n-n) the difference in the concentration of carriers. The current does not pass through the heterojunction in the dark state when increase the doping because the n- type carriers are not generated while the current resistance in the lighting state is higher in the forward bias than the reverse bias because changed the carriers concentration of n- type of the Si (n) substrate and deposited n- type has on

the substrate of the sample. It is noted from figure (4.23) that the electrical current of the Si (p) sample more flow at NiO pure in the dark state because of the low potential barrier formed at the junction (p-p) of the samples. And The increase doping increase the current of the Si (p)/ NiO:Cu (p) flow at in the light and dark state because of the low potential barrier formed at the junction (p-p) of the sample as in figure (4.24).

The figure (4.25) show decrease the current of the Si (p)/ NiO:Cu (p) flow at in the light and dark state because increase of the grain size formed at the junction (p-p) of the sample.

The figure (4.26) show increase the current of the Si (p)/ NiO:Cu (n) flow at in the light and dark state at the junction (p-n) of the sample. by comparison of the Si (n)/ NiO:Cu (n) at the junction (n-n) of the sample because the n- type carriers are not generated while the current resistance in the lighting state is higher in the forward bias than the reverse bias because changed the carriers concentration of n-type of the Si (n) substrate and deposited n- type has on the substrate of the sample. Whether it is the type (p-p) or the similar type (n-n) have the same values of density but the second side of the heterojunction may have the same density as the carriers of silicon type (p) and silicon type (n) but they are different in density for carriers of the compound, which relatively generates a different potential barrier, due to the difference in density values then it is note that the current values are disparit, which reduces its sensitivity to darkness.

It is also noted from the previous figures that the current values are higher for the same voltage values in the lighting state due to the excitation of the heterojunction (p-n) when photons incident, which generate more carriers because of the breaking of the bonds that occur as a result of the incident, which increases the current values. As for the efficiency of the heterojunction prepared, it is noted

that it increases at the doping Si (n) / NiO:Cu (p) (at ratio doping Cu/Ni =10%) then it starts to decrease when the (n) film is deposited on the (n) substrate. Because the electron density increases when the doping increases and table (4.4) indicates open circuit voltage (Voc) and short circuit current (Isc), maximum voltages, current, fill factor, and efficiency of samples from heterojunctions of the Si/NiO:Cu compound. Using a computer program, while it was noticed that the highest value of open circuit voltage is (78mV) for the Si (p) sample with a (p) type film deposited for the NiO pure sample.

It was noted that the best efficiency is with a value of (2.8571429%) when depositing the type (p) film of the NiO:Cu(at ratio doping Cu/Ni =10%) sample on the Si (n) substrate .

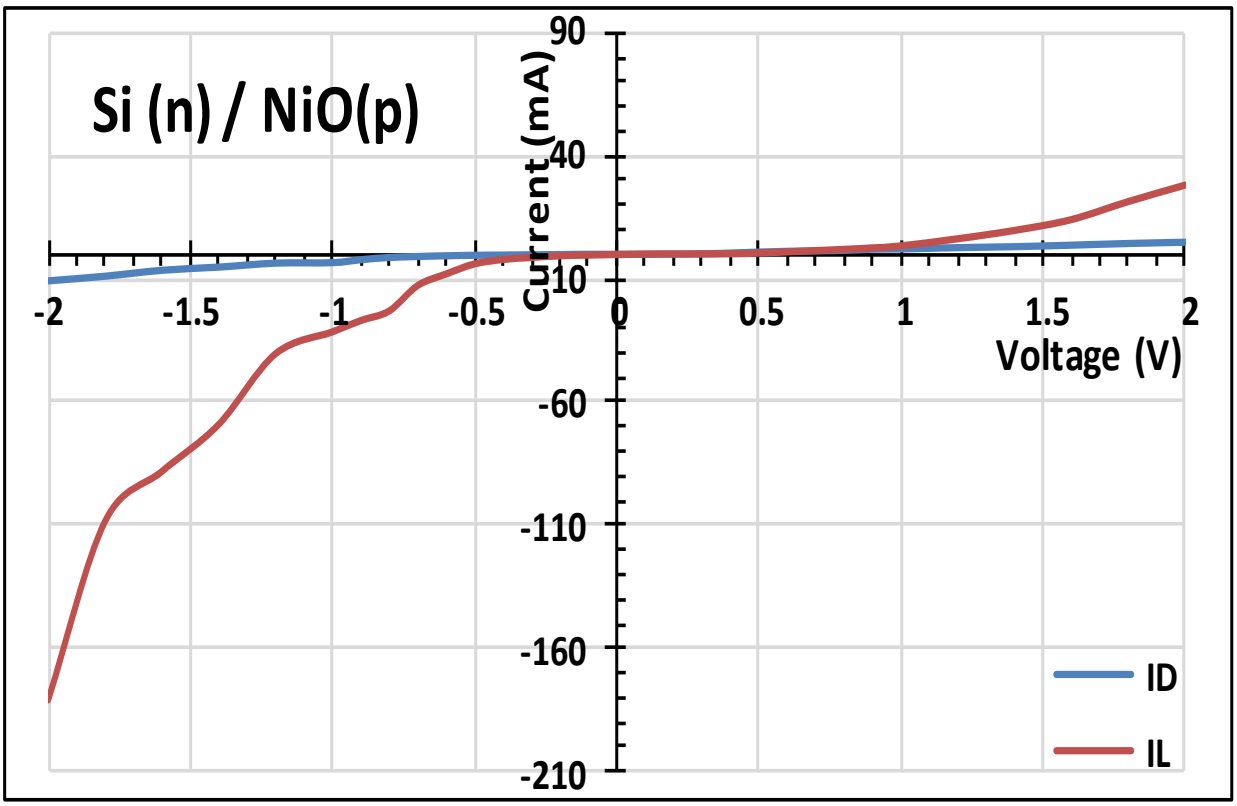

Figure (4.19): I-V Characteristics in Dark and Light for film Si (n) /NiO (P).

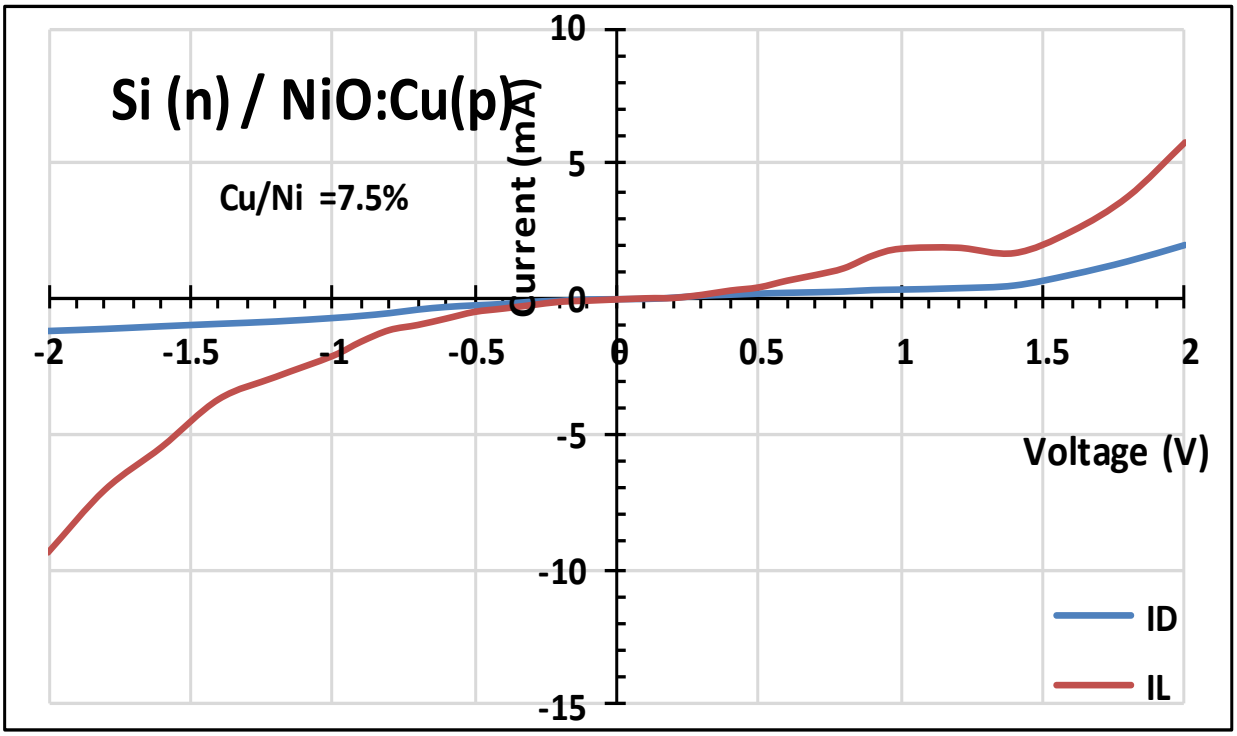

Figure (4.20): I-V Characteristics in Dark and Light for film Si (n) /NiO:Cu $_{Cu/Ni\ =7.5\%}$ (P).

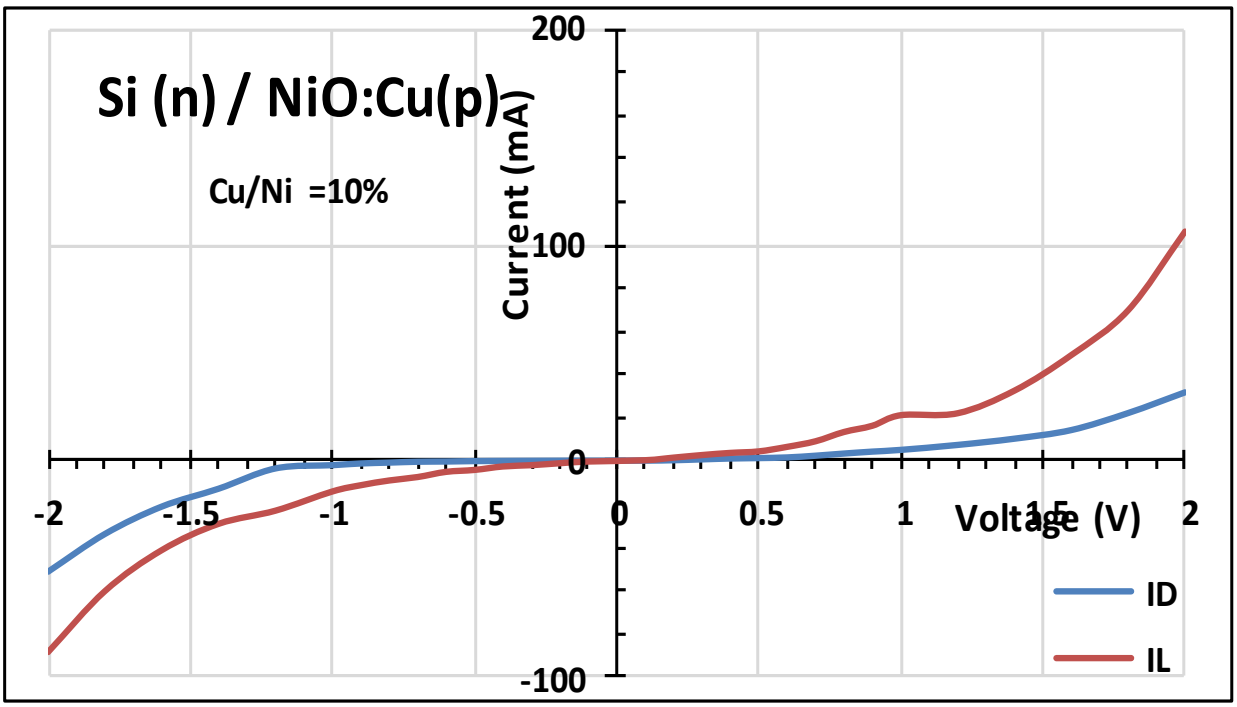

Figure (4.21): I-V Characteristics in Dark and Light for film Si (n) /NiO:Cu $_{Cu/Ni\ =10\%}$ (P).

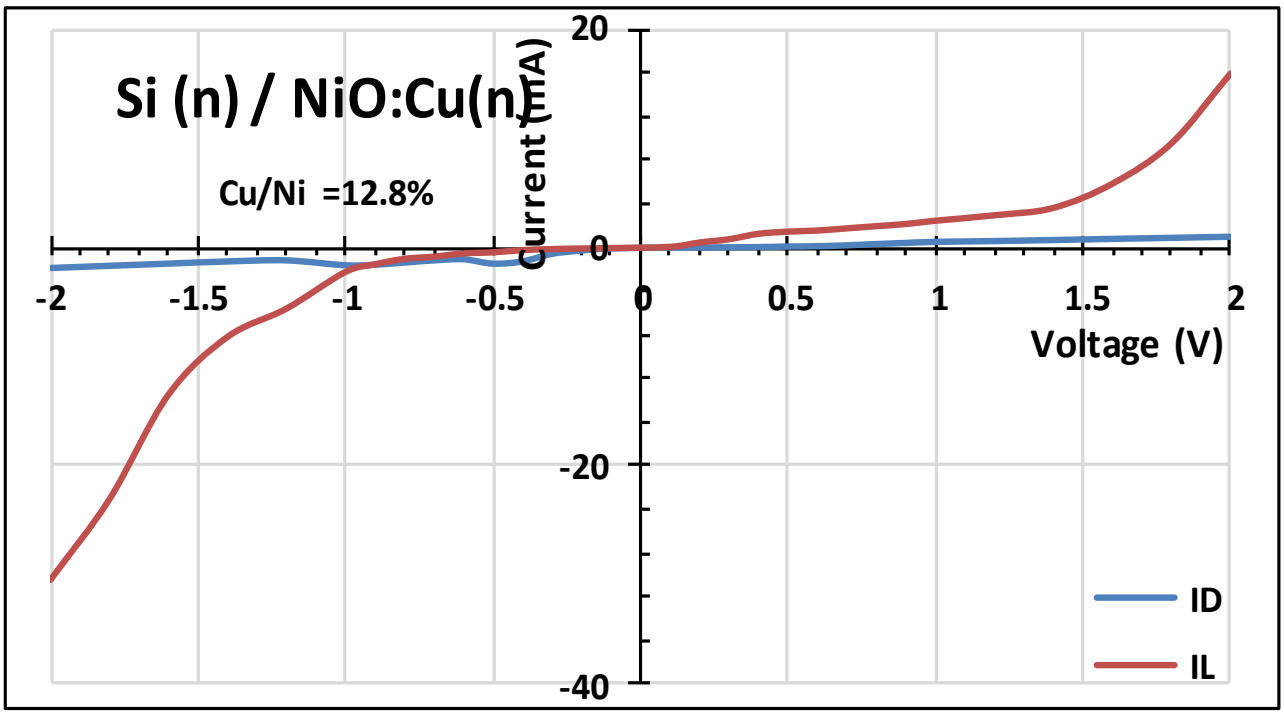

Figure (4.22): I-V Characteristics in Dark and Light for film Si (n) /NiO:Cu $_{Cu/Ni\ =12.8\%}$ (P).

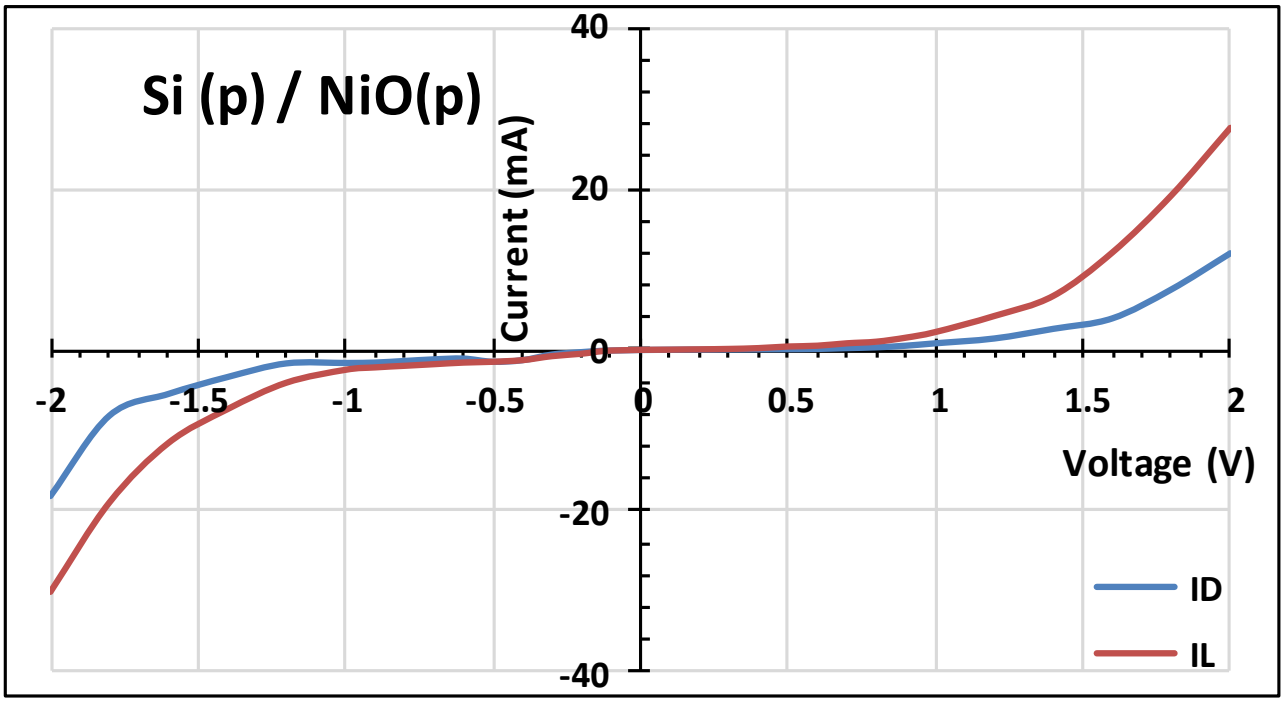

Figure (4.23): I-V Characteristics in Dark and Light for film Si (p) /NiO (P).

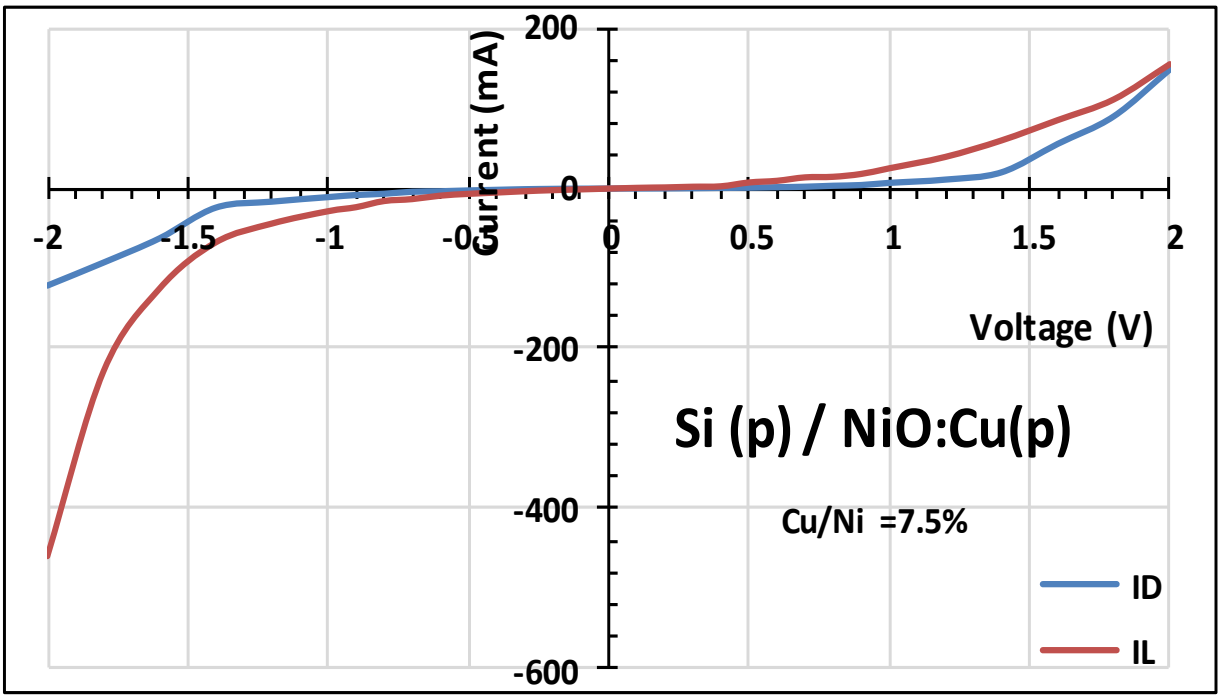

Figure (4.24): I-V Characteristics in Dark and Light for film Si (p) /NiO:Cu $_{Cu/Ni\ =7.5\%}$ (P).

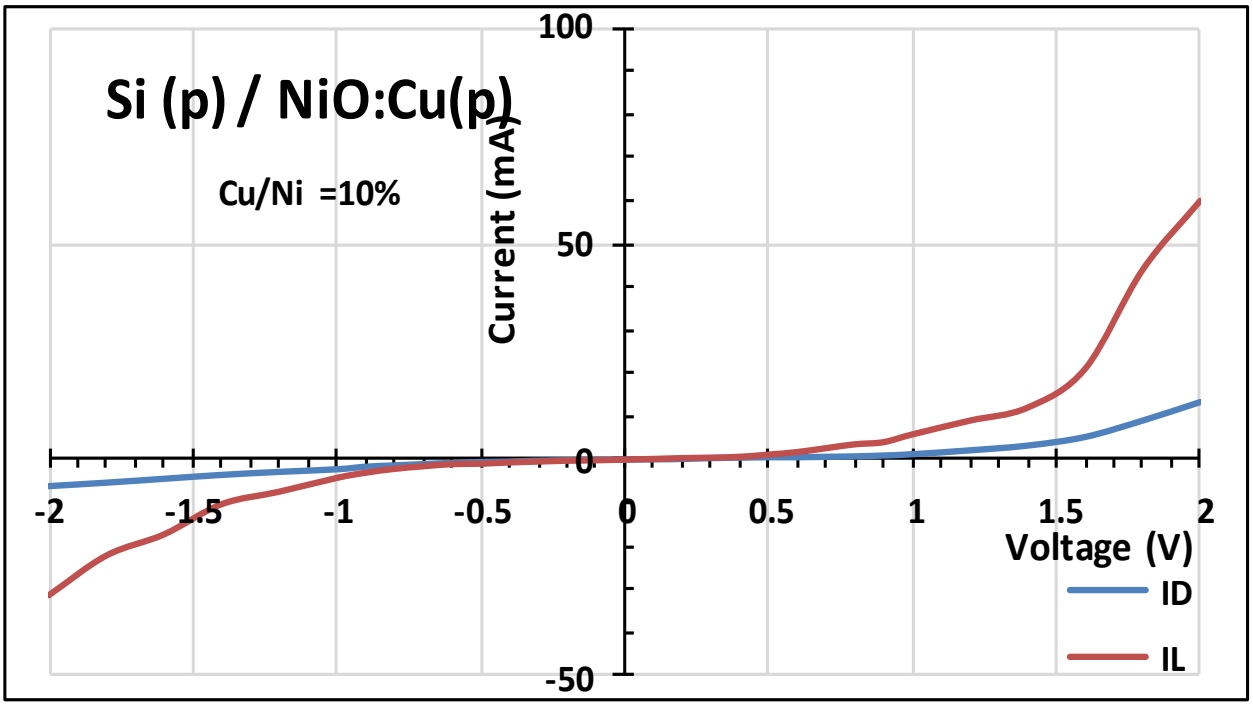

Figure (4.25): I-V Characteristics in Dark and Light for film Si (p) /NiO:Cu $_{Cu/Ni\ =10\%}$ (p).

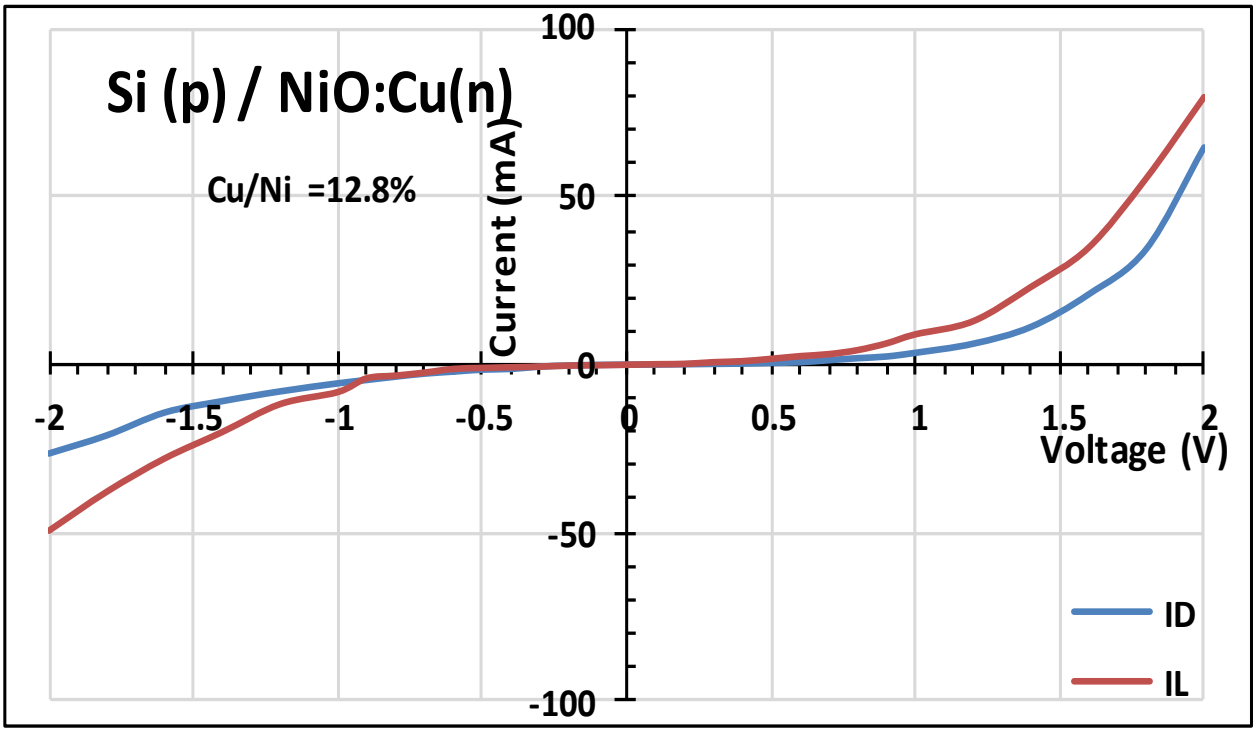

Figure (4.26): I-V Characteristics in Dark and Light for film Si (p) /NiO:Cu $_{Cu/Ni\ =12.8\%}$ (n).

Table (4.4): Values Open Circuit Voltage, Closed Circuit Current and values Maximum for Voltage and Current, Fill Factor, and Efficiency for samples of heterojunction of Si(p,n) / NiO at different doping Cu .

sample	Cu/Ni (At%)	V_{oc}(mV)	I_{sc}(mA)	V_{max}(mV)	I_{max}(mA)	F.F	η%
Si(n)/NiO(p)	0	42	0.082	18	0.05	0.26	1.5306122
Si(n)/NiO:Cu(p)	7.5	35	0.015	20	0.009	0.34	0.3061224
Si(n)/NiO:Cu(p)	10	50	0.13	28	0.06	0.26	2.8571429
Si(n)/NiO:Cu(n)	12.8	21	0.09	10	0.005	0.03	0.0936563
Si (p) / NiO(p)	0	78	0.022	28.00	0.015	0.26	0.7660714
Si(p)/NiO:Cu(p)	7.5	12	0.12	6.5	0.06	0.26	0.6632653
Si(p)/NiO:Cu(p)	10	35	0.058	20	0.03	0.30	1.0204082
Si(p)/NiO:Cu(n)	12.8	32	0.05	15	0.03	0.28	0.7653061

4.7 Conclusions

In this section will show the main conclusions that we have obtained in our research. From overall measurements and observations, one can conclude the following:

1. The method of Aerosol Assistant Chemical Vapor Deposition has proved its efficiency in preparing thin films within nanoscale ranges
2. Increase in the doping Cu increasing which leads to an decrease in the energy gap.
3. The carrier type changes of the films of the NiO:Cu compound from p- type to n-type when the doping increases, so the density of carriers and resistivity is decreases, while the mobility and conductivity increases with increasing doping
4. Noticed a decrease with the disparit of current values in the dark state and an increase in the sensitivity of the samples after lighting in the forward and reverse bias.
5. The best heterogeneous reaction efficiency was observed to be of (2.8571429) value when (p) film of a NiO: Cu sample was deposited on a Si (n) .
6. As for the efficiency of the heterojunction prepared, it is noted that it increases at the doping (Cu/Ni=10%) NiO:Cu(p) /Si (n) then it starts to decrease when the (n) film is deposited on the (n) substrate, Because the electron density increases when the doping increases.
7. There is a variation in the values (Isc,Voc,Imax,Vmax,FF) when depositing isotype (p / p), (n / n) and unisotype (n / p), (p / n).

4.8 Suggestions for Future Work

For future work it can be suggested the following:

1. Fabrication and characterization of a solar cell from multi-junction of NiO:Cu as an upper layer

2. Preparation of (NiO:Cu) heterojunction on different substrate such as GaAs, InSb and Ge and study the optoelectronic properties for heterojunction.

3. Fabrication and characterization of NiO:Cu (p)/NiO:Cu (n) solar cell by chemical spray pyrolysis technique.

4. Preparation of (NiO:Cu) heterojunction using thermal evaporation technique and study optical ,electrical and optoelectronic properties of preparing films.

REFERENCES

References

[1] K. L. Chopra, "Thin Films Phenomena ",McGraw-Hill, NewYork, (1969).

[2] L. Eckcrtova, "Physics of Thin Film ",Plenum press, New York and London, (1977).

[3] R.W. Berry, P.M. Hall & T. Harris "Thin Film Technology " New York, (1979).

[4] K.-L. Choy, Prog. Mater. "Thin Solid Films" Chemical Vapor Deposition 592,611(2003).

[5] K.-L. Choy, " Nanostructured Materials and Nanotechnology: Synthesis and Processing", Academic Press, San Diego, pp. 533–577. (2000).

[6] T. T. Kodas, M. J. Hampden-Smith, " Aerosol Processing of Materials", Wiley-VCH, Weinheim, Germany, (1999).

[7] H. B. Wang, G. Y. Meng and D. K. Peng, "Thin Solid Films", Chemical Vapor Deposition 368, 275.(2000).

[8] X. Hou and K.-L. Choy, "Chemical Vapor Deposition", Chemical Vapor Deposition 631. (2006).

[9] H. Z. Song, C. R. Xian, G. Y. Meng and D. K. Peng, " Thin Solid Films " Chemical Vapor Deposition 434, 244,(2003).

[10] H. B. Wang, C. R. Xia, G. Y. Meng and D. K. Peng, Mater., " Thin Solid Films " , Chemical Vapor Deposition 368, 275. (2000).

[11] Sam Zhang, DeenSun,Yongqing Fu, Hejun Du, "Toughening of hard nonstructural thin films", Surface &Coatings Technology 198 . 2-8, (2005).

[12] I.G.C. Weppelman, P.C. Post, C.T.H. Heerkens, C.W. Hagen and J.P. oogenboom, " Fabrication of narrow-gap nanostructures using electron-

beam induced deposition etch masks", Microelectronic Engineering 153 ,77–82, (2016).

[13] Mai Mostafa Khalaf, Hikmet Gamal Ibrahimov and Etibar Hummat Ismailov, " Nanostructured Materials: Importance, Synthesis and Characterization-A Review", Chemistry Journal, Vol. 02, Issue 03, pp. 118-125, (2012).

[14] UmairYaqubQazi and RahatJavaid, " A Review on Metal Nanostructures: Preparation Methods and Their Potential Applications ", Advances in Nanoparticles, 5, 27-43,(2016).

[15] Ying, J. Y., Nanostructured Materials, Academic, San Diego previously published as: Advances in chemical engineering, V. 27. (2001).

[16] M. G. Yousif, "Solid State Physics", Baghdad University press, part II (1987).

[17] Khaled Abdel-Hamid El-Khatib and Walid Khalaf Hamoudi, "Laser Photonics", University of Technology, (1980).

[18] S. S. Al- Rawi, Sh. J. shakir and Y. M. Husan, " Solid state Physics", Publishing of Mousal University, Arabic Version , (1990).

[19] M. G. Yousef, "Solid State Physics," Baghdad University Press, part I (1982).

[20] S. M. Sze, "Semiconductors Devices Physics and Technology", Translated by F. Hayaty and H. A, Ahmed, Al-Mosual University, press, (1990).

[21] J. S. Blakemore, " Solid State Physics", Gambridge Press, 2nd, (1986).

[22] S. Ben " Solid state Electronic devices", Hall International, Inc, U. S. A, (1990).

[23] K. Alexander, " X-ray diffraction Procedures for Polycrystalline and Amorphous Material", john and Sons, (1974).

[24] B.L.Sharma & R.K. Purohit "Semiconductor Heterojunctions", Pergamon Press, New York, (1974).

[25] S. M. Sze," Physics of Semiconductors devices ",2nd, wiley , New York (1981).

[26] Sobhi Saeed Al-Rawi, "Physics of Electronics", Mosul University Press, (1980).

[27] A. G. Nilens , "Deep Imparity in Semiconductors ", Wiley .Inter Science Publi cation, (1973).

[28] SA. Mahmoud, A. Shereen and AT. Mou'ad, " Structural and optical dispersion characterization of sprayed nickel oxide thin films ". J Mod Phys;2:1178–86 ,(2011).

[29] S. C. Chen, T. Y. Kuo, Y. C. Lin and H. C. Lin, "Preparation and properties of p-type transparent conductive Cu-doped NiO films," Thin Solid Films, vol. 519, no. 15, pp. 4944–4947, 2011, doi: 10.1016/j.tsf.01.058,(2011).

[30] A.M. Reddy, A.S. Reddy and P.S. Reddy, "Thickness dependent properties of nickel oxide thin films deposited by dc reactive magnetron sputtering, " Vacuum, 85, pp. 949-954,(2011).

[31] S. Sriram and A. Thayumanavan, "Structural, optical and electrical properties of NiO thin films prepared by low cost spray pyrolysis technique", Int. J. Mater. Sci. Eng., 1, pp. 118-121, (2013).

[32] R.A. Ismail, S. Gafori and G.A. Kadhim, "Preparation and characterization of nanostructured nickel oxide thin films by spray pyrolysis" , Appl. Nanoscience, 3, pp. 509-514,(2013).

[33] K. H. Kim, C. Takahashi, Y. Abe and M. Kawamura, " Effects of Cu doping on nickel oxide thin film prepared by sol-gel solution process " , Optik (Stuttg)., vol. 125, no. 12, pp. 2899–2901, (2014).

[34] V. Gowthami, P. Perumal, R. Sivakumar and C. Sanjeeviraja, "Structural and optical studies on nickel oxide thin film prepared by nebulizer spray technique", Phys B: Condens Matter . 452. 1–6, (2014).

[35] Y. Zhao, H. Wang, C. Wu, Z.F. Shi, F.B Gao, W.C. Li, B.I. Zhang and G.T. Du, "Structures, electrical and optical properties of nickel oxide films by radio frequency magnetron sputtering " , Vacuum, 103, pp. 14-16, (2014).

[36] M. Jlassi, I. Sta, M. Hajji, and H Ezzaouia, "Optical and electrical properties of nickel oxide thin films synthesized by sol-gel spin coating ", Mater. Sci. Semicond. Processing, 21, pp. 7-13, (2014).

[37] M. M. Gomaa, M. Boshta, B.S. Farag and M.B.S. Osman, "Structural and optical properties of nickel oxide thin films prepared by chemical bath deposition and by spray pyrolysis techniques", J. Mater. Sci.: Mater. Electron, 27, pp. 711-717, (2016).

[38] M. Vigneshkumar, S. Muthulakshmi Suganya, J. Pandiarajan, A. Saranya and N. Prithivikumaran , " Structural and optical properties of nanocrystalline nickel oxide thin film by spray pyrolysis technique ", Int J Tech Res Appl 52–6 , (2016).

[39] A.A. Yadav, U. Chavan , " Influence of substrate temperature on electrochemical supercapacitive performance of spray deposited nickel oxide thin films " , J Electroanal Chem 36–42, (2016).

[40] W. Chen., "Understanding the Doping Effect on NiO: Toward High-Performance Inverted Perovskite Solar Cells," Adv. Energy Mater., vol. 8, no. 19, pp. 1–10, (2018).

[41] R. O. Ijeh., "Magnetic and optical properties of electrodeposited nanospherical copper doped nickel oxide thin films ", Phys. E Low-

Dimensional Syst. Nanostructures, vol. 113, no. December 2018, pp. 233–239, (2019).

[42] S. Benramache, B. Benhaoua and H. Guezzoun, "Study the Effect of Cu Doping on Optical and Structural Properties of NiO Thin Films" , Ann. West Univ. Timisoara - Phys., vol. 67, no. 3, pp. 15–22, (2020).

[43] H. Sato, T. Minami, S. Takata and T. Yamada, " Thin Solid Films " ,236 .27–31, (1993).

[44] Korošec and P. Bukovec," Sol-Gel Prepared NiO Thin Films for Electrochromic Applications," Acta Chimica Slovenica. 53(2):136-147.(2006).

[45] S. Dendouga, S. Benramache and S. Lakel," Influence of Film Thickness on Optical and Electrical Properties of Nickel Oxide (NiO) Thin Films," Journal of Chemistry and Materials Research. 5(4):78-84, (2016).

[46] RC. Tenent, DT. Gillaspie, A. Miedaner, PA. Parilla, CJ. Curtis and AC. Dillon,"Fast-Switching Electrochromic Li+ -Doped NiO Films by Ultrasonic Spray Deposition," Journal of the Electrochemical Society. 157(3):H318-H322,(2010).

[47] M. Stamataki, D. Tsamakis, N. Rilis, I. Fasaki, A. Giannoudakos and M. Kompitsas ,"Hydrogen gas sensors based on PLD grown NiO thin film structures," Physica Status Solid (A). 205(8):2064- 2068, (2008).

[48] KW. Nam, WS. Yoon and KB. Kim," X-ray absorption spectroscopy studies of nickel oxide thin film electrodes for supercapacitors," Electrochimica Acta. 47(19):3201-3209,(2002).

[49] G. M. Chow, and L. K. Kurihara, " Chemical Synthesis and Processing of Nanostructured Powders and Films", (Carl. C. Koch, ed.), Nanostructured

Materials: Processing, Properties and Potential Applications, Noyes Publications, pp. 3–50, (2002).

[50] B. Sppval and G. Herman, "Physics of Semiconductor", Springer Verlag, New York, P.41-45, 245, (1995).

[51] B.L.Sharma & R.K. Purohit "Semiconductor Heterojunctions", Pergamon Press, New York, (1974).

[52] A.G. Milnes and D.L. Feocht, "Heterojunction and Metal-Semiconductor Junction", Academic Press, New York, (1972).

[53] J. M. Hincapié-Zapata, E. Y. Castrillón-González, B. Cruz-Muñoz, M. H. Medina-Barreto, and R. J. Dorantes-Rodríguez, "Instrumentation and control of an aerosol-assisted chemical vapor deposition system (AACVD) " , DYNA, vol. 86, no. 210, pp. 52–57, (2019).

[54] J.M. Hincapié, E.Y. Castrillón, W. Olarte, R.J. Dorantes, and B. Cruz, "Statistical study of the variable speed of an AACVD device implemented in the UTP " , IX International Congress of Physics Engineering, Azcapotzalco, México, (2018).

[55] B.E. Monárrez, P. Amézaga, A. Sáenz, P. Pizá, W. Antúnez, and M. Miki, "Synthesis and characterization of composite Fe-Ti oxides nanoparticles with high surface area obtained via AACVD " , Ceramics International, 44(6), pp. 6990-6996, (2018).

[56] B.E. Monárrez, P. Amézaga, P.G. Hernández, W. Antúnez, C. Leyva, and M. Miki, " Theoretical and experimental analysis of the aerosol assisted CVD synthesis of magnetite hollow nanoparticles ", Journal of Alloys and Compounds, 615(1), pp. S328-S334,(2014).

[57] S. Lim, N. Huang, H. Lim, and M. Mazhar, " Aerosol assisted chemical vapor deposited (AACVD) the TiO2 thin film as a compact layer for the

dye-sensitised solar cell" , Ceramics International, 40(6), pp. 8045-8052, (2014).

[58] J.S. Sagua, K.G.U. Wijayantha, and A.A. Tahir, "The pseudocapacitive nature of $CoFe_2O_4$ thin films ", Electrochimica Acta, 246(20), pp. 870-878, (2017).

[59] P. Pizá-Ruiz, A. Sáenz-Trevizo, Y. Verde-Gómez, P. Amézaga-Madrid, and M. Miki-Yoshida, "Delafossite $CuFeO_2$ thin films via aerosol assisted CVD: synthesis and characterization" , Ceramics International, 45(1), pp. 1156-1162, (2019).

[60] X. Hou and K. L. Choy, "Processing and applications of aerosol-assisted chemical vapor deposition" , Chem. Vap. Depos., vol. 12, no. 10, pp. 583–596,(2006).

[61] C. Y. Xu and M. J. Hampden-Smith, T. T. Kodas, Chem, "Thin Solid Films",7,1539, (1995).

[62] T. Ida ," Bragg's law", Chapter 1 , Advanced Ceramics Research Center, (2013) .

[63] M. Nobial , O. Devos , and B. Tribollet , " Advanced Techniques for Energy Sources Investigations and Testing", Proceeding of the International Workshop ,Sofia , Bulgaria, (2001) .

[64] P. Mallick and C. S. Sahoo," Effect of CuO Addition on the Structural and Optical Properties of NiO Nanoparticles", Nanoscience and Nanotechnology, Vol.3, pp.52-55, (2013).

[65] P.A. Chate, D.J. Sathe and P.P. Hankare, "Electrical and crystallographic properties of nanocrystalline $CdSe_{0.5}S_{0.5}$ composite thin films deposited by dip method" , Journal of Materials Science: Materials in Electronics, Vol. 22, No. 2, pp. 111–115, (2011).

[66] P. Miller and R. Yang, "Scanning tunneling and atomic force microscopy combined", Applied Physics Letters, Vol. 52, pp. 2233 – 2235, (1988).

[67] S. Mandal, R.K. Singha, A. Dhar, and S.K. Ray " Optical and Structural Characteristics of ZnO Thin Films Grown by RF Magnetron Sputtering Materials Research", Bulletin,43, (2008).

[68] J. Millman, "Microelectronics", Murray-Hill, Book Company Kogakusha, (1979).

[69] E. Ponz , J.L. Ladaga and R.D. Bonetto, "Measuring Surface Topography with Scanning Electron Microscopy. I. EZE image: A Program to Obtain 3D Surface Data", Microscope Microanal.,Vol.12, No.2 , p. 170, (2006).

[70] K.D. Leaver and B.N Chapman,"Thin Films",Wickham Publications, London, (1971).

[71] L. M. Abduljabbar,"Study the Effect of Annealing on Optical and Electrical Properties of ZnS Thin Film Prepared by CO_2 Laser Deposition Technique", Dijlah University , Iraqi Journal of Laser, Vol. 13, pp.29-35, (2014).

[72] K. Chopra, "Thin Film Device Application", New York: Plenum Press, Vol. 382, p.323,(1980).

[73] A.M.Al-Dhafiri,"CdS-CuS Single Crystal and Thin Film Solar Cell",Ph.D. Thesis ,University of Durham,(1988).

[74] R. Elliot and A.Gibson, "An Introduction to Solid State Physics and Application", 1st edition, Macillian Inc,, Vol. 471, p. 92, (1974).

[75] S. Elliott, "Physics of Amorphous Materials" , New York: Longman Inc, Vol. 155, p. 98, (1984).

[76] G. Burns, "Solid State Physics", New York: Academic Press, Harcourt Brace Jovanovich, (1985).

[77] P.Domens and M . Cadene , "Phys . Stat . Sol (a) ", ACS Appl. Mater. Interfaces, Vol.59 , No.20 , (1982).

[78] M.A.Omer, "Elemntary of Solid State Physics", Adison Wesely Publishing, Co. London, (1975).

[79] M.A. Abdul Majeed,"Optoelectronics Properties of$(CdO)_{1-x}(SnO_2)_x$/Si Detector Prepared by Pulsed Laser Deposition", M.Sc.Thesis, Babylon University, College of Science,(2015) .

[80] J.I.Pankove, "Optical Processes in Semiconductors" ,Prentice – Hall Inc., Englewood cliffs, Vol. 285, pp. 111,(1971).

[81] S. Darbe, R. Beal, A. Stavrinadis, H. Cao, J. Smith, H.A. Assender, A.A.R. Watt, "Visible Light Absorbing Metal Oxide Solar Cells", MIT-Oxford summer student report, (2009).

[82] M. Jassim ,"Investigation of $(NiO)_{1-x}(CuO)_x$ Thin Films Properties Preparing by Spray Pyrolysis Technique", M.Sc.Thesis,University of Babylon,College of Science,(2015).

[83] O. Stenzel , "The physics of thin film optical spectra", Springer Series in Surface Sciences, pp. 214-220, (2011).

[84] L. Eckortova, "Physics of Thin Films ", Plenum Press, (1977).

[85] N. Hasan and M.Mohammed, "Electrical Properties of $(PbO)_{1-x}(CdO)_x$Thin Films Fabricated by Spray Pyrolysis Technique",Advances in Applied Science Research,Vol. 6,No. 7, (2015).

[86] G. B. Armen, "Hall Effect Experiment", University of Tennessee, (2007).

[87] N. F. Mott and E. A. Davis, "Electronic Process in Non-Crystalline Materials", 2nd Edition, Clarendon Press, Oxford, (1979).

[88] L. Olof,"Hall Effect ", Westinghouse research laboratories , (1952).

[89] S. Ilican, Y. Caglar, M. Caglar, and F. Yakuphanoglu, "Structural, Optical and Electrical Properties of F-doped ZnO Nanorod Semiconductor Thin Films Deposited by Sol-Gel Process", Applied Surface Science, Vol. 255, pp. 2353-2359, (2008).

[90] Amada Loren, "Texturization Processes of Mono Crystalline Silicon with Na_2Co_3/$NaHCo_3$ Solution for Solar Cells", Cienclas Y Tecnologlas I.S.B.N, (2012).

[91] Muslim Fadel and Hoda Sallam, "Study of optical properties of copper oxides membranes prepared by laser deposition", University of Technology, Journal of Al-Nahrain University Vol. 12 No. 4, (2009).

[92] P. Wurfel , "Physics of Solar Cell" : From Principle to New Concepts Wiley – WCH, Weinbein ,(2015).

[93] David Garrido, "Electric Measurements on Crystalline Silicon Concentration Cells", Slovak University of Technology Bratislava,(2008).

[94] R. Ellingson and M. Heben., "Solar Cell Performance Characterization: Current – Voltage, and Quantum Efficiency ",The University of Toledo,(2011).

[95] P. Meakin and R. Jullien: "Restructuring effect in the rain model for random deposition" , J. Physique 48, (1987).

[96] M. Feng., "High-Efficiency and Stable Inverted Planar Perovskite Solar Cells with Pulsed Laser Deposited Cu-Doped NiOxHole-Transport Layers" , ACS Appl. Mater. Interfaces, vol. 12, no. 45, pp. 50684–50691, (2020).

الخلاصة

تم تحضير أغشية الرقيقة من NiO:Cu باستخدام تقنية ترسيب البخار الكيميائي بمساعدة الهباء الجوي وهي طريقة اثبتت كفاءتها في تحضير أغشية رقيقة ضمن المديات النانوية. تم التشويب باستخدام النحاس بنسب مختلفة (Cu/Ni=0, 7.5, 10, 12.8 At.%) لترسيب اغشية على ركائز من الزجاج والسليكون نوع (n) و(p).

تم دراسة التركيب البلوري للأغشية المحضرة بطريقة حيود الأشعة السينية (XRD) وبينت النتائج إن الأغشية المحضرة جميعها متعددة التبلور بالطور المكعبي بأعلى قمة عند المستوى (111) وعند الزاوية ^{o}(37.5) وأظهرت تحسن البنية البلورية من حيث ارتفاع القمم وهناك زيادة في الحجم البلوري للجسيمات النانوية ونقصان في المطاوعة وكثافة الأنخلاعات و ارتفاع ثابت الشبيكة (a_o) عند زيادة التشويب من النحاس وهذا مؤشر لتحسن خصائص الأغشية المحضرة. اما نتائج المجهر الالكتروني الماسح (SEM) تظهر الصور الحبيبات للجسيمات النانوية من خلال زيادة التشويب NiO:Cu مع ارتفاع في الحجم الحبيبي.

تم دراسة الخصائص البصرية للأغشية المحضرة بسمك nm (6± 62 - 45) باستخدام قياسات النفاذية البصرية في المنطقة الطيفية nm (330-1100). ولوحظ ان الانتقال مباشر مسموح وان زيادة التشويب بالنحاس تؤدي الى نقصان في فجوة الطاقة البصرية لأغشية المركب NiO من 3.5eV الى 2.8eV التي تقل عند زيادة سمك الغشاء ,اذ يزداد سمك الغشاء بزيادة التشويب مادة الهدف.الثوابت البصرية كمعامل الانكسار ومعامل الخمود وثوابت العزل تم حسابها لجميع الأغشية المحضرة.

الخصائص الكهربائية تم دراسة تأثير هول. أشارت النتائج إن الأغشية من النوع الموجب (p-type) وتتحول الى النوع السالب (n-type) عند زيادة التشويب الى(Cu/Ni=12.8%) . وبينت خصائص التيار- فولتية في حالتي الظلام والإضاءة ان أغشية المركب حساسة للضوء ، حيث لوحظ انخفاضًا مع تباين في قيم التيار في حالة الظلام وزيادة في حساسية الاغشية بعد الإضاءة في الانحياز الأمامي والعكسي ، لوحظ أن أفضل كفاءة للمفرق المتباين هي بقيمة (2.8571429%) عند ترسيب غشاء نوع (p) لعينة NiO:Cu على ركيزة نوع (n) Si في النسبة (Cu/Ni=10%) ,ثم يبدأ بالانخفاض عندما يتم ترسيب الغشاء نوع (n) على الركيزة من السليكون نوع (n). لوحظ ايضا هناك تباين في قيم (I_{sc} , V_{oc} , I_{max} , V_{max} , FF) عند ترسيب نوع متماثل (p / p) و(n / n) ونوع غير متماثل (n / p) و (p / n).

وزارة التعليم العالي والبحث العلمي
جامعة بابل / كلية العلوم
قسم الفيزياء

تحضير وتشخيص الخلية الشمسية (NiO: Cu / Si) بطريقة الترسيب بالتبخير الكيميائي (AACVD)

رسالة

مقدمة إلى مجلس كلية العلو م / جامعة بابل

كجزء من متطلبات نيل درجة الماجستير في العلوم / الفيزيا ء

من قبل

زيد محمد جاسم زويد

(بكالوريوس علوم في الفيزياء ٢٠١٤)

بإشراف

أ.م.د. صبا عبدالزهرة عبيد الشباع

٢٠٢١ م ١٤٤٣هـ